Contaminant mobilisation by fluid-rock interaction and related transport mechanisms in platinum tailings

Submitted in full requirement for the degree

M.Sc. Engineering- and Environmental Geology

To:

Department of Geology

School of Physical Sciences

Faculty of Natural and Agricultural Sciences

University of Pretoria

By:

Altus Huisamen

Student Number 27188176

2013

Declaration and Acknowledgements:

I, Altus Huisamen, student number 27188176, submit this dissertation to the Department of Geology, University of Pretoria, in accordance with the full requirements and prerequisites for the degree Masters in Sciences (M.Sc. Engineering and Environmental Geology). I declare that everything contained in this dissertation is my own work unless noted otherwise. All external sources have been referenced diligently and all credit for previously published work is acknowledged to the respective authors.

I furthermore acknowledge the following parties:

- My Heavenly Father for guidance and wisdom.
- Mr. Matthys A. Dippenaar and the University of Pretoria for mentorship and valuable input.
- Prof J. Louis van Rooy and the University of Pretoria for mentorship and valuable input.
- Mr. A. Huisamen (snr.) for assistance in the construction of the falling head permeameter.
- Miss. Nelda Breedt for support and motivation.
- Mr. Eduan Hattingh for assistance during the pumping tests.
- Dr. van der Ahee Coetsee and Geo Pollution Technologies for opportunities, mentorship, financial assistance, time and resources.
- Dr. Gideon J. du Toit and Geo Pollution Technologies for opportunities, mentorship, financial assistance, time and resources.
- The entire Geo Pollution Technologies staff for motivation, support and advice.
- Mr. Pieter Badenhorst and the staff of Soil and Groundwater Remediation Services for the direct push probe drilling on the tailings.
- Mr. P.S. Rossouw and the University of Pretoria for mentorship and valuable input.
- Dr. S. Adams and the Water Research Commission for funding.
- Mr. Terry Harck and SolutionHPlus for mentorship and valuable input.
- The relevant personnel at the undisclosed mine site where field work was conducted, for their hospitality and accommodating the research project.
- The Huisamen Family for support and motivation.

Signed:

A. Huisamen
(electronic signature)

27/07/2012

ABSTRACT

Contaminant release and transport in platinum tailings are poorly studied in literature. This study serves to characterise these processes. The tailings facility is located in Steelpoort, Mpumalanga, South Africa on Critical Zone rocks of the Rustenburg Layered Suite in The Bushveld Igneous Complex. Tailings material samples were collected by hand auger- and direct push probe drilling at specific locations to represent the different materials present in the tailings facility. Water samples were collected from monitoring boreholes as well as the Steelpoort River. The samples were analysed using XRD, XRF, ABA, NAG, Reflected Light Microscopy, Acid Leaching Tests and ICP scans. Using the collected data, a geochemical model was constructed for the interpretation of mineral phase dissolution and to trace the mineral phases releasing contaminants. Analysis-, test- and modelling results showed that alteration mineral phases formed within ten years in the tailings material and that the existing alteration phases viz. talc and chlorite, as well as sulphides, are the major contributors of contaminants. Elevated pH values as well as major cation and anion concentrations were found in the fluid discharging from the tailings as well as the in groundwater, with little to no heavy metals, which were traced directly to the chromite phase. This suggests that platinum tailings do not contribute to heavy metal contamination or acid rock drainage but may increase aquifer salinity and alkalinity. The flow through the tailings, underlying vadose zone and fractured rock aquifer was characterised using permeameter- and pumping tests. From the data collected, an unsaturated flow model was developed to characterise the flow through the tailings. From the model, discharge from the tailings was calculated to take place at 0.7m per decade into the underlying vadose zone with fracture flow in the aquifer ranging from 0.46-0.026m/d, as calculated from pumping test results. Contaminant migration into the Steelpoort River is possibly inhibited by the Dwarsriver Fault, based on the chemical data and hydraulic conductivities calculated. Therefore, groundwater is considered to be the major receptor in the system and groundwater users may be negatively impacted by increasing groundwater salinity and major ion concentrations.

LIST OF ABBREVIATIONS

ABA = Acid Base Accounting
AH = Auger hole
Al = Aluminium
As = Arsenic
BDL = Below detection limit
BH = Borehole
BIC = Bushveld Igneous Complex
Ca = Calcium
Cl = Chloride
Co = Cobalt
Cr = Chromium
Cu = Copper
EC = Electrical Conductivity
F = Fluoride
Fe = Iron
GRDM = Groundwater Resource Directed Measures
GW = Groundwater
GWB = Geochemist's Workbench
HCO_3 = Bicarbonate
ICP-OES = Inductively Coupled Plasma Optical Emission Spectroscopy
ICP-MS = Inductively coupled plasma mass spectroscopy
K = Potassium
L = liter
m = meters
mamsl = meters above mean sea level
mbgl = meters below ground level
Mg = Magnesium
mg/l = milligrams per liter
Mn = Manganese
n.a. = not analysed
Na = Sodium
Ni = Nickel
NO_3 = Nitrate
Pb = Lead
ppm = parts per million
Si = Silica
SO_4 = Sulphate
SWL = Static Water Level
TDS = Total Dissolved Solids
Ti = Titanium
TLC = Temperature, Level, Conductivity Meter
TSF = Tailings Storage Facility
V = Vanadium
XRF = X- Ray Fluorescence
XRD = X- Ray Diffraction
Zn = Zinc

TABLE OF CONTENTS

FIGURES

TABLES

1. INTRODUCTION

1.1 Project Background

The transport mechanisms and liberation of contaminants in platinum tailings storage facilities (TSFs) are poorly studied and rarely documented. Previously published studies have focussed mainly on gold-, copper-, zinc and lead tailings. This study highlights the importance of platinum TSFs as a contaminant producer due to mineral dissolution and oxidation. This is because these tailings materials may contain significant amounts of sulphide minerals, similar to gold tailings; appreciable amounts of copper derived from minerals such as chalcopyrite and bornite; and appreciable amounts of zinc derived from minerals such as sphallerite.

The mafic silicate mineral phases in platinum TSFs may also be large scale contributors of elevated major cations and -anions in groundwater, as these minerals are prone to breakdown and dissolution at earth surface conditions. This material also contains appreciable amounts of a spinel mineral which may liberate Cr^{3+}, which might potentially evolve under changing redox conditions to a more lethal form *viz.* Cr^{6+}. Therefore, platinum tailings storage facilities may provide material causing the combined contamination types of the waste rock generated by most other precious metal mining operations. The liberated contaminants may also travel in permeating fluids to aquifer level, reaching the underlying phreatic surface and subsequently allowing contaminant transport through hydrogeological pathways to receptors.

1.2 Objectives

The objectives of this study were:

- To identify the chemical and mineralogical composition of platinum tailings materials
- To investigate the dissolution potential of the mineral phases present in order to assess the contaminant contribution of each phase
- To identify the contaminants liberated by the mineral phases present
- To identify the saturated- and unsaturated hydraulic properties of the tailings material
- To identify the hydraulic properties of the underlying aquifer.

2 LITERATURE REVIEW

2.1 Redox Conditions

The uppermost layer of platinum TSFs, which varies in thickness between tailings, is the area where oxidation and subsequent destabilisation of minerals takes place. Minerals that most tailings have in common, including platinum tailings, are the sulphides of which the oxidation is described by Moncur *et al*. (2004) in a study at the Sherridon copper mine, Manitoba. After 70 years, the redox conditions in the upper 50 cm of the Sherridon tailings had become oxidising to the point of having a pH less than 1. Acidic conditions in the tailings due to sulphide mineral dissolution had caused Al-mineral depletion up to 1 m depth (Moncur *et al*., 2004). Many studies (Geelhoed, 2002; Moncur *et al*., 2009; Garrels & Christ, 1965; Piatak *et al.*, 2004; Koski *et al*., 2008; Lefebvre *et al*., 2001; Linklater *et al*., 2005; Molson *et al*., 2005; Yellishetty *et al.*, 2009) have found similar results. Acidic solutions that could potentially form from sulphide dissolution may also cause oxide minerals and silicates in TSFs, both products of platinum mining, to dissolve. The general redox conditions of mine waters permeating through TSFs are shown in *Figure 1*.

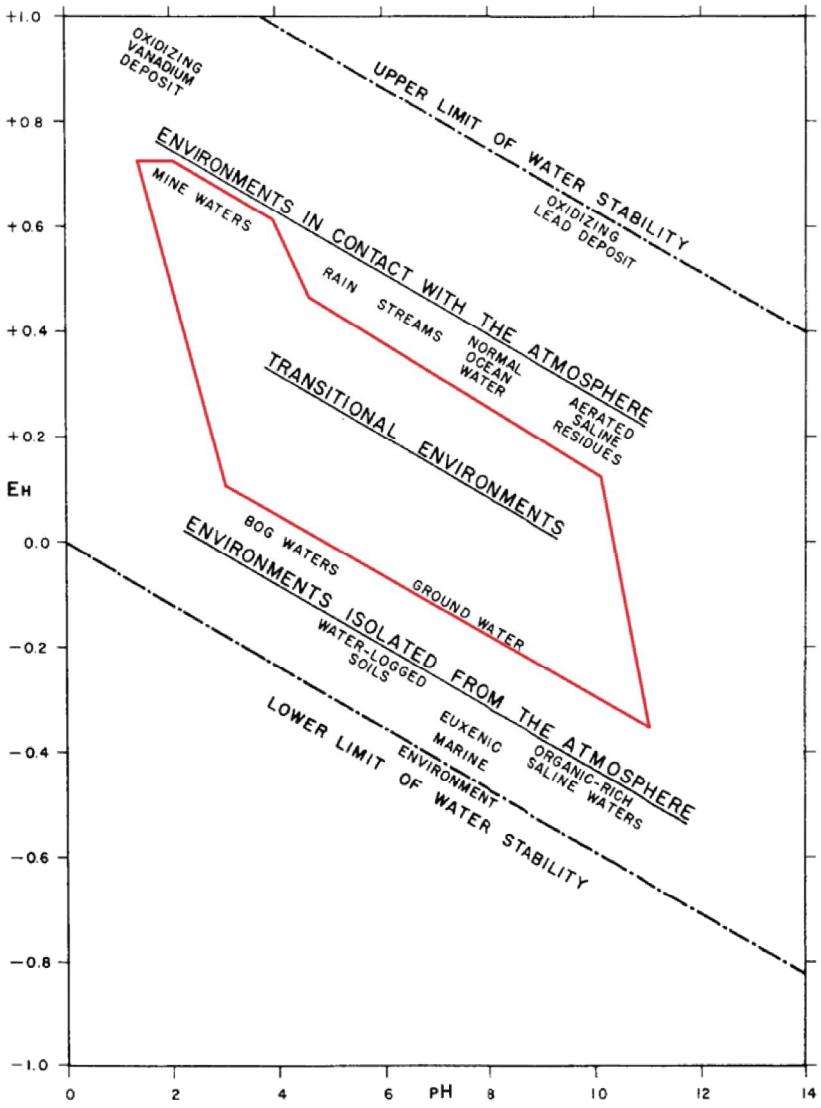

Figure 1: Redox conditions in different waters under 1 atmosphere total pressure and temperature of 25° C (Garrels and Christ, 1965).

Garrels and Christ (1965) illustrate with the use of this Eh-pH diagram, the general redox conditions in the uppermost part of tailings, a layer that is exposed to atmospheric gases and permeating fluids, rendering it oxidising. The general pH and Eh of mine tailings is assumed to be less than 5 and higher than 0.6 respectively, confining the stable minerals, species or ions present in the tailings to the prevailing redox conditions. This type of environment may be termed as oxic (Essington, 2004). However the limits of these redox conditions may vary with different temperatures, pressures, gas partial pressures as well as dissolved species (Garrels and Christ, 1965). This study will also accommodate changes in pressure-temperature conditions in the system to improve literature interpretation.

Redox conditions shift from oxidising to reducing from the top to the bottom of TSFs, as can be observed from the red stability field in *Figure 1*, and may result in the subsequent stabilisation and precipitation of different solid phases. However it is important to note that the original oxidised and dissolved reactant will very rarely be significantly re-precipitated, as many minerals require higher temperature and pressure conditions than those present, to form. An example would be the dissolution of Albite below.

$$2NaAlSi_3O_8 + 2H^+ + 9H_2O \rightarrow 2Na^+ + 4H_4SiO_4(aq) + Al_2Si_2O_5(OH_4) \qquad \textit{Equation 1}$$

Albite forms from silica rich magmas under temperatures ranging from 700–1000 C and is therefore thermodynamically unstable at surface conditions (Winter, 2004). Its re-precipitation will therefore be inhibited (Hem, 1985). Therefore neo-mineralisation may take place deeper in the TSF, inhibiting pollution. However, different species will also remain in solution. It is these species that may eventually reach groundwater and possibly cause contamination of the said environment. Redox conditions in groundwater are indicated by *Figure 1*. These conditions facilitate multiple Fe- sulphide species, SO_4^{2-}, various Cu species and precipitates, Cr^{6+} (Geelhoed *et al.*, 2004) and other heavy metal species in solution (Garrels and Christ, 1965).

2.2 Mineral Stability and Metal Liberation

Platinum mines in South Africa generally mine the Merensky platinum reef and the UG2 chromite reef. According to Vermaak and Hendriks (1976) the mineralogical composition of the pegmatoidal Merensky reef includes silicate- and oxide minerals such as:

- Orhopyroxene (Enstatite- $Mg_2Si_2O_6$; Ferrosillite- $Fe_2Si_2O_6$)
- Chromite- (Fe, Mg) Cr_2O_4
- Postcumulus feldspar (Anorthite- $CaAl_2Si_2O_8$)
- Postcumulus clinopyroxene (Diopside- $CaMgSi_2O_6$; Hedenbergite- $CaFeSi_2O_6$; Augite- (Ca, Na) (Mg, Fe, Al) Si_2O_6)
- Olivine and quartz-bearing facies also occur sporadically

The base metal sulphides present, according to Vermaak and Hendriks (1976) include:

- Pyrite (FeS_2)
- Pyrrhotite ($Fe_{1-x}S$)
- Chalcopyrite ($CuFeS_2$)
- Pentlandite ($(Fe, Ni)_9S_8$)

Precious minerals in the Merensky reef are generally associated with the base metal sulphides and the discreet phases present, according to Vermaak and Hendriks (1976) include:

- Braggite (Pt, Pd)S
- Cooperite PtS
- Laurite RuS
- Minor Sperrylite $PtAs_2$

According to the PHREEQC geochemical modelling databases (Appelo and Postma, 2010), each of these minerals has its own distinct reaction constant when dissolved in fluids indicating a product- or reagent favoured reaction. This takes place under different hydrogen ion concentrations i.e. pH conditions for each mineral, indicating its stability. Dissolution reactions and their subsequent reaction constants, of some of the mentioned minerals that may be found in platinum TSFs, are paraphrased from the PHREEQC databases in *Table 1* (Appelo and Postma, 2010).

Table 1: Fluid-mineral reaction constants of various minerals in mafic tailings material (Appelo and Postma, 2012).

Mineral Phase	Dissolution Reaction	Reaction Constant (log K)
Enstatite	$MgSiO_3 + 2H^+ = + 1H_2O + 1Mg^{2+} + 1SiO_2$	11.3269
Ferrosilite	$FeSiO_3 + 2\ H^+ = + 1\ Fe^{2+} + 1\ H_2O + 1\ SiO_2$	7.4471
Chromite	$FeCr_2O_4 + 8\ H^+ = + 1\ Fe^{2+} + 2\ Cr^{3+} + 4\ H_2O$	15.1685
Anorthite	$CaAl_2(SiO_4)_2 + 8\ H^+ = + 1\ Ca^{2+} + 2\ Al^{3+} + 2\ SiO_2 + 4\ H_2O$	26.5780
Diopside	$CaMgSi_2O_6 + 4\ H^+ = + 1\ Ca^{2+} + 1\ Mg^{2+} + 2\ H_2O + 2\ SiO_2$	20.9643
Hedenbergite	$CaFe(SiO_3)_2 + 4\ H^+ = + 1\ Ca^{2+} + 1\ Fe^{2+} + 2\ H_2O + 2\ SiO_2$	19.6060
Forsterite	$Mg_2SiO_4 + 4\ H^+ = + 1\ SiO_2 + 2\ H_2O + 2\ Mg^{2+}$	27.8626
Fayalite	$Fe_2SiO_4 + 4\ H^+ = + 1\ SiO_2 + 2\ Fe^{2+} + 2\ H_2O$	19.1113
Pyrite	$FeS_2 + 1\ H_2O = + 0.2500\ H^+ + 0.2500\ SO_4^{2-} + 1\ Fe^{2+} + 1.7500\ HS^-$	-24.6534
Chalcopyrite	$CuFeS_2 + 2\ H^+ = + 1\ Cu^{2+} + 1\ Fe^{2+} + 2\ HS^-$	-32.5638
Pyrrhotite	$FeS + 1\ H^+ = + 1\ Fe^{2+} + 1\ HS^-$	-3.7193

From these examples it can be seen that reaction constants are positive for silicate minerals, indicating a product favoured dissolution. Reaction constants for sulphide minerals are negative, indicating a reagent favoured dissolution. The chromite reaction constant is positive indicating product favoured dissolution. Reaction constants of these dissolution reactions may be fixed, but their reaction rates, however, are not. According to Yadav and Chakrapani (2006), pH conditions influence dissolution rates of minerals at high and low values, accelerating dissolution, whereas neutral pH conditions favour mineral stability and lowers solubility as illustrated by *Figure 2.*

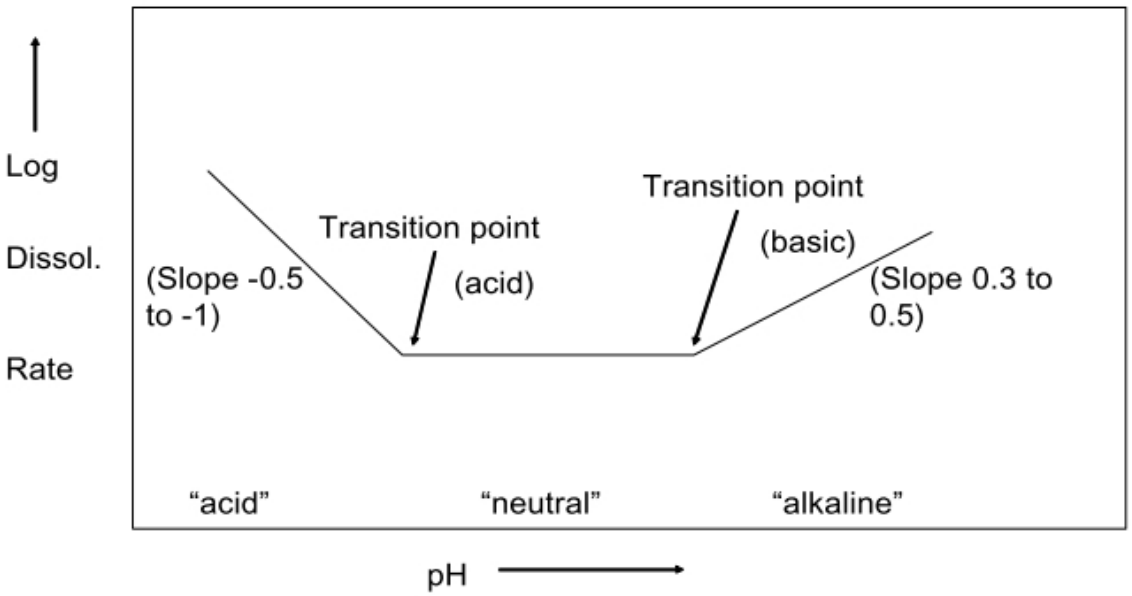

Figure 2: Logarithmic mineral dissolution rates at different pH levels (Yadav and Chakrapani, 2006)

This curve of dissolution is termed amphoteric and is constructed using the species in solution under different pH conditions, *viz.* the Cr^{6+} species is stable and abundant in solution, at a pH of 8 as illustrated by Geelhoed (2007) in *Figure 3*.

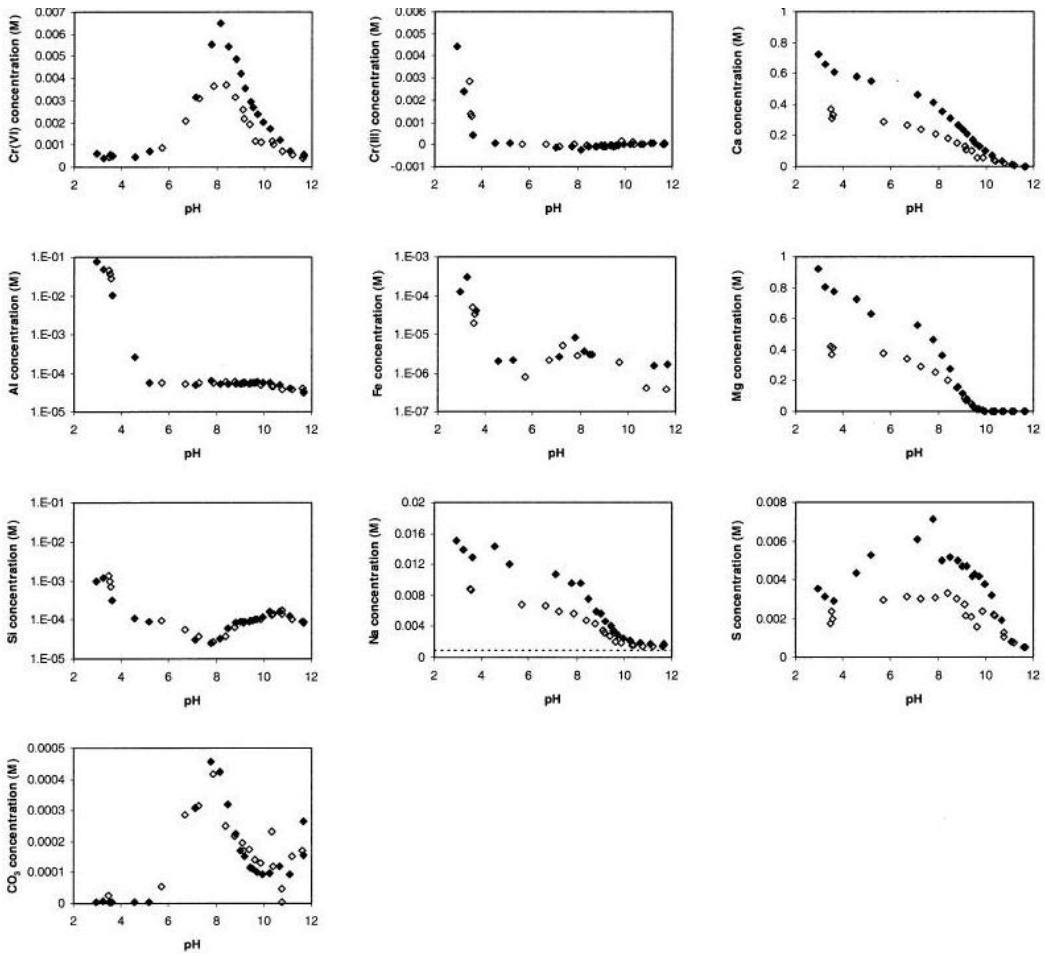

Figure 3: Concentrations of ions in solution under different pH conditions (Geelhoed, 2007)

Now that the mineral dissolution reaction constants are known, as well as the minerals found in platinum TSFs, an approximation can be made regarding the stability of these minerals under mine water redox conditions. Approximations and interpretations from Eh-pH diagrams can also be made to determine stable species and complexes under these conditions. Inferences from these stability diagrams can also be made about the precipitates that might form along the chemical evolution path of the permeating water, at different points in the TSF.

Some of the solid phases and species that are stable in platinum tailings are shown in and discussed below for each unique system.

2.2.1 Ferrous- and Ferric Hydroxides

Figure 4 indicates the stability of transitory, meta-stable iron species that may form in solution in a purely H_2O-Fe solution (Garrels and Christ, 1965). As mentioned, these species are of a transitory nature but remain stable in solution long enough to be noteworthy (Garrels and Christ, 1965). The most important species on this diagram with respect to platinum TSFs is $Fe(OH)_3$. Theoretically, if the tailings were kept at a temperature of 25° C and a pressure of 1 atmosphere from top to groundwater level, this species of iron would be found throughout the chemical stability field of the permeating fluid down to aquifer level. However, the chemistry of the tailings is not this simple and many more species are present. This diagram still gives an indication of which oxidation state of iron might be stable throughout the permeating fluid's path, *viz*. Fe^{3+} according to the inferred stability field.

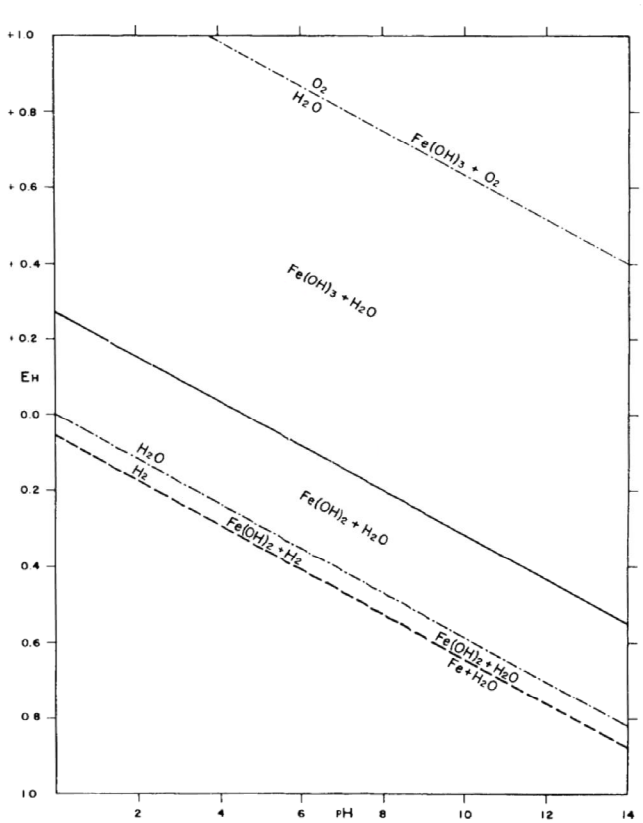

Figure 4: Eh-PH stability diagram of the Fe-O-H system 1 atmosphere total pressure and temperature of 25° C (Garrels and Christ, 1965)

2.2.2 Ferrous- and Ferric Oxides and- Sulphides

As mentioned, sulphur may be a significant component in platinum TSFs due to its presence, in varying oxidation states, in sulphide minerals which may be present in tailings. When sulphur is added to the system, iron speciation and the stability of these species and solid phases, changes somewhat from *Figure 4*. This change is evident in *Figure 5* (Garrels and Christ, 1965) where the stable form of iron occurs in the heamatite phase along with dissolved sulphate ions. This occurs under the assumption that temperature remains at 25° C and pressure at 1 atmosphere with 10^{-1} as the activity of dissolved sulphur. This phase is stable from the oxidative top of the tailings to groundwater level as indicated by the inferred stability field in red. This renders other solid phases such as pyrite, pyrrhotite and pure magnetite phases theoretically unstable anywhere in the tailings, making them prone to dissolution. *Figure 6* also illustrates this concept by indicating which solid phases of iron are present in the tailings under different Eh-pH conditions as well as which iron ion is present. Instability of the previously mentioned meta-stable solid phases may cause significant metal and sulphate contamination to groundwater. However, chemistry in the tailings is, more complex than a simple four-component system.

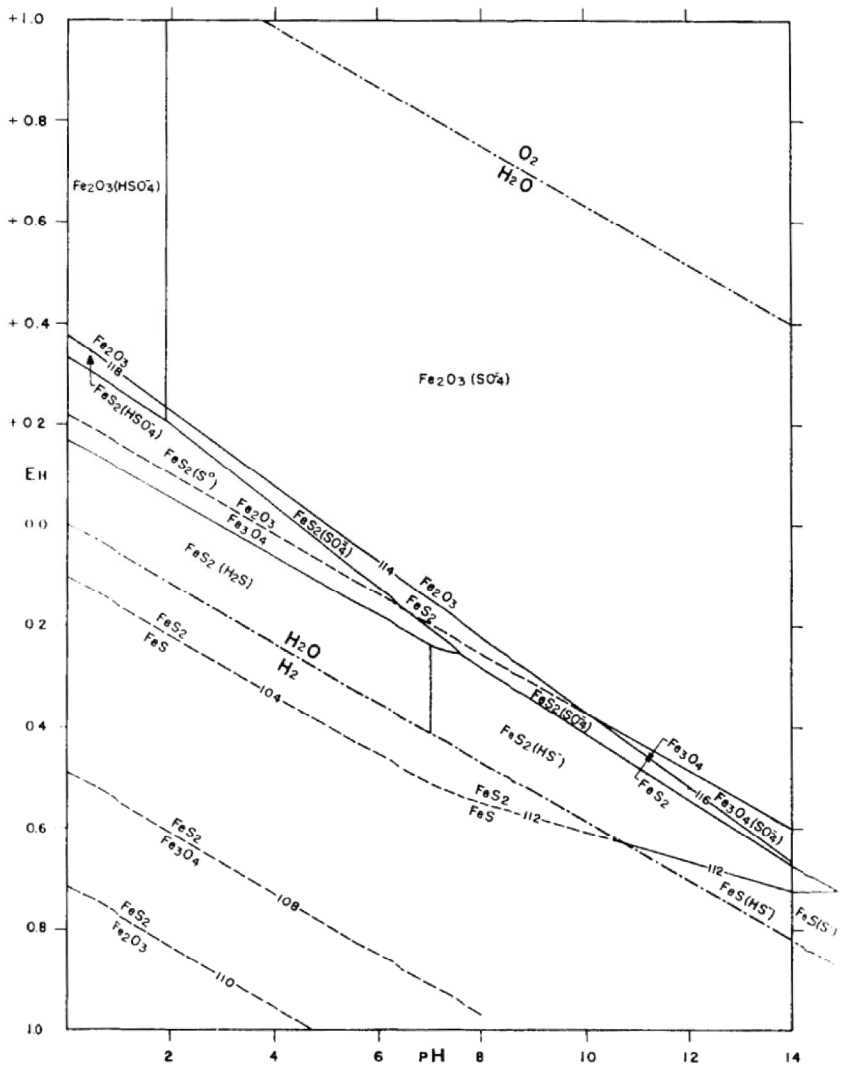

Figure 5: Eh-pH stability diagram of the Fe-S-O-H system at 1 atmosphere total pressure and temperature of 25° C (Garrels and Christ, 1965)

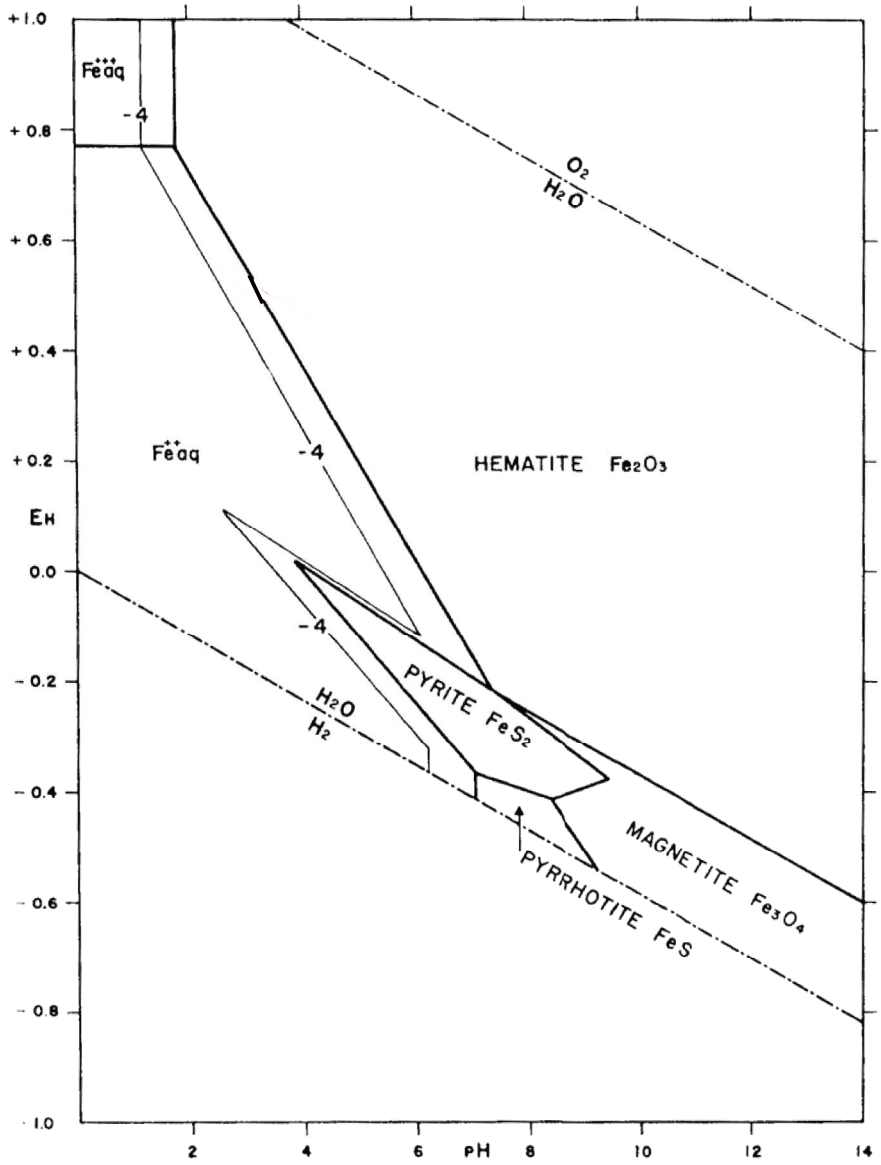

Figure 6: Eh-PH stability diagram of solid phases in the Fe-S-O-H system at 1 atmosphere total pressure and temperature of 25̊ C (Garrels and Christ, 1965)

2.2.3 Ferrous- and Ferric Oxides and – Silicates

*Figure **7*** illustrates a Fe-Si-O-H system. This diagram shows heamatite as the stable solid phase throughout the stability field of the permeating fluid from the oxidising upper zone of the TSF to groundwater level. Although Si is present in the system in the form of enstatite in this diagram, this solid phase remains unstable and will dissolve and speciate into the fluid. This in turn could also act as a control on the dissolution of other minerals (Essington, 2004). This diagram also illustrates pure magnetite as an unstable phase in tailings and at groundwater level.

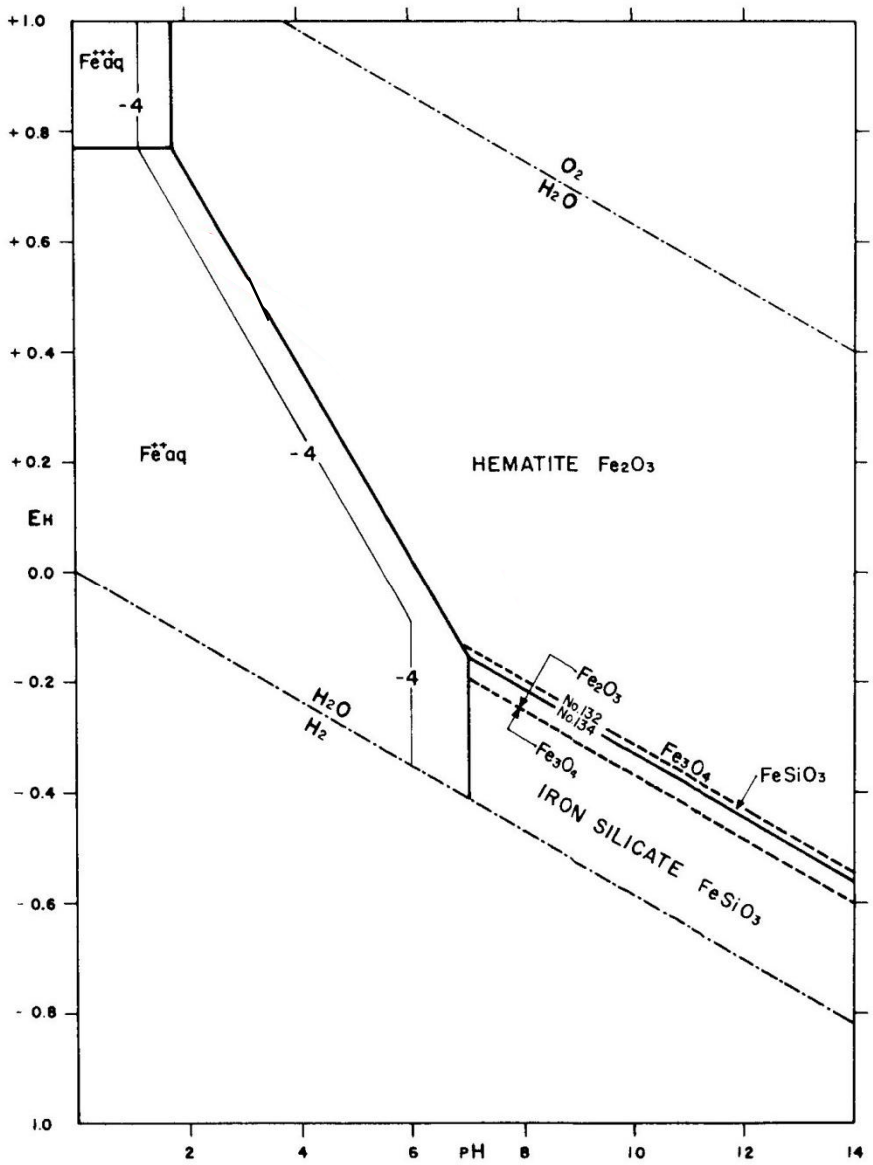

Figure 7: Eh-PH stability diagram of the Fe-Si-O-H system at 1 atmosphere total pressure and temperature of 25° C (Garrels and Christ, 1965)

2.2.4 The Cu-Fe-S-O-H system

This system is of special interest in the study of contamination from TSFs. This is because the principle contaminant and cause of acid mine drainage in tailings is conventionally accepted as sulphide minerals. *Figure 8* illustrates the thermodynamic conditions under which these minerals are stable relative to the stability field followed by permeating fluids through the tailings to groundwater level. Metals such as Fe^{2+} and Cu^{2+} are stable in solution in the upper tailings and as the solution migrates, heamatite once again becomes stable with Cu^{2+} remaining in solution as a stable species. Fe^{2+} activity therefore becomes lower while Cu^{2+} activity only lowers from 10^{-4} to 10^{-6} as the cuprite-heamatite stability field is approached. When these thermodynamic conditions are reached by the permeating fluid, cuprite and heamatite exist as distinct solid phases. These phases then destabilise to form native Cu and heamatite which evolve with the permeating fluid into solid phases of chalcocite and hematite in groundwater level thermodynamic conditions. An important point to note from this diagram is that pyrite, chalcopyrite and pyrrhotite are all unstable throughout the

fluid's redox path, when compared to Figure 1, and may destabilise to liberate Fe, Cu and different sulphur species causing contamination to groundwater.

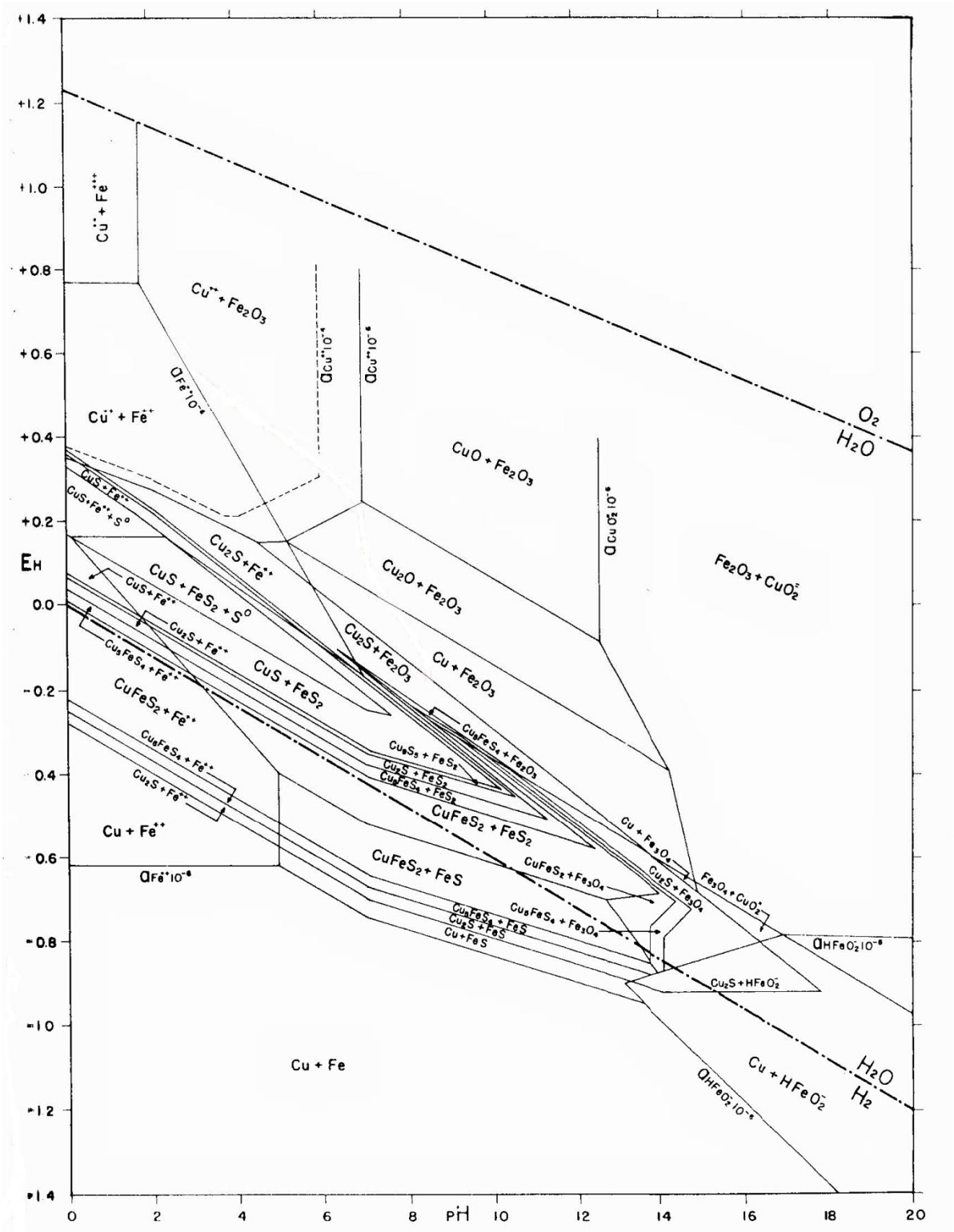

Figure 8: Eh-PH stability diagram of the Fe-Cu-S-O-H system at 1 atmosphere total pressure and temperature of 25° C (Garrels and Christ, 1965)

2.2.5 Sulphur Speciation

In *Figure 9* (Garrels and Christ, 1965), it is evident that the only stable sulphur species along the entire stability field, when compared to Figure 1, is SO_4^{2-} at an activity of 10^{-1}. Therefore other sulphur species will be significantly less abundant. The sulphur stability diagram is discussed individually for exactly this reason. SO_4^{2-} anion species are the main indicators of acid mine drainage, being the only stable form of dissolved phase sulphur in tailings and groundwater. These sulphates are free to mobilise and react with any mineral and fluid encountered along the indicated redox path, in Figure 1, and form sulphuric acid with water. Sulphuric acid is highly corrosive and is a major contaminant in surface water and groundwater. It also lowers pH significantly, accelerating the dissolution rates of the minerals present and causing unfavourable thermodynamic conditions for most solid phases, affecting their thermodynamic stability.

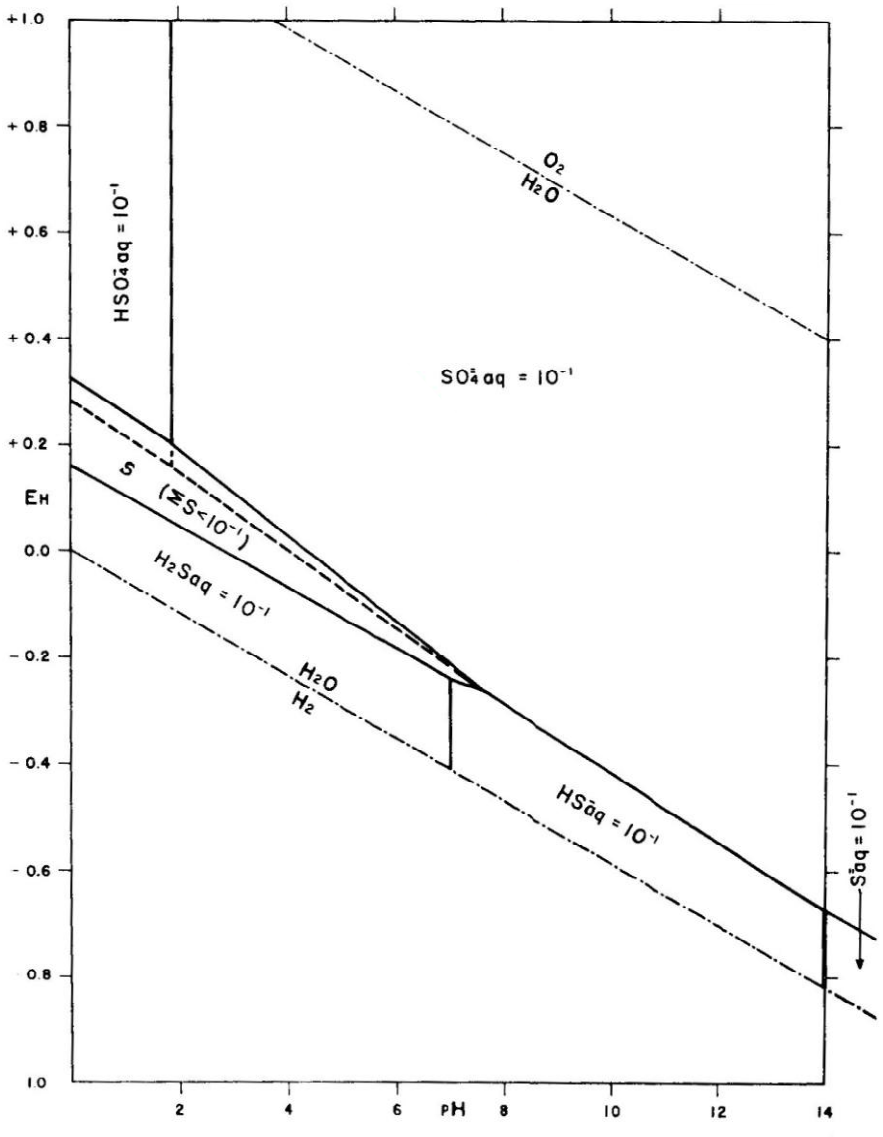

Figure 9: Eh-PH stability diagram for the S-O-H system at 1 atmosphere total pressure and temperature of 25° C (Garrels and Christ, 1965)

2.2.6 Chromite Dissolution and Chromium Speciation

As mentioned, chromite dissolves in water according to:

$$FeCr_2O_4 + 8\,H^+ = 1\,Fe^{2+} + 2\,Cr^{3+} + 4\,H_2O \qquad \textit{Equation 2}$$

This chemical reaction has a positive reaction constant which is indicative of a product favoured dissolution reaction with Fe and Cr being liberated, according to the PHREEQC databases. The ion of specific interest, liberated by this reaction is Cr^{3+}. This ion could be liberated throughout the entire stability field of acidic permeating fluids in tailings, even as an amorphous phase, as can be observed in *Figure 10*. The ion keeps its trivalent charge even in the redox conditions found in groundwater according to this figure. However, this ion might be oxidised in a higher Eh range, to its more lethal, hexavalent state (Geelhoed, 2002). Research conducted by Geelhoed (2002), indicates that high levels of Cr^{6+} may be present at a pH of 8 as indicated by *Figure 11*.

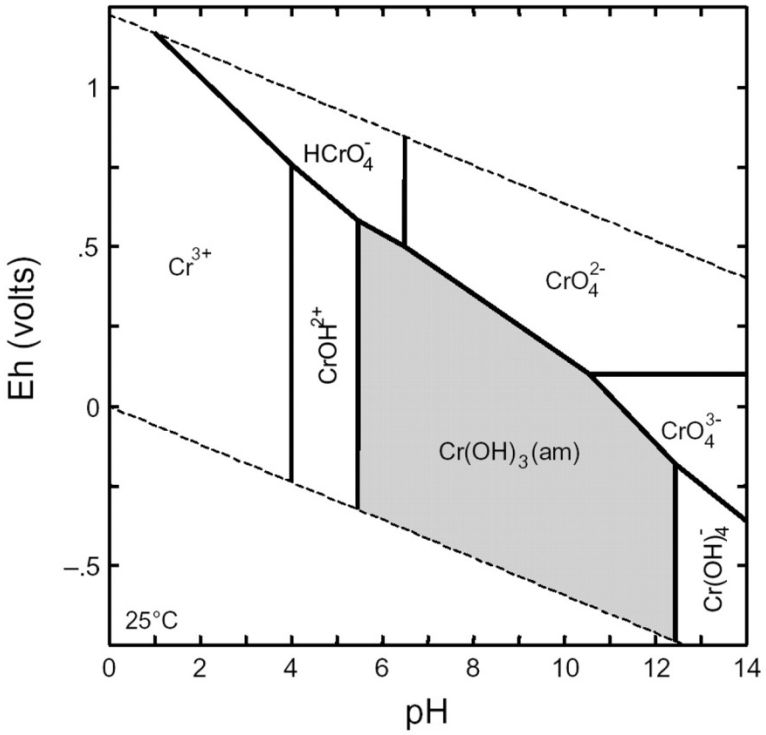

Figure 10: Eh-pH stability diagram of the Cr-O-H system at 1 atmosphere total pressure and temperature of 25° C (Indiana.edu, 2011)

Therefore, if the character of the tailings or groundwater changes to higher Eh or pH levels, or an oxidising agent such as Mn is released in significant concentrations, Cr^{6+} may become present in the system causing toxicity and environmental degradation. Eh can be considerably influenced and raised to up to +700 mV by increases in O_2 concentration (Radojevic and Bashkin, 2006). This is especially of concern in platinum TSFs as Cr is concentrated in this setting whereas its occurrence in natural systems is of trace abundance (Kotas and Stasicka, 1999).

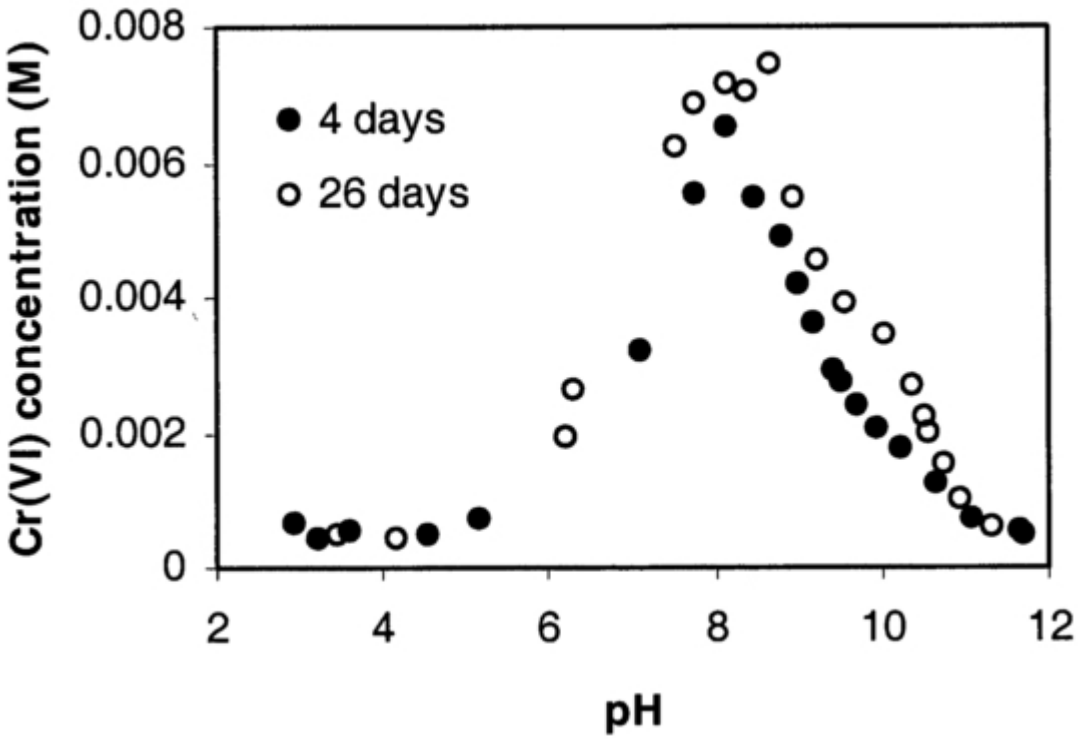

Figure 11: Scatter plot indicating Cr^{6+} concentration against pH value (Geelhoed,2002)

2.2.7 Silicate Weathering

Perhaps one of the major overlooked contaminators in platinum TSFs is the mafic silicate minerals. These minerals are abundant in the major platinum producing lithologies in South Africa, located in the Bushveld Igneous Complex (Vermaak and Hendriks, 1976). Silicate minerals such as olivine, pyroxene and calcic plagioclase species are found in many Bushveld tailings and contain cations such as Mg, Fe, Ca, K, Na and Cr. These ions may also be substituted in solid solutions by heavier metals such as Zn, Mn, Ti, Ni and others (Klein & Dutrow, 2008).

According to Wilson (2004) weathering of the primary silicate minerals is related to the inherent susceptibility of the mineral to weathering, which is in turn related to chemical composition, crystal structure and the distribution of defects. These defects may include dislocations and exsolutions which may contribute to the controls on the weathering reactions. All these defects are increased during the crushing and milling process. However, thermodynamic formation conditions may also play a role in mineral breakdown as phases formed at high pressures and high temperatures are more meta-stable at earth surface conditions. A lower energy state may subsequently be obtained from mineral breakdown in accordance with Ostwald's Step Rule (Bethke, 2011). This indicates that silicate phases in the Bushveld lithologies would be more prone to weathering than those found in felsic intrusions. This idea is supported by Wilson (2004) by indicating that the primary weathering sequence follows the reverse of the magmatic crystallisation series as proposed by Bowen (1928).

Most silicate minerals show an amphoteric dissolution curve when dissolution rates are plotted against pH as illustrated by Yadav and Chakrapani (2006). This indicates that higher dissolution rates are induced by high and low pH values respectively. Acid- or alkaline drainage is a common problem associated with mining activity and therefore may increase the concentrations of liberated cations from silicate minerals.

Platinum tailings material contains both mafic mineral phases and produce acid- or alkaline drainage. Therefore, increased cation release can be expected from the material. However, these cations may also act as buffers in solution, forming stable complexes with anions such as SO_4 which may inhibit acid formation (Essington, 2004). Complexes may also be adsorbed to secondary mineral surfaces, inhibiting rapid contaminant release.

2.3 Transport mechanisms

Contaminant transport following mineral dissolution, in natural systems as well as tailings material, occurs by diffusion, dispersion and advection. Each of these processes plays a governing role in the amount of contamination that may reach an aquifer.

2.3.1 Molecular Diffusion

The first and most important step in the determination of molecular diffusion close to dissolving mineral surfaces, is to calculate the ionic strength of the solution in which the mineral or aggregate is immersed (Essington, 2004). This will be discussed in more detail later in this section. Ionic strength is calculated using the equation below.

$$\boldsymbol{I = \frac{1}{2}\sum C_i.\left(Z_i^2\right)} \qquad \textit{Equation 3}$$

Where:

I = Ionic strength of the solution which is defined by Essington as the amount of charges in solution

C_i = The concentration of the ion in solution (M)

Z_i = The charge of the ion.

The I-value obtained from this equation, is used to calculate an activity coefficient for the ion in question. This can be calculated by using the Debyë-Hückell equation, Extended Debyë-Hückell equation or the Davies equation. The Davies equation is the most robust of these three equations as it can be used for solutions with ionic strengths of 0 to 0.5. Therefore the Davies equation, given by the equation below, is most often used in these types of calculations.

$$\boldsymbol{log\gamma_i = -\left[AZ_i^2\left(\frac{I^{\frac{1}{2}}}{1+I^{\frac{1}{2}}} - 0.3I\right)\right]} \qquad \textit{Equation 4}$$

Where:

γ = The activity coefficient of the ion in question

i = The ion in question

A = An equation constant of 0.5

Z = The charge of the ion in question

I = The ionic strength of the solution.

The γ_i value calculated from the Davies equation is then used to calculate the activity of the free, unspeciated ion in solution by multiplying the concentration of the ion with its activity coefficient.

The diffusion of an ion into solution close to a dissolving mineral surface can now be calculated using Fick's first law. This law states that a substance put into solution will tend to diffuse towards

constant concentration throughout the solution (Mondofacto, 1997) The equation for this calculation is given below, as defined by the University of Arizona's website (2007).

$$\boldsymbol{J} = -\boldsymbol{D}.\left(\frac{\Delta \boldsymbol{C}}{\Delta \boldsymbol{x}}\right) \qquad \textit{Equation 5}$$

Where:

J = The mass flux i.e. the movement of matter from one point to another per time unit

D = The diffusivity of a material. A constant that describes the material's diffusion speed

ΔC = The change in concentration of the ion in question

Δx = The change in distance that the material is diffusing.

An understanding of how an element diffuses from a dissolving mineral surface can now be obtained from Fick's law. This may influence dissolution kinetics and subsequently reaction kinetics and becomes another controlling factor, apart from thermodynamic conditions, on the amount of contaminant liberated and reaching groundwater from tailings material. Modern geochemical modelling software does not account for this mechanism and assumes instantaneous diffusion rather than a gradual process. However, diffusion may be such a negligible transport mechanism in moving fluids that other transport mechanisms may override it completely.

Diffusion will take place where a mineral is dissolving and subsequently reacting with a permeating fluid. The area where this is most likely to occur is the oxidising upper area of the TSF where metals and other contaminants are readily liberated. As the dissolved ion diffuses to lower parts of saturated tailings material, an inhibiting factor may come into play *viz*. adsorption. Mineral edges and surfaces may be altered, partially inducing a temporary or permanent negative charge. This causes diffusing ions in solution to be adsorbed onto mineral surfaces, lowering the activity of the specific ion in solution. This may, along with mineral precipitation, reduce contaminants reaching the underlying aquifer of the TSF.

2.3.2 Mechanical Dispersion

Mechanical dispersion of a solute in a fluid can be described as the pathway it follows through a matrix as illustrated in *Figure 12*. However, dispersion can be influenced by adsorption, diffusion speed, matrix type, fluid behaviour and other parameters. According to Kalmaz and Barbieri (1980), parameters controlling dispersion can be grouped into three categories:

- Media dependent such as intrinsic permeability
- Substance dependant such as decay constant
- Substance-environment dependence such as distribution coefficients in numerical models.

The most important parameters controlling dispersion in porous media are also paraphrased from Kalmaz and Barbieri (1980) as:

- Dispersion coefficient- a function of velocity and dispersivity
- Pore Velocity- a function of hydraulic gradient, permeability, effective porosity
- Equilibrium constant- a function of distribution coefficient, unit weight and porosity of the porous media
- Decay constant.

Therefore, when taking all these parameters into account, it can be concluded that the dispersion of solutes through the tailings material as well as aquifer media, is a physical process depending strongly on the properties of the media as well as the chemical characteristics of the solute.

However, lateral dispersion in the tailings material is minimal as fluids principally permeate due to gravity and the general movement vector is therefore vertical to sub-vertical. Lateral dispersion is therefore kept to a minimum in the tailings material. However, mechanical dispersion at aquifer level may cause pluming of dissolved contaminants as their movement occurs under the influence of hydraulic head and lateral- and vertical dispersion may now also take place.

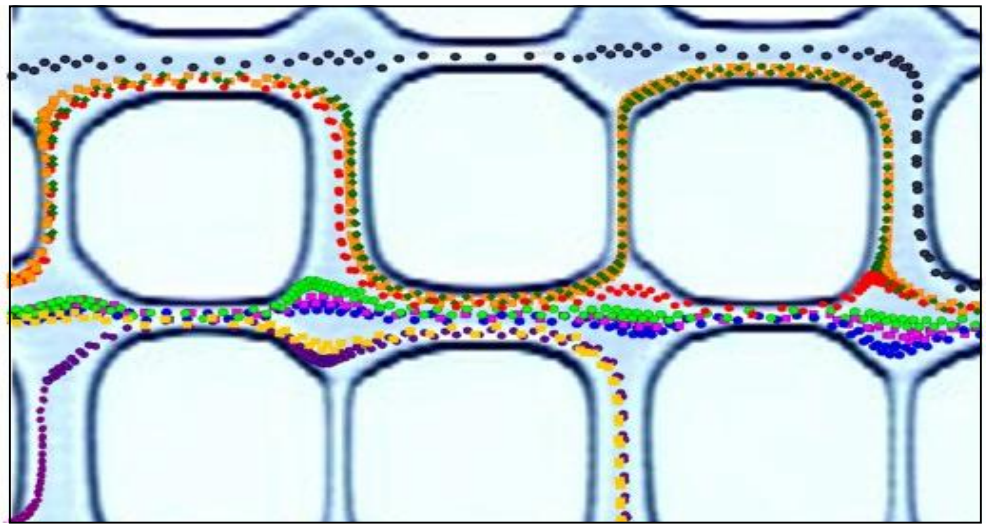

Figure 12: Schematic representation of mechanical contaminant dispersion through a matrix (Keller, 2004)

2.3.3 Hydrodynamic Dispersion

Bear and Bachmat (1967) defined hydrodynamic dispersion as a soluble substance, called a tracer, in a fluid flowing through a porous medium which spreads out, increasingly occupying a portion of the flow domain. Hydrodynamic dispersion is a function of three macroscopic transport parameters. These parameters are the permeability of a porous medium; the coefficient of mechanical dispersion of that medium; and the coefficient of molecular diffusion of that medium. Each of these parameters measures a different characteristic of the flow through the porous medium. Permeability measures the medium's ability to convey fluid movement; the coefficient of mechanical dispersion measures the temporal spreading of a solute in space; and the coefficient of molecular diffusion measures the spreading of a solute in a fluid when the fluid is stagnant (Bear and Bachmat, 1967). Therefore, hydrodynamic dispersion is a combination of mechanical and molecular spreading of a solute in a solvent during flow which is defined by a combination of diffusion and dispersion. This is of special concern at tailings level as fluid movement through the material is slow (Craig, 2004) and advection is unlikely to take place through preferred pathways as the media may be homogeneous and isotropic.

2.3.4 Advection

Advection is the transport of solutes via groundwater below the phreatic surface, under a hydraulic gradient, as illustrated by *Figure 13*. For a contaminant to rapidly progress away from its source, advection via groundwater along with dispersion is required.

This can only take place if groundwater is moving under a hydraulic gradient (Verral *et al*., 2008). If a positive hydraulic gradient is present, advection will take place in the flow direction of the hydraulic gradient and is of special concern below the tailings, as contaminants may reach a receptor much more rapidly due to elevated flow velocities relative to that of fluids at tailings level. However, advection, like dispersion, also depends on physical properties of the aquifer, as well as chemical properties of the contaminant.

Contaminants, such as metals, produced from tailings material will move via groundwater, if reached, in the form of advection. A smaller amount of dispersion may take place, depending on the aquifer properties, and even less diffusion depending on the contamination state of the water and the adsorptive properties of the aquifer material. Therefore, aquifers underlying TSFs, with a high hydraulic gradient, intrinsic permeability and porosity should be monitored much more closely for contaminant advection.

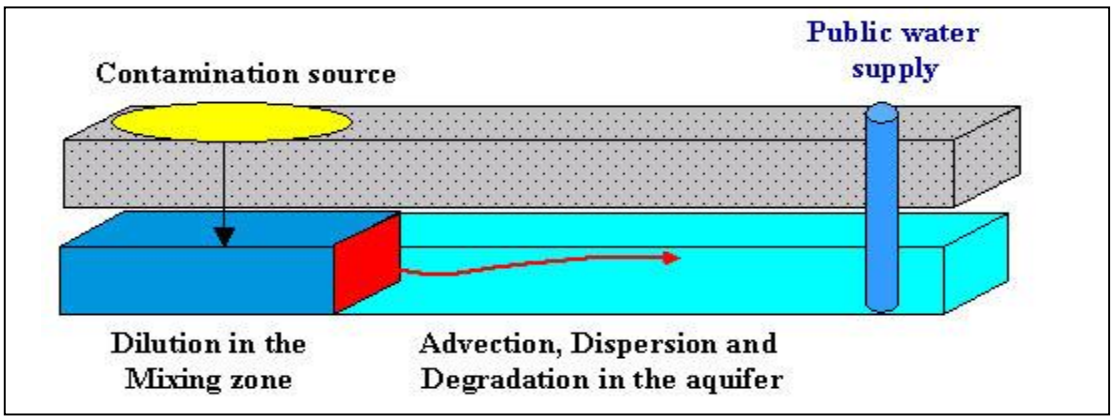

Figure 13: Conceptual model indicating contaminant transport by advection (Strassberg et al. 2011).

2.4 Analysis methods

To correctly characterise tailings material and the contaminants released from TSFs, different methods should be employed. Each method yields information about the tailings material's mineralogical and subsequent chemical composition; the leaching potential of the tailings material; the physical and hydraulic characteristics of the tailings material and underlying rock mass; the chemical composition of permeating fluids; the chemical composition of groundwater; and the potential contaminants present in or being liberated from the tailings material.

2.4.1 X-Ray Fluorescence Spectroscopy and X-Ray Diffraction

X-Ray Fluorescence Spectroscopy (XRF) is used to determine the chemical composition of the tailings material in terms of oxides. Each oxide then represents a weight percentage of the sample being

analysed. From this analysis, it can be determined which contaminants are possibly concentrated in the tailings material as metals or other contaminants.

X-Ray Diffraction (XRD) on the other hand gives the composition of the tailings material sample in terms of the minerals present. This data can then be used in conjunction with thermodynamic data on the phases present to determine the possible dissolution of minerals, reaction kinetics, dissolution rates and mineral stability under a given set of conditions. It is important to note that XRD can only report the crystalline phases present above an abundance of 1 weight%.

2.4.2 Reflected Light Microscopy

Reflected light microscopy may be used to determine the presence of sulphide and oxide minerals in rock material. These minerals appear opaque in direct light microscopy which is performed by transmitting light through a thin section of rock. Reflected light microscopy is performed using mounted, polished sections, from which light is reflected, projecting an image of the opaque minerals such as sulphides and oxides, through the microscope oculars. By utilising direct observation and the optical properties of the minerals present, the relative amounts and compositions of these minerals can be determined and noted. This information is useful in determining the amount of contamination that may be released from these minerals, especially with respect to sulphides.

2.4.3 Acid-Base Accounting and Net Acid Generation

Acid-Base Accounting (ABA) is a static test which assesses the potential of a rock to produce or neutralise acid. This test is used as a first approximation of the acidity or alkalinity of leachate produced by the rock in the presence fluids. Components analysed in an ABA test are as follows:

- Acid Generating Potential (AGP) – this test determines the amount of acid that could potentially be generated by the rock material.
- Acid Neutralisation Potential (ANP) – this test determines the amount of acid that could potentially be consumed by the rock material. ANP is also expressed as kg of $CaCO_3$ per ton of rock to represent the amount of theoretical $CaCO_3$ available in the rock material, to neutralise acid.
- Net Acid Generation (NAG) Potential - This value is obtained by subtracting the ANP from the AGP. A positive value indicates potentially acid forming rock whereas a negative value indicates potentially non-acid forming rock. Vice versa to this is the Net Neutralising Potential (NNP) of the rock.

The potential of the rock to generate acid is classified according to a screening method utilising the NNP, percentage S as sulphide and the ANP:AGP ratio as follows:

- Rock material with an NNP less than zero kg $CaCO_3$ per ton will theoretically have a nett potential to produce acidic leachate. Rock material with an NNP higher than zero kg $CaCO_3$ per ton will theoretically have a net potential to neutralise acidic leachate. However, research shows that -20 kg $CaCO_3$ per ton to 20 kg $CaCO_3$ per ton is defined as an area of uncertainty in determining net acid generation or neutralisation potential. Therefore, rock material with an NNP above this value is considered to reduce acid. Rock material with an NNP below this range is considered to be likely to reduce acid.

- The ANP:AGP ratio can also be used to classify rock material as acid generating or –reducing with the method described by Price (1997) in *Table 2*.

Table 2: Screening method for classifying the acid generation potential of rock material (Price, 1997).

Potential for Acid Generation	NP:AP screening criteria	Comments
Rock Type I. Likely Acid Generating.	< 1:1	Likely acid generating.
Rock Type II. Possibly Acid Generating.	1:1 – 2:1	Possibly acid generating if ANP is insufficiently reactive or is depleted at a faster rate than sulphides.
Rock Type III. Low Potential for Acid Generation.	2:1 – 4:1	Not potentially acid generating unless significant preferential exposure of sulphides along fracture planes, or extremely reactive sulphides in combination with insufficient reactive ANP.
Rock Type IV. No Potential for Acid Generation.	>4:1	No further acid testing required unless materials are to be used as a source of alkalinity.

2.4.4 Inductively Coupled Plasma Analyses

Inductively coupled plasma optical emission spectrometry (ICP-OES) and -mass spectroscopy (ICP-MS) are used for analysing water samples for heavy metal and trace element concentrations, respectively. These analyses may be used to obtain concentrations of contaminants produced in acid leach tests as well as contaminants present in groundwater samples obtained from field work conducted around TSFs. Therefore the concentrations and subsequent activities of contaminants liberated from tailings material become evident and may be used in calculations pertaining to their transport and attenuation.

2.4.5 Permeameter Tests

Permeameter tests provide hydraulic conductivities and intrinsic permeabilities of the tailings material. This is a critical factor in determining flow velocities of contaminants produced by TSFs and how rapidly these contaminants may reach natural systems. Permeameter tests may be of falling- or constant head nature. The tests are performed by percolating a fluid, normally water, through a column of material and measuring the loss of head per unit time in falling head tests. In constant head tests, the amount of fluid added continuously to maintain a constant head per unit time is measured. However, for very fine, silt-sized particles such as tailings material, a falling head permeameter test is preferred (Craig, 2004).

2.4.6 Pumping Tests

Pumping tests are performed to estimate the hydraulic properties of an aquifer such as hydraulic conductivity, transmissivity and storativity. This is done by pumping a well that has been developed in the aquifer, which causes a subsequent stress by changing the hydraulic head in the said well.

This hydraulic head is measured by means of a dipmeter or data logger from the top of the well casing while pumping the well. This, subsequently, also gives the change in head over time which is

termed the drawdown and is illustrated in *Figure 14* (Weight, 2008). A pumping test therefore has three phases, *viz*. planning, which includes a desk study and gathering of information with regards to previous test work, geology, pumping rates and any other information; data acquisition, which includes the actual pumping of the well and field measurements of waterlevels as mentioned; and data analysis, which entails the interpretation of the acquired data by using different analytical methods such as that of Theis (SANS, 2003).

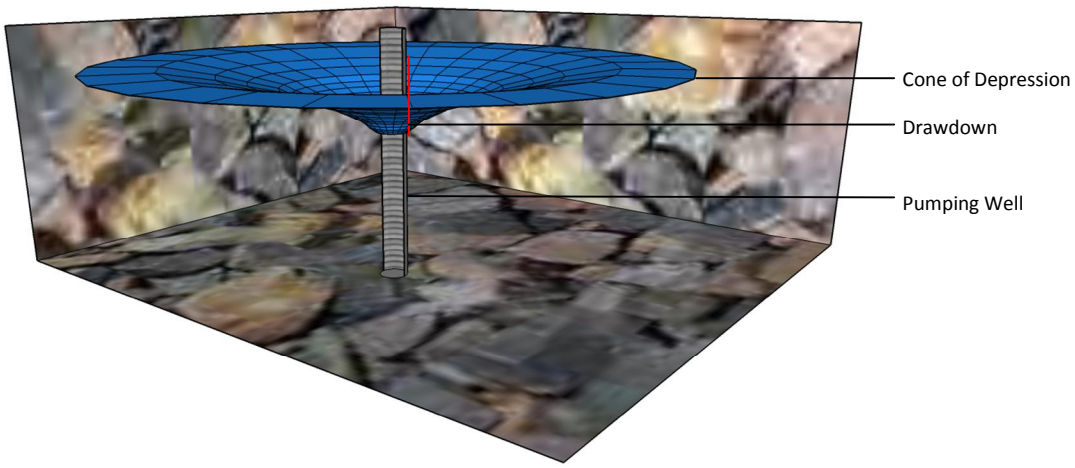

Figure 14: Schematic representation of a cone of depression and subsequent drawdown caused by a pumped well.

Different types of pumping tests exist *viz.* step-drawdown tests, which measure the performance of a well; and constant discharge tests, which measure the hydraulic properties of the aquifer (SANS, 2003). However, only constant discharge tests will be addressed in this study as the well tested is intended as a monitoring well and will be used to determine the hydraulic properties of the aquifer as well as boundary conditions to groundwater flow. These tests, performed over extended periods, yield information about the hydraulic conductivity and transmissivity of the aquifer by extending the cone of depression much further, which gives a long term estimate of the flow through the lithological unit/s (Dippenaar, 2008).

Interpretation of the acquired data can be done using several different methods. The earliest of these being developed by Theis in the 1930's (Weight, 2008). However, these methods must be applied with caution *viz.* the Theis method assumes the following as paraphrased from Weight (2008):

- No edge effects (aquifer is of infinite areal extent)
- Uniform thickness (pumping well fully penetrates and receives water from the full thickness of the aquifer)
- Constant heat source (constant pumping rate)
- Homogeneous and isotropic (aquifer is uniform in character and the hydraulic conductivity is the same in all directions)
- No sources or sinks (water is discharged instantaneously from storage and not from external sources by either adding or removing water).

Additional assumptions inherent to the Theis equations are:

- Pumping well is 100% efficient
- Laminar (Darcian) flow prevails throughout the well and aquifer.

These assumptions are almost never true in reality due to the complexity of geological features in nature with influences from rivers, streams, confining layers, discontinuities, fault- and shear zones, dykes, constructed barriers and the like (Weight, 2008).

These assumptions are used, almost universally, for different pumping test data analysis methods. However, these methods do provide an estimate of the hydraulic properties of an aquifer.

For fractured rock aquifers, such as the one that will be investigated in this study, a useful method is that of Moench developed and published in 1984. Moench developed a method which extends the normal transient block-to-fracture flow double porosity model by adding a fracture skin effect attributed to mineralisation in the said fracture. Moench (1984) found that if this mineralised fracture skin is of sufficient thickness, the flow from blocks to fractures becomes a pseudo steady-state process regulated by the hydraulic conductivity of the fracture skin and the applicability of the pseudo steady- state double porosity model becomes more plausible. An important finding by Moench (1984) is that at early time on a semi-logarithmic, time-drawdown plot, the early time curve indicates well bore storage with the flatter middle time section indicating fracture dewatering and a sharper gradient late time curve indicating matrix block dewatering. Van Tonder *et al*. (2002) found that changes in the slope of the semi-logarithmic curve might also indicate no-flow boundaries present by doubling (single no-flow boundary) or quadrupling (double no-flow boundary) of the slope.

3. STUDY AREA

The Tailings Storage Facility investigated in this study is located in the north of Mpumalanga Province, South Africa, on the Rustenburg Layered Suite of the Bushveld Igneous Complex, as illustrated in *Figure 15*.

The TSF is located at an undisclosed mine on the eastern limb of the BIC between Steelpoort and Mashishing (Lydenburg) in Mpumalanga.

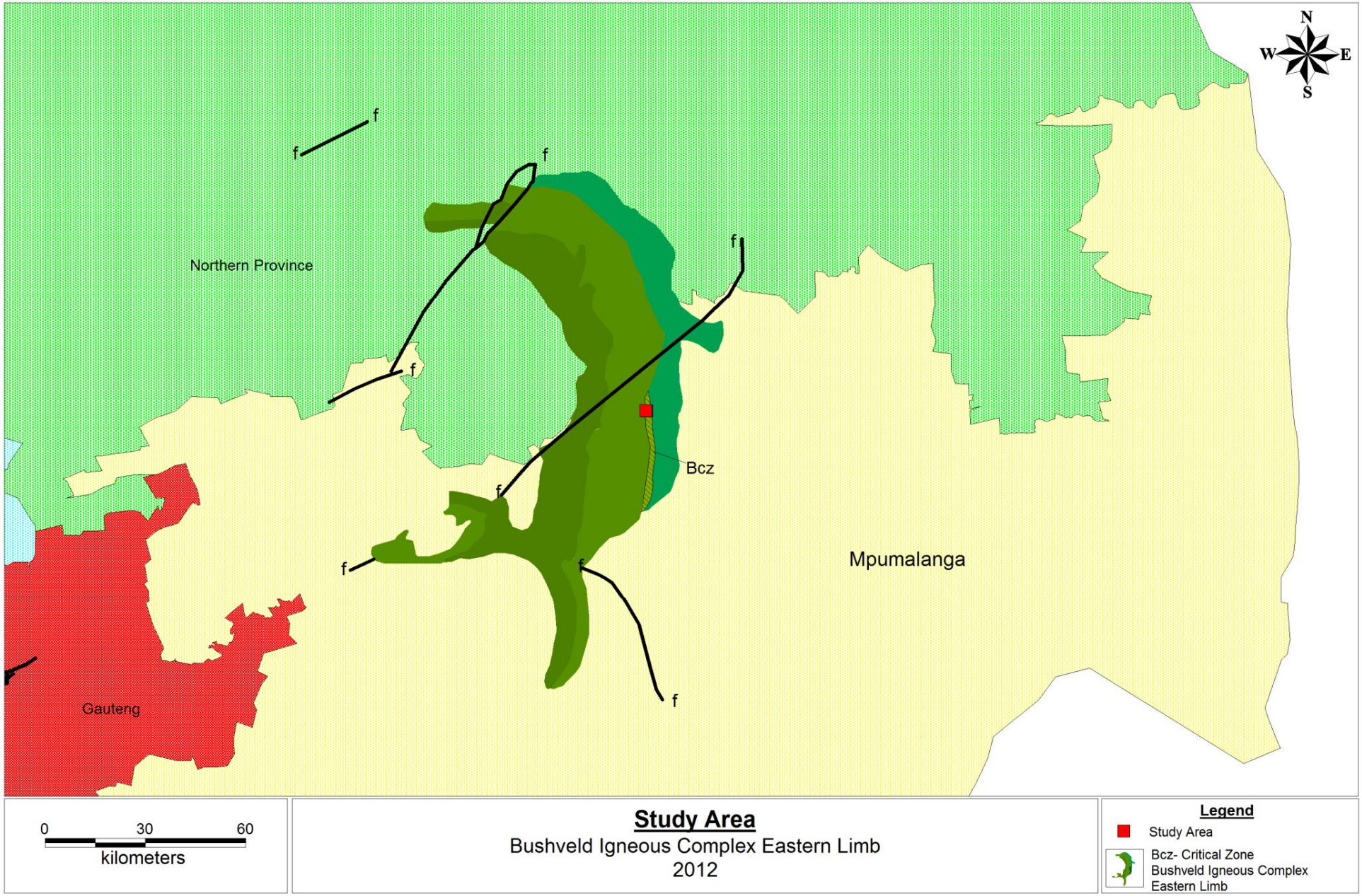

Figure 15: Study area located on critical zone lithologies of the eastern limb of the Bushveld Igneous Complex

3.1 Tailings Storage Facility

The Tailings Storage Facility under investigation is located in the north of Mpumalanga Province. UG2 and Merensky Reef lithologies from the eastern limb of the Bushveld Igneous Complex are generally mined in this area. The material present in the TSF is graded at -86 µm and is of a mafic to ultramafic nature. Therefore, metal content is high, specifically Fe and Mg, with salts precipitating on surface due to chemical reactions with acidic permeating fluids. This can be observed in *Figure 15*.

The mine where the investigated TSF is situated commenced full operation in 2008, three years from the initiation of the project phase. Currently, only the UG2 reef is being mined, producing the mafic minerals in the TSF. The Tailings Storage Facility is divided into 3 terraces. Sampling positions TAH01 and TAH03 are in the upper and lower terraces respectively, representing the second oldest and oldest cycles of tailings disposal. To ensure structural stability of the upper terrace, a second terrace was created in which sampling position TAH02 is situated, which represents the youngest cycle of tailings disposal. The TPH samples were collected from the upper terrace. It is assumed that all precious metals are removed from the processed ore.

3.2 Climate

As paraphrased from Stimmie *et al*. (2001), rainfall in the Steelpoort basin and subsequently in the Steelpoort area occurs predominantly in the summer months between October and March. January generally has the highest amount of rainfall. Average annual rainfall in the area is between 630 mm and 1000 mm, which is generally superseded by evapotranspiration figures. Thunderstorms are common in the Steelpoort basin with a low infiltration rate of soil in mountainous areas.

Rainfall data obtained from the South African Weather Service representing rainfall from the last decade partially supports these figures with annual rainfall reaching 643.2 mm and 663.6 mm in 2001 and 2010 respectively. This is illustrated by *Figure 17* and also supports the findings of Stimmie *et al*. (2001), indicating that rainfall predominantly occurs between October and April.

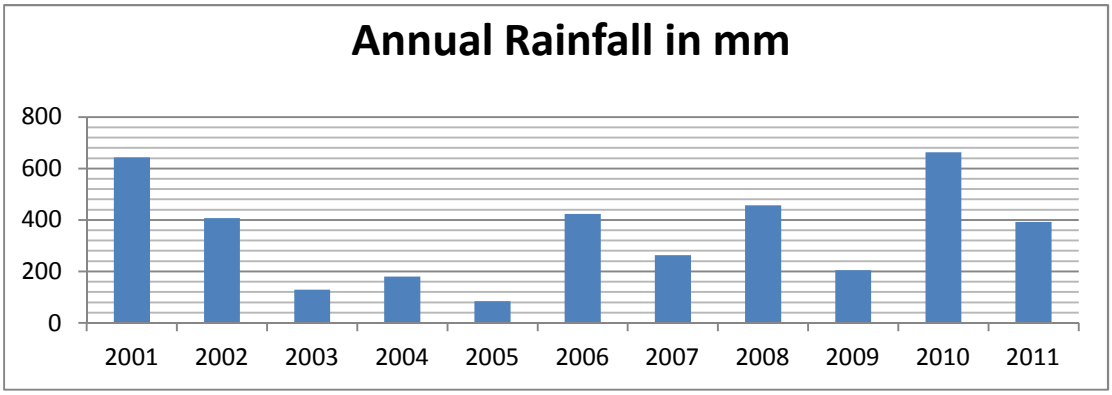

Figure 16: Annual rainfall in mm from 2001 to 2011, in the Steelpoort catchment, as measured by the SAWS weather station near Lydenburg

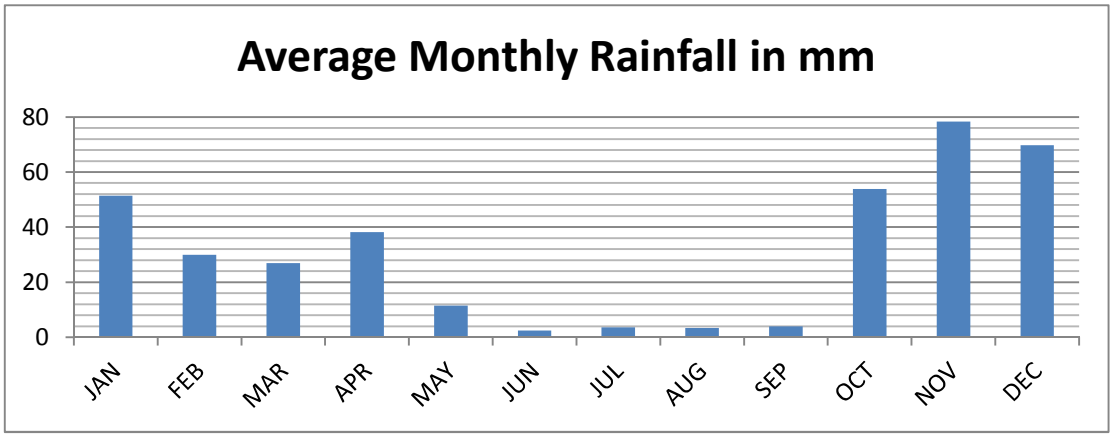

Figure 17: Average monthly rainfall in mm from 2001 to 2011 in the Steelpoort catchment, as measured by the SAWS weather station near Lydenburg

Stimmie et al. (2001) also found that average annual temperatures show little fluctuation. Temperatures range from 19°C to 22°C in summer while temperatures in winter range between 13°C and 19°C. Evaporation rates are also up to 80% higher in summer than in winter.

3.3 Regional Hydrology

As seen in *Figure 18* the topography around the mining area is mountainous with abundant valleys and regional surface flow following the topography towards the northeast via the Steelpoort river. The TSF is bound to by steep topography to the east and west with possible high runoff occurring during precipitation events. The Steelpoort river is the closest perennial surface water body to the tailings.

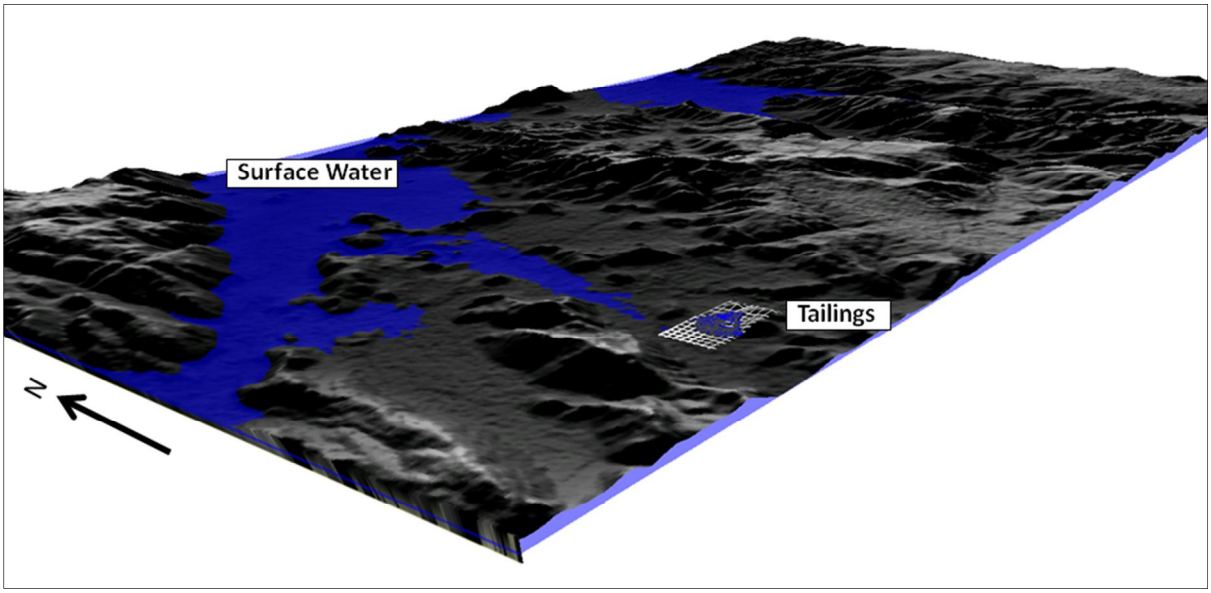

Figure 18: Simulated flooding indicating surface drainage to the northeast

Based on the data sourced from DWAF's GRDM3 database, the tailings facility falls within the B41G quaternary catchment within the Olifants Water Management Area. The catchments eco status category can be classified as A which is pristine. A summary of the relevant GRDM data is shown in *Table 3*.

Table 3: GRDM Data

GRDM Data	
Quaternary Catchment	B41G
Area	442.1 km^2
Mean Annual Precipitation	650mm/a
Mean Annual Run-Off	66mm/a
Base Flow	17mm/a
Population	0 Count
General Authorisation	0m^3/ha/a
Present Eco Status	A
Recharge	45.91mm/a
Current Usage	1.66m^3/a
Exploitation Potential	3 m^3/a
Average Depth to Groundwater	17.7mbgl

3.4 Regional Geology

The TSF under investigation is located on Critical Zone lithologies of the Bushveld Igneous Complex. According to Cawthorn et al. (2006), the Critical Zone consists of layered chromitite, pyroxenite, norite and anorthosite on scales of millimetres to tens of meters. The Critical Zone consists of 3 sub-zones as discussed below, from lower to upper:

3.4.1 Lower Critical Zone

The Lower Critical Zone consists of an 800 m thick sequence of pyroxenite cumulates with chromite disseminated throughout, almost ambiguously (Cawthorn et al., 2006). This sequence also contains an olivine interval as well as seven, distinct chromite seems of varying thickness.

3.4.2 Middle Critical Zone

The Middle Critical Zone marks the boundary between the Upper Critical Zone and Lower Critical Zone in the form of the MG2 chromitite layer where noritic-anorthositic cumulates first occur.

The base of this zone is marked by harzburgite- pyroxenite assemblages, while the upper part represents a different magmatic cyclic unit and includes anorthosite, subsequently changing the lithology (McCandless *et al*., 1999).

3.4.3 Upper Critical Zone

The Upper Critical Zone marks the transition to the famous Merensky Reef in the Main Zone of the Bushveld Igneous Complex. Here, cumulus anorthite is abundantly present along with the UG1 and UG2, as well as UG3 in the case of the eastern limb chromitite seams (Cawthorn *et al*., 2006).

3.4.4 Geological Structures

The TSF under investigation is bounded by the Dwarsriver- and Steelpoort thrust faults to the west and east respectively (South African Geological Map Series, 1986). The Dwarsriver fault is illustrated in *Figure 15* to the north of the study area. The Steelpoort fault, south-east of the study area, was probably active from Transvaal (2060 Ma) to post-Bushveld (2050 Ma) times (Hartzer, 1995). This fault is characterised by medium to high grade metamorphic assemblages, specifically andalusite and cordierite, indicating its compressive, thrust nature, as well as medium to high emplacement temperatures of the Lebowa Granite Suite (Hartzer, 1995). These faults are also preferred pathways for groundwater movement as the aquifer underlying the TSF is of secondary, fractured porosity. Therefore any contamination reaching the aquifer will potentially move by advection, along these secondary structures.

3.5 Conceptual Model

Based on the literature review performed and data obtained from the mine, a conceptual site model was developed to provide a conceptual understanding of the hydrogeological, geochemical and geological characteristics of the tailings-aquifer system (*Figure 19*).

The deposition of the tailings takes place using a jet method where finer tailings are deposited in the tailings dam with coarser tailings being deposited on the bank where the jet is located. Utilising this method, tailings banks are gradually generated over time from the coarser material. This method was used to generate three consecutive tailings terraces for stability of the pile. Keeping this in mind, sampling of the material was equally spaced between the three terraces to intercept the finer material. Samples of the coarser material were collected across the entire profile of the highest tailings bank to obtain representative samples of the entire tailings profile to soil level. This would also give a good indication of the moisture content distribution in the tailings to obtain data for the flow gradient and phreatic surface in the tailings.

Data on the groundwater monitoring system implemented by the mine was also provided. From this data, a generalised hydrogeological profile could be developed and was classified into two aquifer systems *viz.* a shallow, weathered aquifer system and a deeper, fractured rock aquifer system. The data also provided water levels in the monitoring boreholes, which were generally measured at depths within the weathered aquifer.

From the geological maps, it was evident that the Dwarsriver fault was present in a northeast-southwest orientation adjacent to the tailings and was therefore included as an important part of the conceptual model. The geological map also indicated the presence of alluvial sediments adjacent to the Steelpoort river and this was noted as a possible third aquifer system, but less relevant to the study in terms of the localised flow under the tailings facility.

The development of the conceptual model provided a clear conceptual understanding of possible redox conditions and flow directions in the system and aided in the planning of sample and data collection for the development of the geochemical and unsaturated flow models.

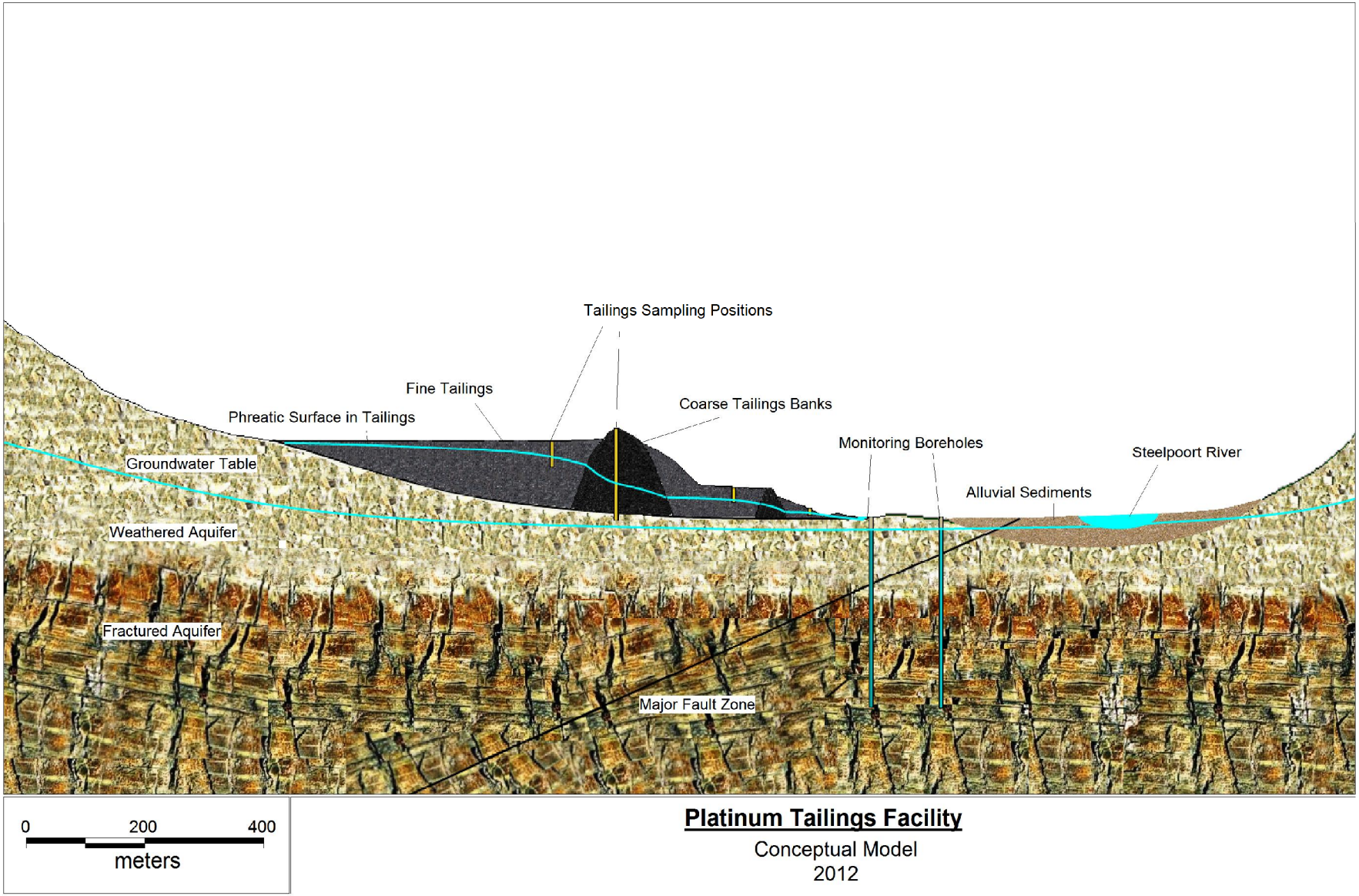

Figure 19: Conceptual Model of the Platinum Tailings Storage Facility

4. DATA ACQUISITION

Samples were collected from the Tailings Storage Facility on 7 and 8 July 2011 as well as 20 February 2012. The tailings material was subsequently analysed to provide an understanding of the chemical composition and -behaviour in order to model the liberation of potential contaminants. The material, as well as the underlying aquifer, was also hydraulically tested to provide an understanding of the hydraulic properties to obtain flow and contaminant transport properties. This was also helpful in determining hydraulic boundary conditions.

4.1 Sampling Methods

4.1.1 Hand Auger Drilling

Hand auger drilling was employed to sample the tailings material in 2011. This method was chosen as it is cost effective, the tailings material is readily removed via this method and it provides a generalised profile of different materials within the TSF. A schematic representation of the Johnson Soil®, Thompson type, hand auger (75mm diameter) used for drilling is depicted in *Figure 20*. Disturbance of the natural material profile was considered to be of lesser importance as the material distribution and grading is anthropogenically created and uniform throughout each profile drilled. The chemical composition of the tailings material also remains unaltered as this is an unlubricated, low-impact drilling method.

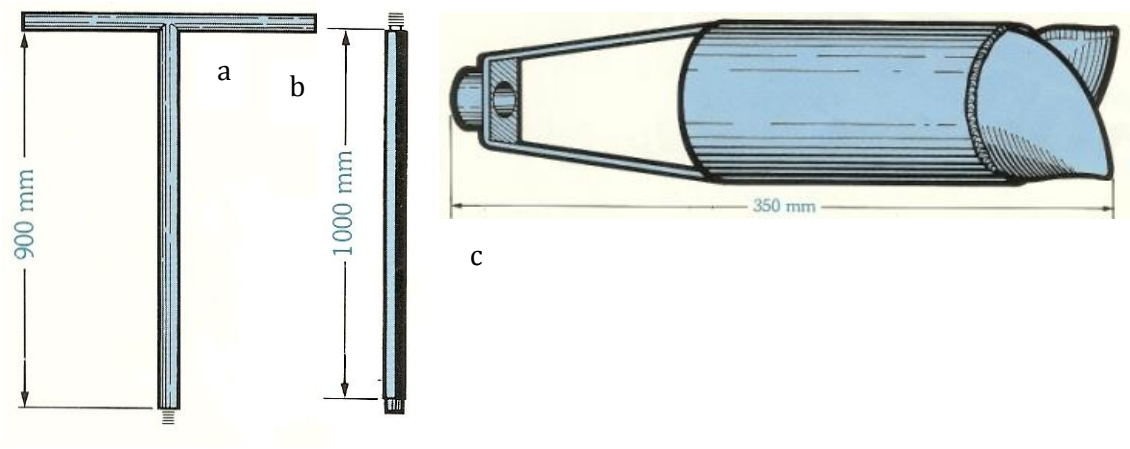

Figure 20: (a) Standard T- piece, (b) Auger extension rod, (c) Auger bucket head (Johnson Soil, 2011)

4.1.2 Direct Push Probe Drilling

Direct push probe drilling was employed to sample the tailings material in 2012. Although more expensive, this method provides undisturbed samples in PVC tubes and completely retains the material structure, moisture content distribution and chemical properties. This would provide even more detail on the conditions in the tailings material than that obtained by hand auger drilling. This method also provided a depth much greater than that reached by the hand auger sampling, down to soil level below the tailings facility.

The drill used is the AMS PowerProbe 9100VTR Diesel model, illustrated on the tailings facility in *Figure 21*. This rig uses its own static self-weight, combined with hydraulic down pressure and rapid hydraulic hammering to advance hollow stem augering equipment into subsurface lithologies.

Figure 21: Direct push probe drilling on the tailings storage facility on 20 February 2012.

Contained within the hollow stem auger equipment is a PVC tube of standard 1.2m length that is advanced into the subsurface material. When drilling has advanced 1.2m, the PVC tube is retracted with a sample of the material, an extra auger stem is added and a new PVC tube inserted. Drilling then continues to advance another 1.2m into the subsurface. This method is specifically designed to drill into- and sample soft sediments.

4.2 Sampling Locations

Samples were collected at the locations indicated in *Figure 22*. These four locations were chosen based on the constraints of spatial representation, accessibility and moisture content. Tailings material at these locations was moist enough to provide cohesion during extraction by hand auger drilling, but also dry enough to provide a safe, stable platform to drill on without the hole collapsing due to pore fluid pressures.

Auger holes were drilled into the top, middle and bottom terraces of the TSF in 2011 as indicated in *Figure 22*. These three locations provide a spatial representation of each cycle of tailings disposal forming the entire TSF.

The direct push probe hole was drilled in the terrace bank of the uppermost disposal terrace in 2012. This location was stable enough to allow the drill rig to remain stationary without sinking into the tailings facility. The samples obtained from this area would also represent the tailings in its entirety as a depth down to the original soil level could be reached with this drilling method. This would provide samples representing the very first tailings disposal up to the latest cycle of disposal.

Figure 22: Aerial photograph of the tailings storage facility indicating sampling positions

4.3 Sampling Depth and Frequency

Hand auger sampling of the tailings material in 2011 was performed with each advance of an auger bucket length i.e. 20cm. The samples collected and the extent of each are tabulated below in *Table 4*.

Table 4: Samples collected from the Tailings Storage Facility by Hand Auger

	TAH01	TAH02	TAH03
Sample Depth in Meters Below Groundlevel (mbgl)	0-0.2	0-0.2	0-0.2
	0.2-0.4	0.2-0.4	0.2-0.4
	0.4-0.6	0.4-0.6	0.4-0.6
	0.6-0.8	0.6-0.8	0.6-0.8
	0.8-1.0	0.8-1.0	0.8-1.0
	1.0-1.2	1.0-1.2	1.0-1.2
	1.2-1.4	1.2-1.4	Depth of refusal
	1.4-1.6	1.4-1.6	
	1.6-1.8	1.6-1.8	
	1.8-2.0	1.8-2.0	
	2.0-2.2	2.0-2.2	
	2.2-2.4	2.2-2.4	
	2.4-2.6	2.4-2.6	
	2.6-2.8	2.6-2.8	
	2.8-3.0	2.8-3.0	
	3.0-3.2	3.0-3.2	
	3.2-3.4	3.2-3.4	
	3.4-3.6	Excavation ceased	
	3.6-3.8		
	Excavation ceased		

Sampling was stopped in auger holes TAH01 and TAH02 after collapse, due to pore fluids, started to occur at the indicated depths of refusal in *Table 4*. Sampling was stopped in auger hole TAH03 after anorthositic gravel was encountered at the depth of refusal indicated in *Table 4* and further progress could not be made. Important points to note are:

- Samples from TAH01 were wet below 3.2 mbgl
- Samples from TAH02 were wet below 0.3 mbgl
- Samples from TAH03 were wet below 0.1 mbgl
- A stale, sulphuric smell was encountered at 2 mbgl in TAH02.

Samples were collected at the above-mentioned frequency to ensure a complete profile is represented and analyses performed yield complete results with minor to no gaps in the acquired data.

The direct push probe sampling in 2012 was a continuous sampling run with sample tubes being returned every 1.2 m of drilling. The samples collected and the extent of each are tabulated below in *Table 5*.

Table 5: Samples collected from the Tailings Storage Facility by Direct Push probe Drilling

	TPH
Sample Depth in Meters Below Groundlevel (mbgl)	0-1.2
	1.2-2.4
	2.4-3.6
	3.6-4.8
	4.8-6.0
	6.0-7.2
	7.2-8.4
	8.4-9.6
	9.6-10.0
	End of hole

Sampling was stopped due to the encountering of hard, anorthositic gravel at the bottom of the tailings, which was present in the underlying soil. Therefore, the PVC tube could not advance further without being damaged and causing a loss of sample material. However, a very complete profile of the tailings material, down to soil level, was obtained for the tailings material using this drilling method.

4.4 Sample Containment

The samples collected from the Tailings Storage Facility in 2011 were contained in 300 x 400 mm industrial plastic bags and sealed tightly with 100 mm plastic cable ties to retain the natural moisture content of the material. The direct push probe samples were contained in the original sampling tubes and sealed with wax paper and plastic caps at both ends to completely isolate the sample.

This prevents the material from desicating, clumping and hardening, making it more manageable to extract smaller samples from the bulk samples for analyses. Moisture content was also retained to preserve the in situ pH and Eh of the samples as far as possible, to ensure representative data obtained from any analyses performed on the material.

4.5 Analyses Performed

Different lab analyses and tests were performed on the tailings material sampled from the Tailings Storage Facility. This was done to determine the mineralogical composition, elemental composition, sulphide content, acid generation potential and contaminant leachability of the tailings material at different depths in the TSF. The methods employed are explained below.

4.5.1 Quantitative and Qualitative X-Ray Diffraction

The samples were prepared for XRD analysis using a back loading preparation method. They were analysed in the Department of Geology Analytical Facility of the University of Pretoria using a PANalytical X'Pert Pro powder diffractometer with X'Celerator detector and variable divergence-and receiving slits with Fe filtered Co-Kα radiation. The phases were identified using X'Pert Highscore plus software. The relative phase amounts (weight %) were estimated using the Rietveld method

(Autoquan Program). Errors are on the 3 sigma level. Amorphous phases, if present were not taken into consideration in the quantification.

4.5.2 X-Ray Fluorescence Spectroscopy

The samples were prepared as pressed powder briquettes. The ARL9400 XP+ Sequential XRF and Uniquant software was used for analyses in the Department of Geology Analytical Facility of the University of Pretoria. The software analysed for all elements in the periodic table between Na and U, but only elements found above the detection limits were reported. The values were normalised, as no LOI was done to determine crystal water and oxidation state changes. All elements were expressed as oxides.

4.5.3 Reflected Light Microscopy

Four samples obtained from the direct push probe samples were prepared as polished sections in the Department of Geology Analytical Facility of the University of Pretoria. These sections were petrographically analysed using an Olympus Petrographic Microscope connected to an external light source. The microscope has 5x, 10x and 50x magnification oculars available. Reflected light petrographic analyses were performed to identify oxide- and sulphide minerals in the samples which represented different depths in the tailings storage facility.

4.5.4 Acid-Base Accounting and Net Acid Generation Potential

In an Acid-Base Accounting analysis, two major parameters are quantified. These parameters are the acid generation potential and the acid neutralisation potential.

A tailings sample was submitted to WaterLab® in Pretoria where it was analysed for total sulphur content from which the percentage of sulphur present as sulphides were analytically calculated. The acid generation potential was calculated by multiplying the percentage of sulphur present as sulphides with a factor of 31.25 (Price, 1997). Acid generation potential is expressed as kg of $CaCO_3$ per ton of rock. This indicates the mass of theoretical calcite neutralised by the produced acid.

To calculate the acid neutralisation potential of the sample, a known volume of hydrochloric acid was added to the sample, followed by a titre of sodium hydroxide to determine the amount of unreacted acid. Acid neutralisation potential is also expressed as kg of $CaCO_3$ per ton of rock to represent the amount of theoretical $CaCO_3$ available in the rock material, to neutralise acid.

The net acid generation potential of the tailings material was then calculated by subtracting the acid neutralisation potential from the acid generation potential. A positive value indicates potentially acid forming rock whereas a negative value indicates potentially non-acid forming rock.

4.5.5 Acid Leach Tests and Inductively Coupled Plasma- Mass Spectroscopy

The acid leach test results were obtained by performing the UIS Analytical Laboratories® Acid Rain Test on the samples as received by the laboratory. A 100 g fraction of each sample was rotated for 18 hours in 2000 ml of carbonated water at a pH between 3.6 and 3.8. The solution was filtered after the extraction process and the pH value was measured before analysis. The solution obtained from each sample was analysed for trace elements with the Perkin Elmer Elan 6100 instrument using inductively coupled plasma- mass spectroscopy. The ions analysed in each solution were Ag, Al, As,

Au, B, Ba, Be, Bi, Ca, Cd, Co, Cr, Cu, Fe, Ga, Ge, Hg , K, Li, Mg, Mn, Mo, Na, Ni, Pb, S , Sb, Se, Si, Sn, Sr, Th, U, Ti, Tl, V, W, Zn, Zr, F, Cl, NO2, NO3, PO4, SO4 and results were expressed as milligrams of each element per 1000 ml of solution.

4.6 Hydraulic Testing

Hydraulic testing was performed on the tailings material and underlying aquifer in the form of permeameter tests and pumping tests respectively. These tests aid in the determination of contaminant movement velocities and directions in the TSF itself as well as in the aquifer. The calculated parameters and graphic analyses of data provide boundary conditions for flow and also aid in the characterisation of a source and pathway. This adds clarity to the prediction of possible receptors and where contamination might possibly migrate to if present. The test methods are described below.

4.6.1 Permeameter Tests

Two permeameter tests were performed on the tailings material to determine hydraulic conductivity. The tests were conducted for 8 hours as steady state flow was already established after 2 hours. The permeameter is illustrated in *Figure 23*. It was constructed using a calibrated rain gage; flexible PVC tubing with 10 mm diameter; 5 mm thick Perspex lids which were grooved; a 500 mm Perspex column of 5 mm thickness and an internal diameter of 150 mm; 8 marine grade turnbuckles; 2 mm thick steel cables; 2 valves to control flow and finally sealed with silicon to prevent any leakage. The Perspex column was filled with the tailings material which was premixed with water, after which additional water was added to ensure that the maximum degree of saturation possible was obtained. The column was sealed after insertion of the tailings and wall mounted to run the test.

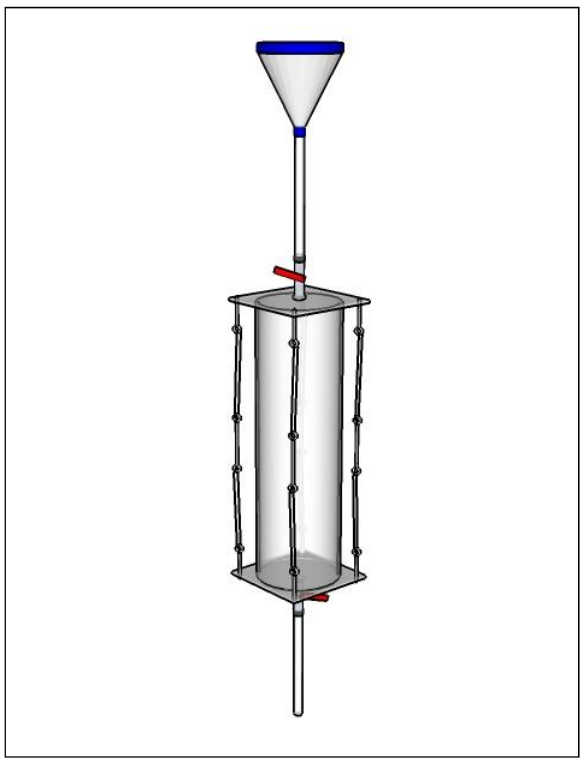

Figure 23: Schematic representation of the falling head permeameter used to obtain transport- and hydraulic properties of the tailings material.

4.6.2 Pumping Tests – AQTESOLV

Two pumping tests were conducted around the tailings storage facility between 14 and 16 March 2012 on existing monitoring wells to determine the hydraulic properties of the underlying aquifer. The tests were performed on two wells located between the tailings and the Steelpoort river which is considered to be a possible receptor of contamination. A pump was inserted to a depth where a known water strike was encountered during drilling as indicated by information received from the mine. The wells were pumped at a low discharge rate equal to the observed blow yield obtained during drilling, with waterlevel readings being noted at differing intervals to obtain high resolution data. This was performed using a TLC dipmeter. The low yielding wells were each pumped for a limited time period as steady state conditions were reached within 2 to 3 hours of pumping, and left to recover to a level as close as possible to the original datum waterlevel.

The data obtained from these tests were then interpreted using AQTESOLV software to determine the hydraulic parameters of the aquifer such as hydraulic conductivity, transmissivity, fracture depths, no flow boundary conditions as well as aquifer storativity. AQTESOLV is a software package used to analyse pumping tests, slug tests and constant-head tests.

4.7 Geochemical and Flow Modelling

The data collected from the field work, testing and analyses, were used to construct and calibrate geochemical and unsaturated flow models. The models were used to predict the future flow and chemical behaviour of the tailings, as well as to attempt to explain the processes that are currently taking place in the material. Each model and its application are explained in the paragraphs below.

4.7.1 Geochemical Modelling – The Geochemist's Workbench 9.0 Standard

The modelling software used to interpret the obtained geochemical data from the Tailings Storage Facility, is The Geochemist's Workbench® Standard 9.0 (GWB). As paraphrased from the developer's website (Rockware, 2011), The Geochemist's Workbench® is a set of software tools for solving water quality problems, including those encountered in environmental protection and remediation, the petroleum industry and mine wastewater planning. The software provides a platform for:

- Water data storage
- Unit conversion
- Evaluation of replicates and standards
- Flagging of exceedances
- Balancing chemical reactions
- Creating Pourbaix and activity diagrams
- Solution speciation calculations
- Mineral saturation calculations
- Gas fugacity calculations
- Predicting ion sorption and surface complexation
- Creating Piper, Stiff, series, time series, cross plot, ternary and other aqueous geochemistry diagrams
- Calculating polythermal and sliding fugacity reactions
- Incorporating mineral dissolution/precipitation kinetics and redox kinetics

- Specifying custom rate laws
- Modelling microbial metabolism and growth
- Obtaining Debye-Huckel or Pitzer activity coefficients
- Specifying flow-through and flush configurations
- Plotting flash (scaling) diagrams
- Modelling stable isotope fractionation.

The model was used to predict solution speciation of permeating fluids through the TSF as well as stable mineral phases that could potentially form. Rate constants for dissolution kinetics of existing, meta-stable mineral phases present in the tailings material were obtained from literature. The activities of different ionic species in the fluids permeating the TSF were also determined using activity coefficient equations available from the software.

4.7.2 Unsaturated Flow Modelling – HYDRUS

The modelling software was used to evaluate the unsaturated flow parameters of the tailings material is HYDRUS® 1D 4.0, a FORTRAN® based numerical unsaturated flow modelling software. This software can be used to calculate unsaturated hydraulic conductivities, vapour flow, heat flow and solute transport in variably saturated soil materials using the Richards equation.

As paraphrased from Šimůnek and van Genuchten (2009), the program may be used to analyse water and solute movement in unsaturated, partially saturated, or fully saturated porous media. The flow region may be composed of nonuniform soils. Flow and transport can occur in the vertical, horizontal, or a generally inclined direction. The water flow part of the model can deal with prescribed head and flux boundaries, boundaries controlled by atmospheric conditions, as well as free drainage boundary conditions. The governing flow and transport equations are solved numerically using Galerkin-type linear finite element schemes. This version of HYDRUS also includes a Marquardt-Levenberg type parameter optimization algorithm for inverse estimation of a variety of soil hydraulic and/or solute transport and reaction parameters from measured transient or steady-state flow and/or transport data.

5. RESULTS AND DISCUSSION

5.1 Analytical Results

The chemical results obtained for each analysis are interpreted and discussed in detail below and provide insight into different chemical and mineralogical aspects of the TSF-vadose zone-aquifer system.

5.1.1 X-Ray Diffraction

The X-Ray Diffraction analyses that were performed on the tailings material, took place at the StoneMan laboratory at the University of Pretoria. The analysis results are attached under Appendix A. The mineral phases present in the tailings material and underlying vadose zone are summarised below in *Table 6* and *Table 7* respectively.

Table 6: Mineral phases present in the tailings material on site

Mineral	Chemical Formula
Annite	$KFe_3(Al, Si)_3O_{10}(OH, F)_2$
Anthophyllite	$(Mg_{0.76}, Fe_{1.24})(Mg_{4.95}, Fe_{0.05})Si_8O_{22}(OH)_2$
Diopside	$(Ca, Mg)Si_2O_6$
Enstatite	$(Mg_{1.568}, Fe_{0.432})Si_2O_6$
Magnesiohornblende	$Na_{0.46}Ca_{1.7}Mg_{3.44}Fe_{1.72}Al_{1.08}Si_{6.92}O_{23}(OH)$
Lizardite	$Mg_3Si_2O_5(OH)_4$
Chromite	$NiCr_2O_4$
Anorthite	$CaAl_2Si_2O_8$
Talc	$Mg_3Si_4O_{10}(OH)_2$
Chlorite (Clinochlore)	$Mg_{5.1}Al_{1.2}Si_3Cr_{0.7}O_{10}(OH)_8$
Phlogopite	$KMg_3(Al, Si)_3O_{10}(OH,F)_2$
Muscovite	$KAl_3Si_3O_{10}(OH)_2$
Tremolite	$Ca_2Mg_5Si_8O_{22}(OH)_2$
Chalcopyrite	$CuFeS_2$

Table 7: Mineral phases present in the vadose zone on site

Mineral	Chemical Formula
Chlorite (Clinochlore)	$Mg_{5.1}Al_{1.2}Si_3Cr_{0.7}O_{10}(OH)_8$
Quartz	SiO_2
Kaolinite	$Al_2Si_2O_5(OH)_4$
Enstatite	$(Mg_{1.568}, Fe_{0.432})Si_2O_6$
Chromite	$NiCr_2O_4$
Anorthite	$CaAl_2Si_2O_8$

The variation in mineral content, as weight percentages, is graphically illustrated for each sample with depth in the figures below. These graphs display stacked totals with each colour representing a different mineral phase to illustrate the above mentioned variations, as well as the mineral abundances relative to each other for each assemblage at each sample depth. Material that was not accounted for and fall outside of the 1% error margin for accuracy may be present in the form of colloidal phases as XRD analysis only detects crystalline phases or analytical value rounding. Also, excess weight percentages may be due to analytical value rounding.

Figure 24 illustrates minor variations in enstatite, hornblende and anorthite abundances of up to 8%. This may be due to variations in the mineralogy of the hanging wall and footwall of the UG2, but may also indicate changes in different depositional cycles and mixing of material in a mostly uniform material. This figure also illustrates abundances of talc in excess of 5 weight% as well as the increase of the lizardite phase with depth. This figure represents the oldest cycle of tailings disposal at the facility.

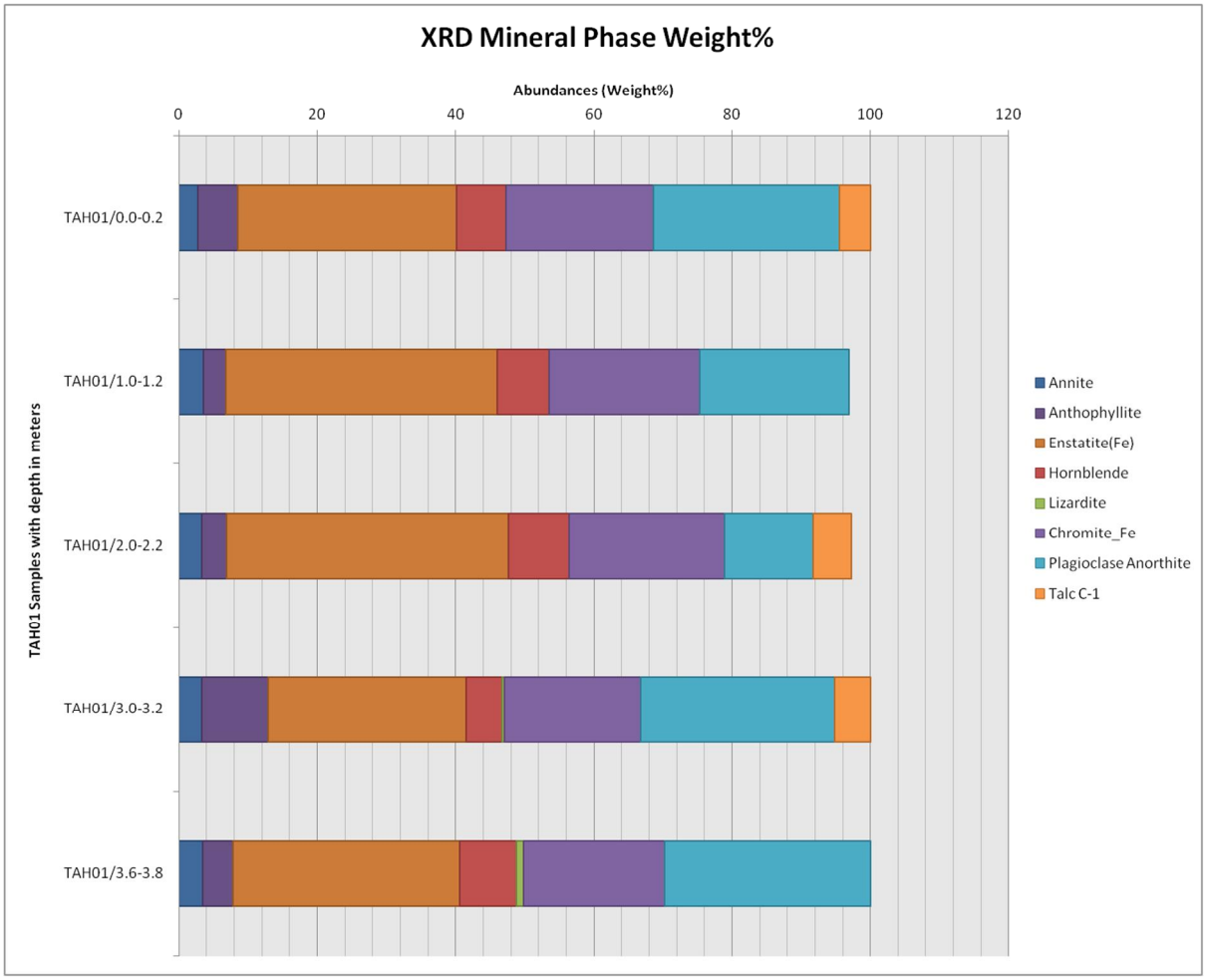

Figure 24: Mineral phase abundances with depth in TAH01

Figure 25 illustrates variations in enstatite, anorthite and hornblende as well as the complete replacement of the annite and anthophyllite phases with depth. The variations in enstatite and anorthite may be attributed to hanging wall and footwall variations in mineralogy during disposal cycles, but may also be a product of several different disposal cycles and mixing ratios. Lizardite can also be observed to be depleted within the first meter of the profile. This may indicate slightly older, more hydrated tailings material which has undergone more extensive weathering and dissolution present in the material during the deposition of this portion of the tailings profile. The depletion of annite and anthophyllite may be due to mineral structure changes with varying degrees of weathering, fluid content and oxygen availability in the rock before extraction. This could indicate the deposition of younger tailings material higher in the profile. At an approximate depth of 3 meters, annite can be observed to have been replaced with ferrian phlogopite which could be a result of magmatic mixing during the formation of the rock, changing this phase into its more Mg-rich end member phase. Magmatic mixing may also be responsible for diopside in the tailings at depth with Mg in the crystal structure of enstatite being substituted with Ca during the formation of a younger lava after its systematic depletion from the system. Its presence at depth in the tailings profile could therefore be explained by the mining of shallower, younger rock from the Critical Zone. This figure represents the second oldest cycle of tailings disposal.

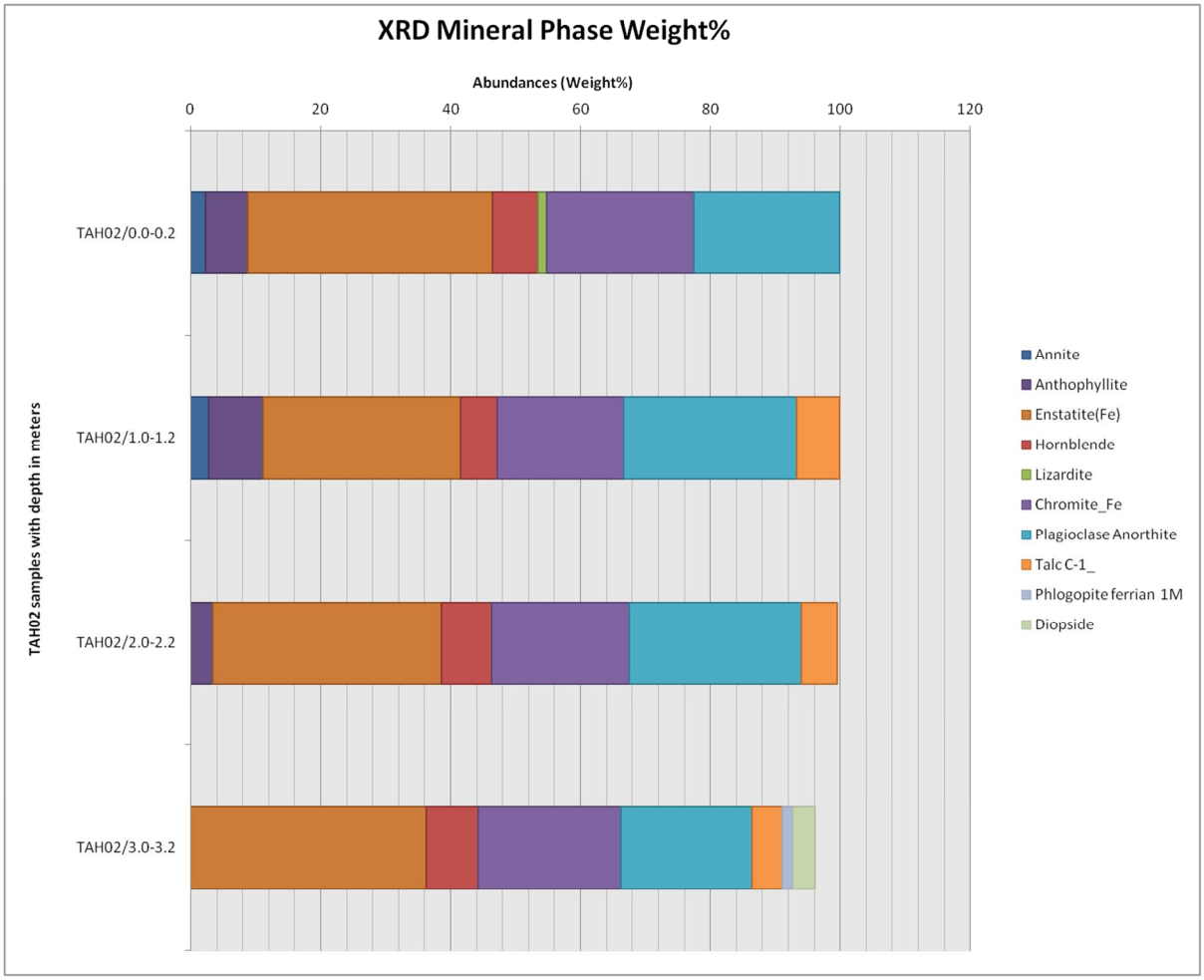

Figure 25: Mineral phase abundances with depth in TAH02

Figure 26 illustrates lesser variation in the enstatite phase with depth but much more so for the anorthite phase, as well as the complete replacement of the anthophyllite and diopside phases. This profile was obtained at the foot of the tailings, near a toedrain and variations may be due to material that has been transported from the tailings by geomorphic processes. The abundance of enstatite remains constant in each of the samples while diopside and anthophyllite is depleted. This is interpreted as differences in hanging wall and footwall mineralogy, as the profile does not show similar mineral abundance trends to the other two sampling localities where anthophyllite becomes depleted with the increase in diopside. However, this profile is interpreted to be extensively weathered as talc is an abundant phase with no lizardite present, as observed in the other profiles. Therefore, this profile is interpreted to have a mixed mineralogical signature and represents an area of mixing in the tailings material.

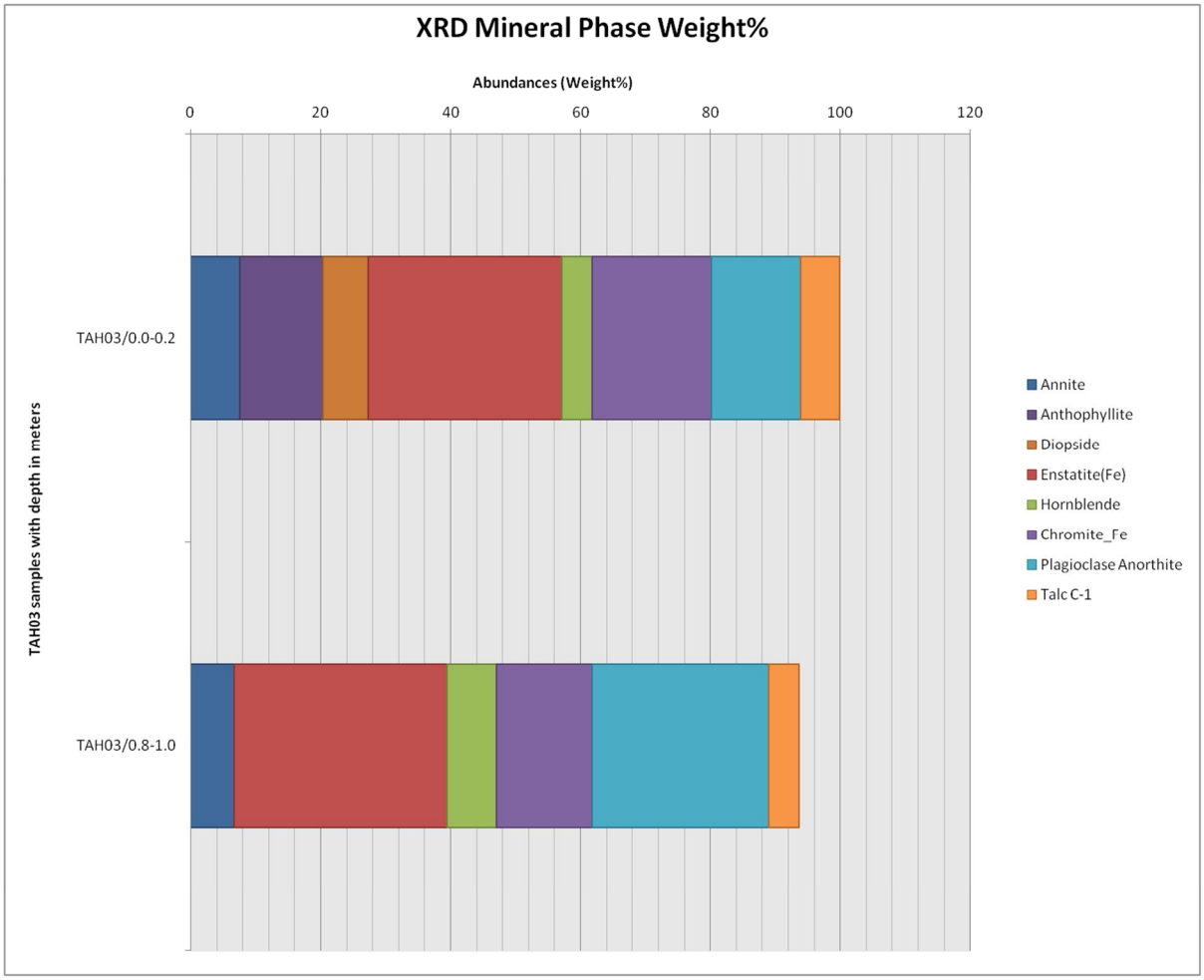

Figure 26: Mineral phase abundances with depth in TAH03

Figure 27 illustrates the mineral phase abundances in the direct push probe hole, drilled in the top terrace of the tailings as illustrated in *Figure 22*. Samples TPH0-1.2T to TPH8.4-9.6B represents tailings material from the top to the bottom of the TSF. Sample TPH9.6-10 represents the underlying soil material and natural vadose zone on site. From this figure, it is evident that throughout the TSF, the major composition of the material is an anorthite-enstatite-chromite assemblage with minor amounts of other mineral phases present. However, these phases are useful in interpretation of the origin and chemical evolution of the magmatic sequence throughout the profile, by acting as indicator minerals. Variations in enstatite and anorthite are inversely proportional to each other across the entire depth of the tailings profile. However, a point to be noted is that enstatite abundance is lower, shallower in the profile down to approximately 1.5 m and decreases abruptly at 8.4 m depth in sample TPH7.2-8.4B. This may have a skewing effect on the average mineralogical composition of the tailings but is interpreted as undulations in the reef and could possibly represent outliers in the data set due to a sudden localised change in reef composition. The higher abundance of quartz and kaolinite at this depth is explained as a zone of mixing in the tailings material between the tailings and natural soil material.

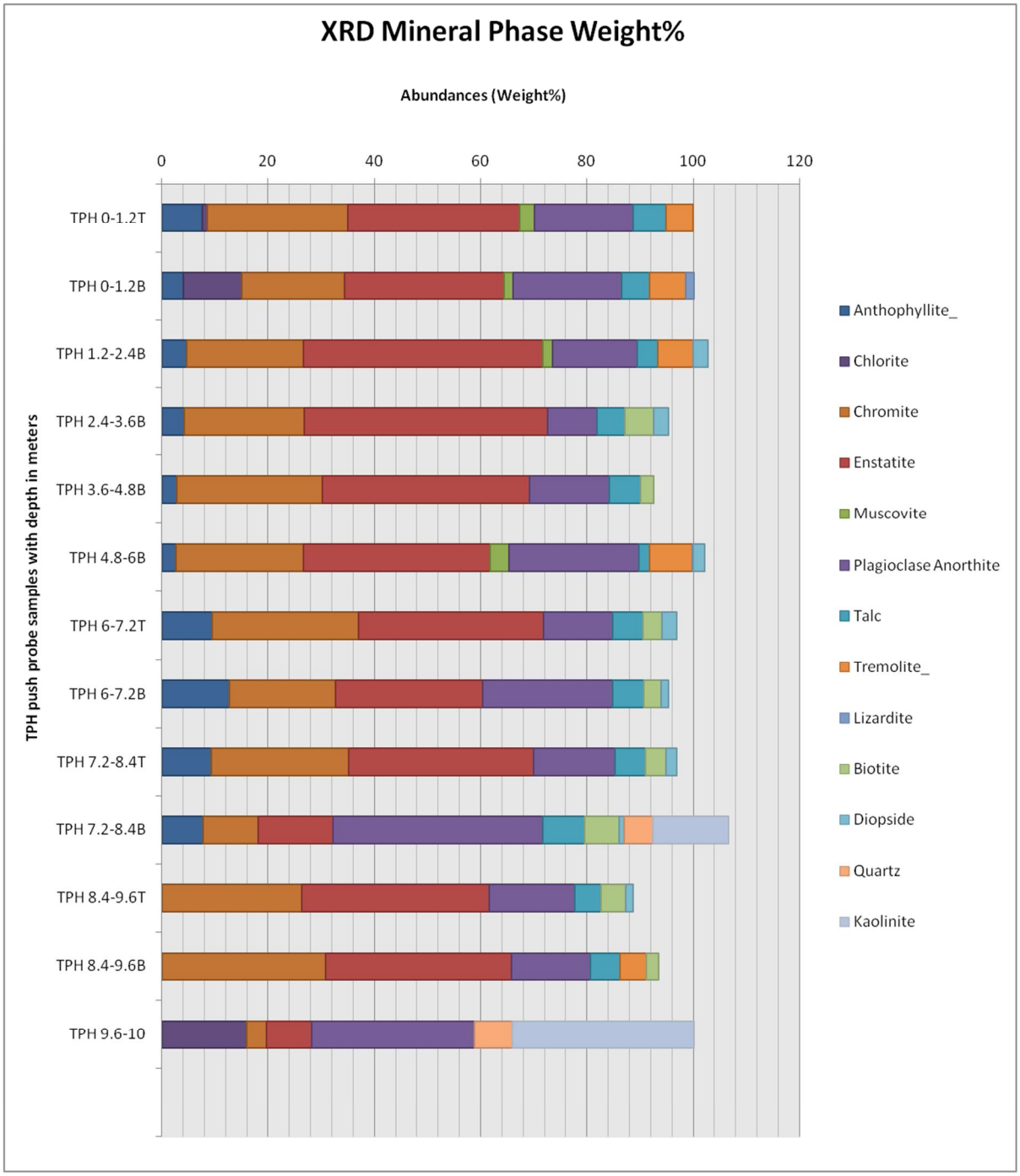

Figure 27: Mineral phase abundances with depth in TPH

Chlorite, muscovite and anthophyllite phases can all be observed to be minor phases in the tailings profile, linking with anomalous chemical compositions in the reef hanging wall and footwall due to various processes. The biotite and diopside phases increase with depth which is to be expected as these minerals decrease with depth as the mine progresses through the magmatic sequence from more intermediate to more mafic mineralogical assemblages. Talc and lizardite can also be found throughout the tailings profile, approximately inversely proportional to the abundance of the enstatite phase, which may indicate talc formation as a secondary mineral after enstatite breakdown by subsurface hydrothermal alteration. Another important point to note is that the weight percentage of chromite in each of the profiles discussed in this section showed little to no variation,

indicating its stability under a wide range of redox conditions as well as temperature and pressure conditions during the formation of the reef.

The mineral phases found in the soil profile constituting the natural vadose zone on site, predominantly consisted of anorthite, chlorite and kaolinite. Chlorite can be directly linked to the weathering of orthopyroxene minerals such as enstatite while kaolinite is a product of anorthite breakdown in the soil environment. Chromite was also found as a minor phase in the soil profile which may indicate mixing from tailings material. However, its low abundance may also indicate natural mixing from the underlying bedrock and its high resistance to weathering in the natural soil environment and redox conditions. Quartz is another minor mineral phase in the soil profile and is an abundant final product of the weathering cycle.

5.1.2 X-Ray Fluorescence Spectroscopy

The X-Ray Fluorescence analyses that were performed on the tailings material, took place at the Department of Geology Analytical Facility of the University of Pretoria. The major- and trace elements that were detected in the material were expressed as weight percentages in terms of oxides, tabulated below in *Table 8* and *Table 9* respectively. The analysis results are attached under Appendix B.

Table 8: Major element oxides as detected by XRF.

Major Element Oxides as Detected by XRF			
SiO_2	CaO	V_2O_5	CuO
TiO_2	Na_2O	ZRO_2	ZnO
Al_2O_3	K_2O	SO_3	Co_3O_4
Fe_2O_3	P_2O_5	WO_3	CeO_2
MnO	Cr_2O_3	BaO	SrO
MgO	NiO	Cl	MoO_3

Table 9: Trace elements as detected by XRF

Trace Elements as Detected by XRF			
As	Sr	Co	La
Cu	Th	Cr	Ce
Ga	U	F	Ba
Mo	W	S	Cl
Nb	Y	Sc	Rb
Ni	Zn	V	
Pb	Zr	Cs	

The variation in element oxide content, as weight percentages, is graphically illustrated for each sample with depth in the figures below. These graphs display stacked totals with each colour representing a different element oxide to illustrate the above mentioned variations, as well as the elemental abundances relative to each other for each assemblage at each sample depth.

Figure 28 illustrates variations in Si, Fe, Al, Mg, Ca, Cr and Na which are the most abundant major elements in the profile. Si decreases by 10% with depth up to 2.2 m where it starts to increase. Inversely proportionate to this element is the variations in Fe and Cr. Mg content stays relatively constant with Ca content following the same trend of variation as Si. This may indicate a direct link

to anorthite as the primary Ca bearing phase and may also control chromite stability to a certain degree as Cr weight percentages vary in an inversely proportionate manner to Si weight percentages.

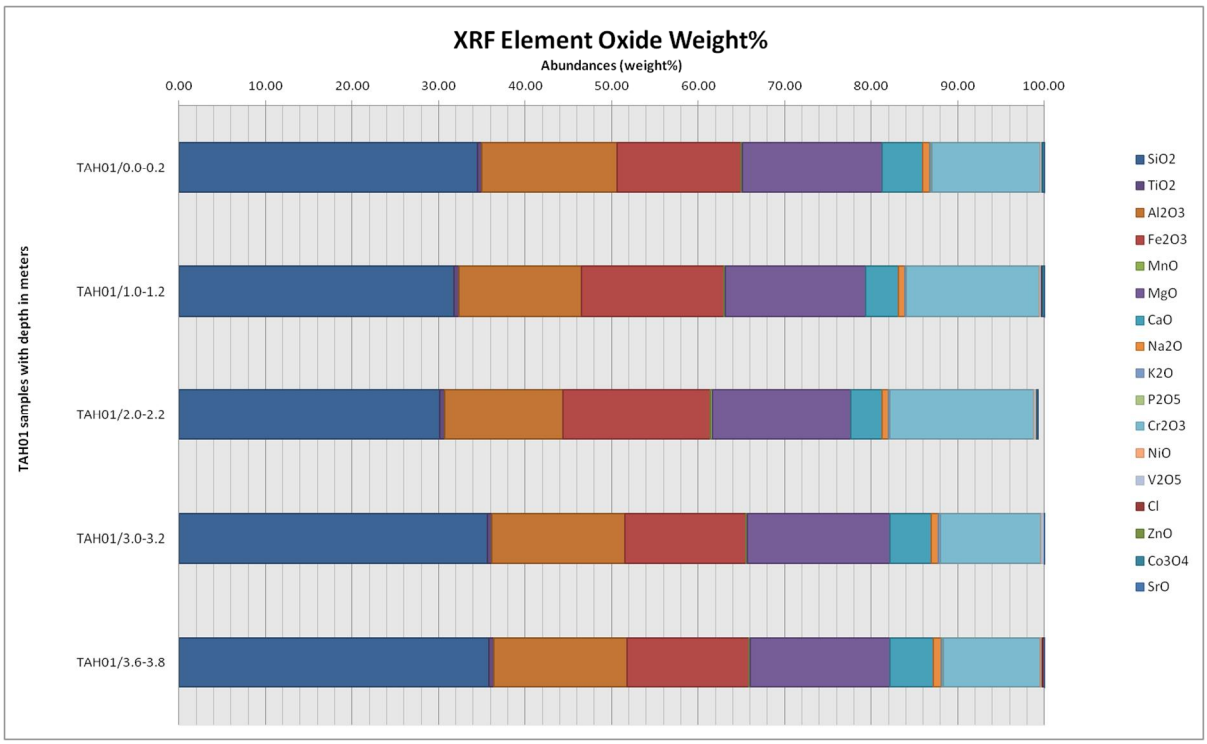

Figure 28: Element oxide abundances with depth in TAH01

Figure 29 illustrates a much more subtle variation in Si, Iron, Al, Mg, Ca, Cr and Na than that observed in TAH01. However, this figure illustrates the inversely proportionate relationship between Si and Cr content with Si content increasing slightly and then decreasing with depth. This may indicate a direct link to anorthite as the major Si bearing phase in the profile as its variation in abundance in this profile is much less pronounced. Fe, Al, Mg and Ca all remain approximately constant throughout the profile.

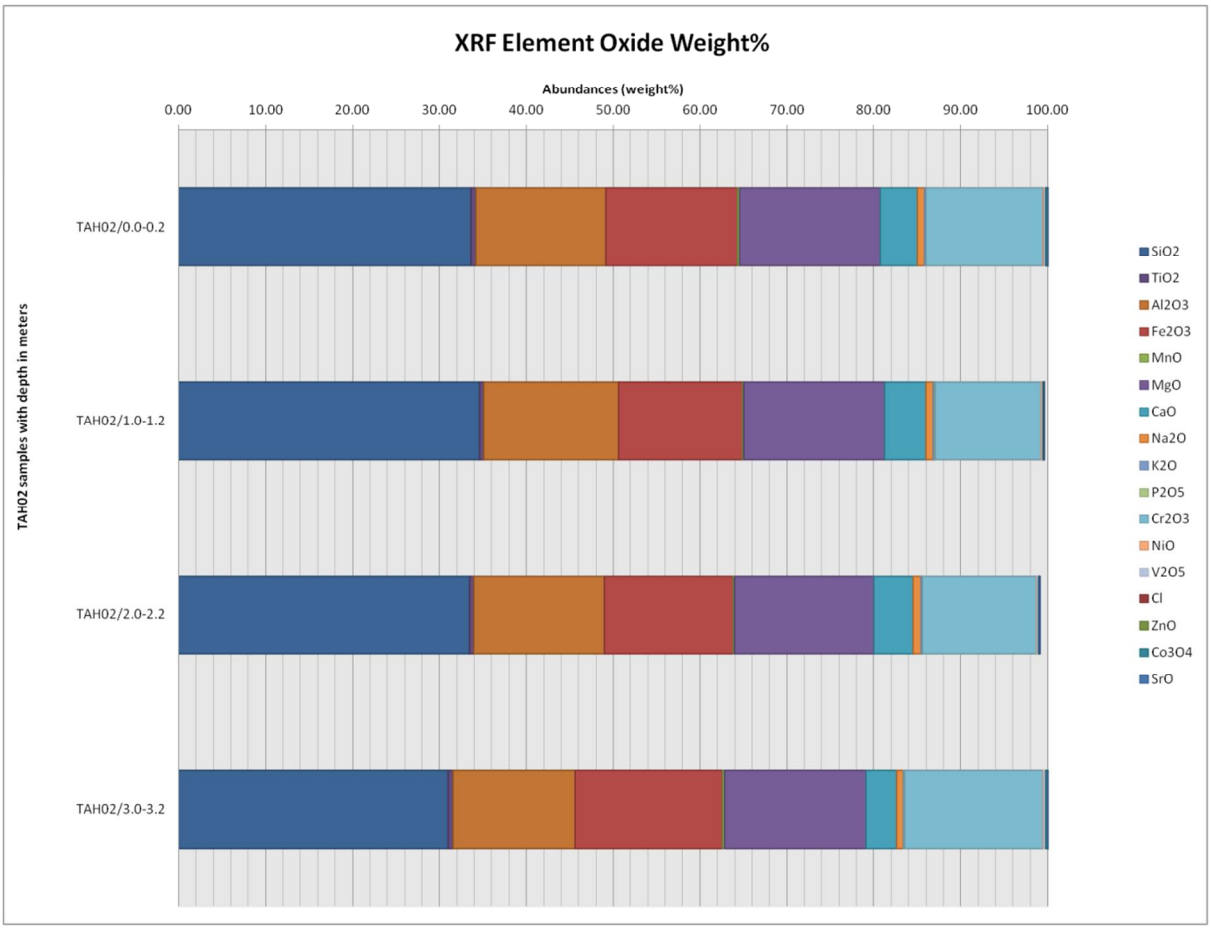

Figure 29: Element oxide abundances with depth in TAH02

Figure 30 illustrates more pronounced variations in Si content with depth and illustrates its inversely proportionate relationship with Cr much more obviously. Minor decreases in Fe content as well as Mg content can be observed with depth with increased Al content with depth. Therefore, chromite crystallisation may have been inhibited in the later stages of this magma which provided more suitable conditions for feldspar crystallisation, which is also indicated by the increase in Al and Ca content with depth.

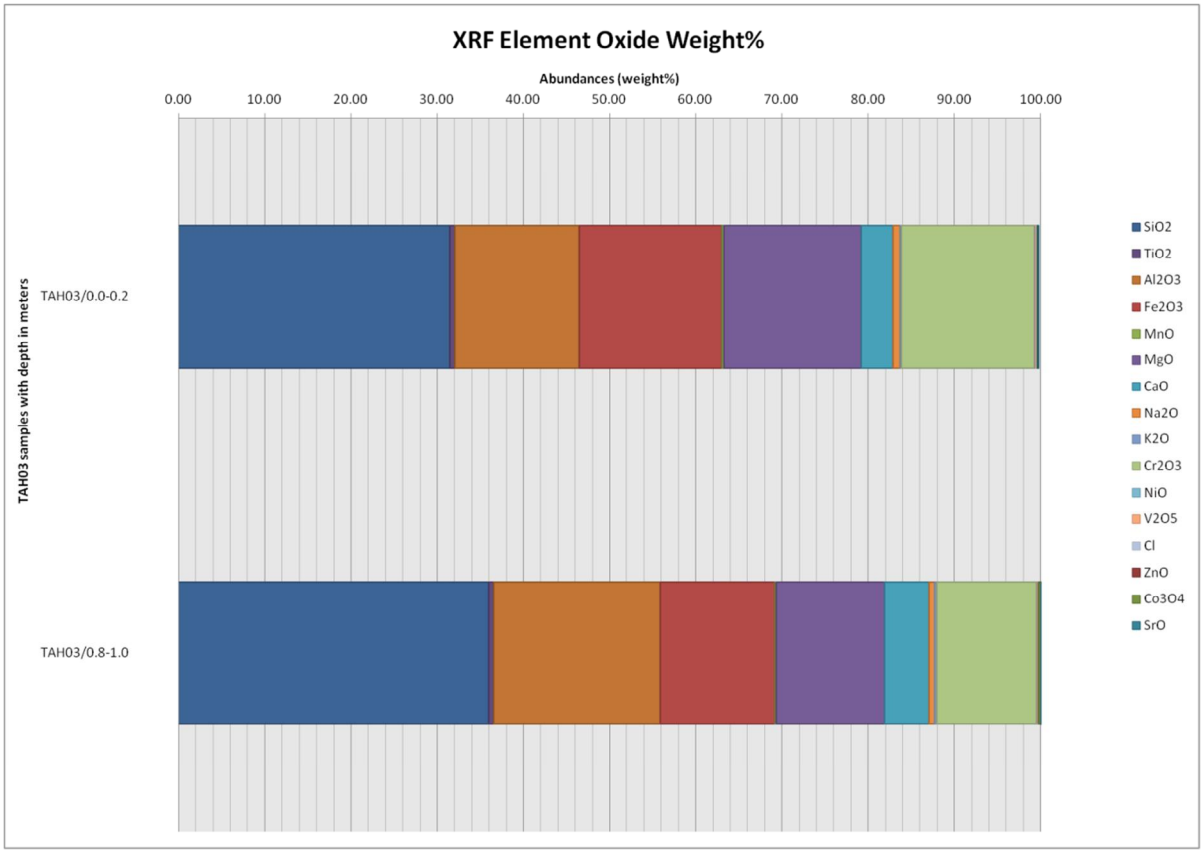

Figure 30: Element oxide abundances with depth in TAH03

Figure 31 illustrates major element oxides in the tailings material down to 9.6 m after which the major element oxides in the soil material comprising the natural vadose zone, are illustrated for depths between 9.6 and 10 m. The inversely proportional relationship between Si and Cr content is illustrated in this diagram, as well as throughout the tailings material down to soil level. The explanation given for this relationship for TAH03 also holds in this instance. An increase in Ca and Al content can also be observed at 9.6m which may indicate a higher abundance of anorthite. This could be because of increased enstatite weathering due to fluid ponding at this specific depth in the tailings material as enstatite is slightly more prone to weathering and dissolution than the anorthite phase. However, it is more likely that this is due to the mineralogy at shallower mining depths as well as mixing with the natural soil profile. In the rest of the tailings profile, Fe and Mg contents remain fairly constant. At soil level, Mg is almost entirely depleted with much lower Fe and Cr abundance and major increases in Ca, Al and Si. This may be attributed to long term weathering and pedogenesis, causing advanced breakdown and dissolution of the enstatite phase, with the remaining phases being constituted of secondary minerals and more felsic minerals, stripped of their once elevated Mg and Fe content.

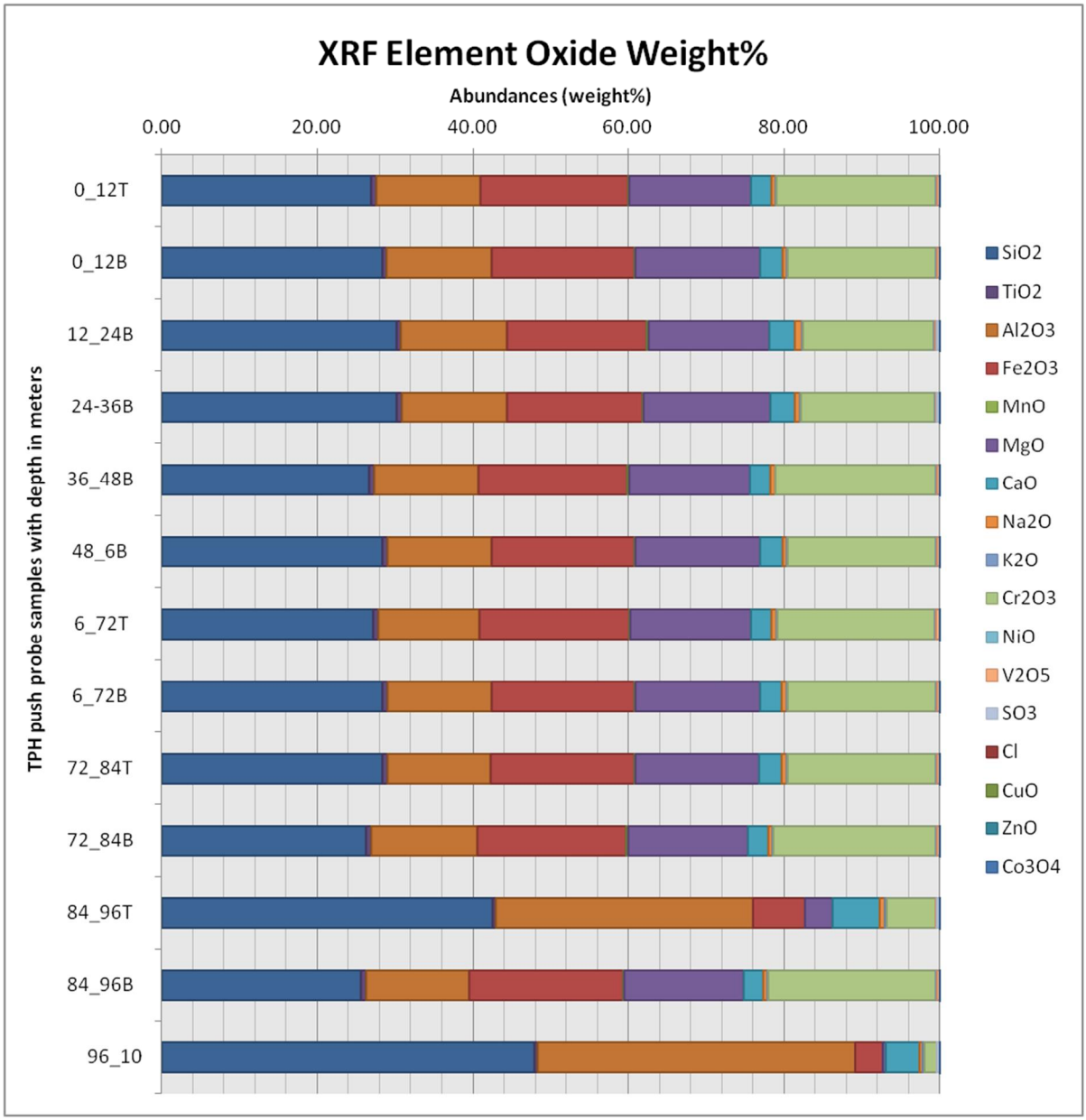

Figure 31: Element oxide abundances with depth in TPH

Figure 32 illustrates trace element oxides in the tailings material down to 9.6 m after which the trace element oxides in the soil material comprising the natural vadose zone, are illustrated for depths between 9.6 and 10 m. Zn, Ni and V variation can be observed to be directly proportionate to Cr variation throughout the profile indicating a direct link to chromite abundance in the profile. Ba and Cl abundance can be observed to be inversely proportionate to Ni abundance. This may indicate a link to silicate mineral phases such as anorthite which has approximately the same trend of abundance throughout the profile even down to soil level. The ratio of Rb to Sr and U may also indicate that the tailings material is variably saturated as Sr and U partitions readily into the fluid phase and these trace elements may have been concentrated in the material during the sample drying process. S can also be observed to follow an increasing trend with depth which may indicate significant decreases in oxygen to facilitate sulphide mineral dissolution. Cu can also be observed to remain approximately constant throughout the profile.

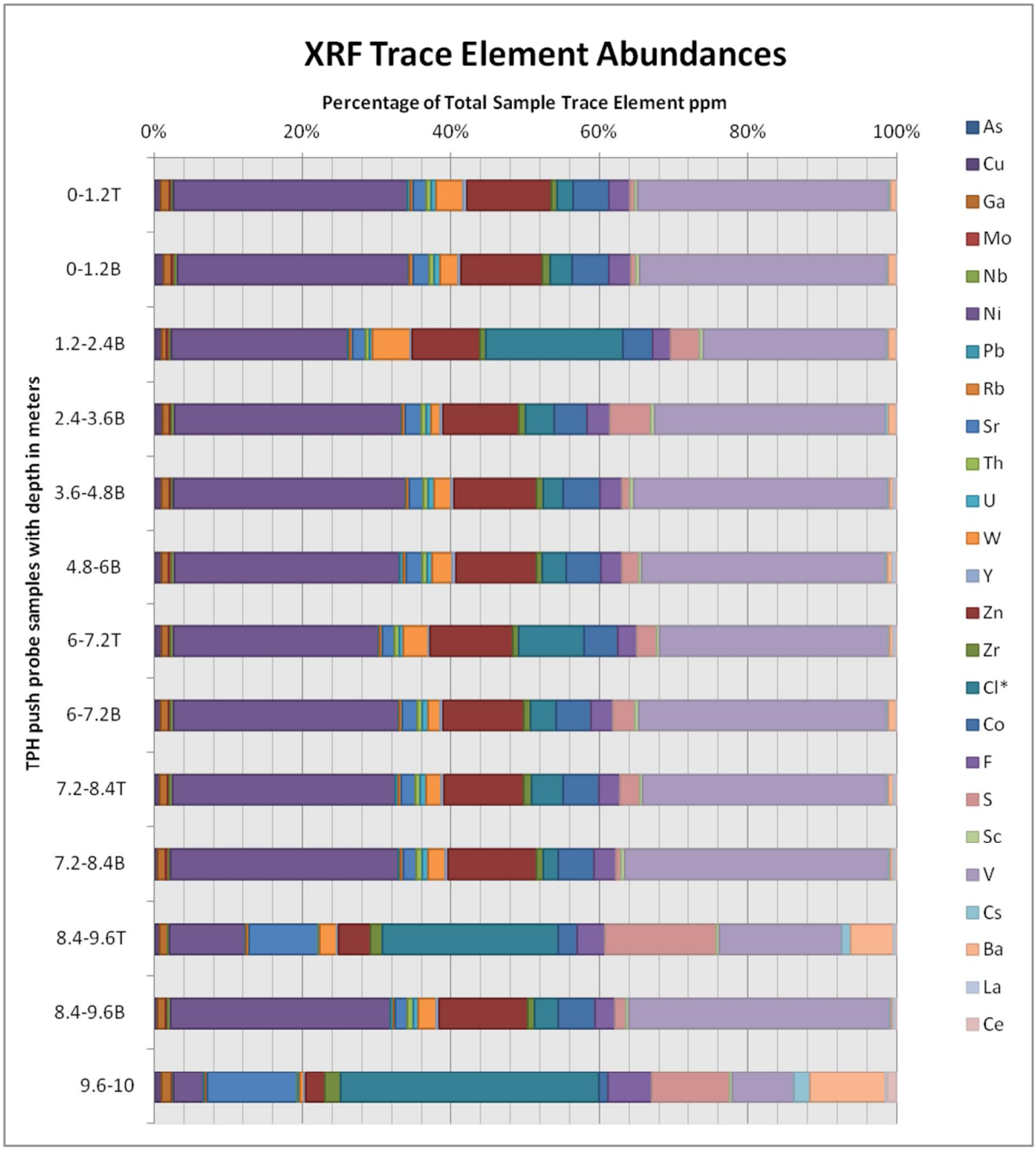

Figure 32: Trace element abundances with depth in TPH

5.1.3 XRF Element Correlations and Mineral Tracing

Figure 33 illustrates the correlation of specific trace elements with specific major elements from the XRD data discussed in the previous section. These elements were correlated to be able to observe a trend and attempt to link a certain trace heavy metal to a certain major ion which could then be linked to a specific mineral phase. Ca was correlated with Si and fitted with a linear trend line which fitted the data with an R^2-value of approximately 0.76 which is considered to be a moderately good fit. Si was found to be 5 times as abundant as Ca in the system. Anorthite and Diopside was concluded to be the major Ca bearing silicate phases in the system, with a ratio of one mol of Ca to 2 moles of Si each, based on abundances.

Al was correlated with Si and fitted with a linear trend line which fitted the data with an R^2-value of approximately 0.96 which is considered to be a good fit. Al was found to be 0.74 times as abundant as Si in the system. Anorthite, the biotite series, chlorite, muscovite and magnesiohornblende were identified as Al bearing phases. However, anorthite is the most abundant Al bearing phase and was therefore concluded to be the major Al bearing silicate phase in the system, with a ratio of 2 moles of Al to 2 moles of Si.

Mg was correlated with Si and fitted with a linear trendline which fitted the data with an R^2-value of approximately 0.91 which is considered to be a good fit. Si was found to be approximately 4 times as abundant as Mg in the system. Enstatite was concluded to be the major Mg bearing silicate phase in the system, with a ratio of 2 moles of Mg to 2 moles of Si, based on abundances.

Na was correlated with Si and fitted with a linear trendline which fitted the data with an R^2-value of approximately 0.67 which is considered to be a poor fit. Si was found to be approximately 12 times as abundant as Ca in the system. Due to the poor fit and correlation of the data, Na could not conclusively be traced to a specific silicate phase. However, the only XRD identified silicate phase containing Na is magnesiohornblende. Therefore, this phase may be a source of Na in tailings pore fluids. However, precipitated Na salts or amorphous phases may be more likely to be the source of Na based on the low abundance of the hornblende phase.

K was correlated with Si and fitted with a linear trendline which fitted the data with an R^2-value of approximately 0.8 which is considered to be a good fit. Si was found to be 130 times as abundant as K in the system which indicates only a slight positive correlation between these elements. The biotite series and muscovite was concluded to be the major K bearing silicate phases in the system, with a ratio of one mol of K to 3 moles of Si each. However, based on relative abundances and the correlation between these elements, the silicate phases cannot be conclusively isolated as the sole source of K and amorphous phases and K-rich precipitates are thought to be more likely sources of this element.

The trace heavy metals V, Co and Ni were all correlated with Cr. Each dataset was fitted with a linear trendline. Each trendline showed an R^2-value above 0.95 which is considered to be an excellent fit. Concentrations of Cr relative to these elements were found to be up to 544 times more abundant. However, based on the fit of the trendline to the data, the high correlation regression coefficient and chromite being the only Cr bearing phase in the system, it can be concluded confidently that these trace heavy metals are sourced from the chromite phase. An important point to note is that chromite is insoluble in most redox conditions as illustrated by the literature review section. Acidic conditions are required to dissolve this mineral phase and it may therefore pose a low contamination potential in terms of heavy metals.

Pb was also correlated with Cr abundances and fitted with a linear trendline which fitted the data with an R^2-value of approximately 0.23 which is considered to be a very poor fit. Therefore, Pb cannot be conclusively stated to be sourced from the chromite phase and could possibly exist in amorphous Pb-sulphide phases.

Cu was correlated with S and fitted with a linear trendline which fitted the data with an R^2-value of approximately 0.065 which is considered to be a very poor fit and that no correlation exists. However, the only Cu bearing phase in the system was found to be chalcopyrite which contains one mole of Cu for every two moles of sulphur. Therefore, the XRF data for these elements may not indicate a correlation of these elements, but petrographic data suggests otherwise.

Cu was then correlated with Fe in an attempt to illustrate the association with chalcopyrite. The data was fitted with a linear trendline which fitted the data with an R^2-value of approximately 0.23 which is considered to be an improvement but still a very poor fit. However, the only Fe bearing phase in the system containing one complete mol of Fe, was found to be chalcopyrite. Therefore, petrographic data again suggests otherwise.

Fe was then correlated with S in an attempt to illustrate the association with chalcopyrite. The data was fitted with a linear trendline which fitted the data with an R^2-value of approximately 0.15 which is considered to be a poor fit. However, the only Fe and S bearing phase in the system containing one complete mol of Fe and two moles of sulphur, was found to be chalcopyrite. Therefore, petrographic data suggests a possible alternative. Chalcopyrite is therefore suggested to be the main source of Cu, Fe and S species in the system.

Fe was correlated with Si and fitted with a linear trendline which fitted the data with an R^2-value of approximately 0.98 which is considered to be a good fit. However, a negative correlation between Si and Fe was observed, confirming the sulphide phase, chalcopyrite, to be the main source of this metal in the system. Pyroxenes and amphiboles were, however, not disregarded as iron contributors, but are thought to play a less significant role. *Figure 33* shows the correlations of the abovementioned results.

Figure 33: Correlation of major and trace element abundances obtained from XRF analysis.

5.1.4 Reflected Light Microscopy

Reflected light microscopy was performed on four polished sections, as tabulated in *Table 10*, at the University of Pretoria. This petrographic work was performed using an Olympus Petrographic Microscope with 5x, 10x and 50x magnification.

Table 10: Samples selected from different depths in the TPH direct push probe hole for reflected light microscopy

Selected sample for petrography	Sample depth
TPH1.2T	0.01m
TPH2.2.4B	2.4m
TPH6.7.2T	6.01m
TPH8.4.9B	9.6m

Figure 34 illustrates two grains of chalcopyrite identified in the entire polished section, prepared for the sample returned from a depth of 0.01 m. Each grain also shows a certain degree of alteration, indicative of active weathering processes which may have decreased the abundance of this mineral phase.

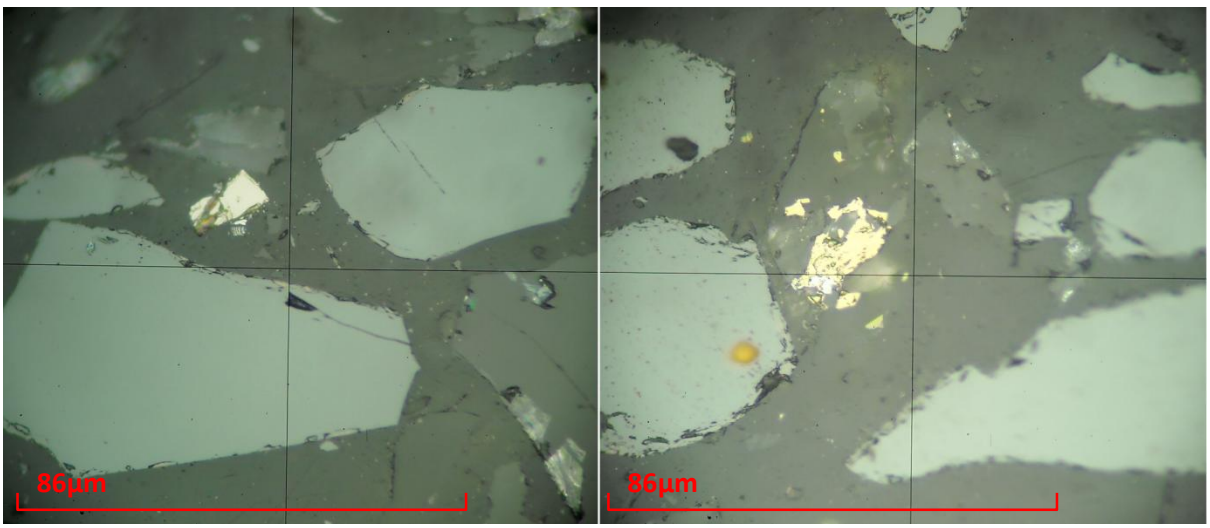

Figure 34: Reflected light microscopy images for sample TPH1.2T at 50x magnification.

Figure 35 illustrates pyrite (left) as well as chalcopyrite in a silicate phase (right). These are the only sulphide phases identified throughout the polished section, prepared from the sample returned from a depth of 2.4 m in the tailings material. The sulphide phases at this depth appear to be slightly more abundant with less alteration which may indicate a shorter exposure period to oxidising weathering conditions.

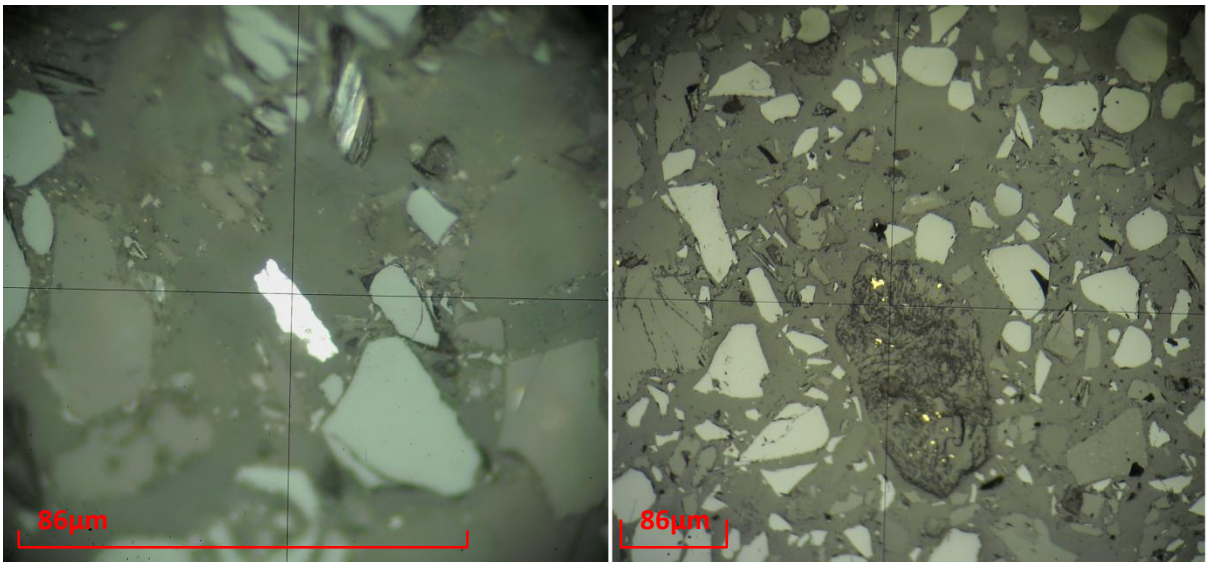

Figure 35: Reflected light microscopy images for sample TPH2.2.4B at 50x magnification (left) and 10x magnification (right).

Figure 36 illustrates a single occurrence of chalcopyrite throughout the entire section at 50x magnification. This section was prepared for the sample TPH6.7.2T, returned from a depth of 6.01 m in the tailings material. This grain appears to be unaltered by weathering which could be due to its isolation from oxygen at depth in the tailings. However, adjacent to it, a grain of chalcopyrite appears to be altered. This may be due to abundant fluids in the tailings material at this depth. However, this cannot be stated conclusively.

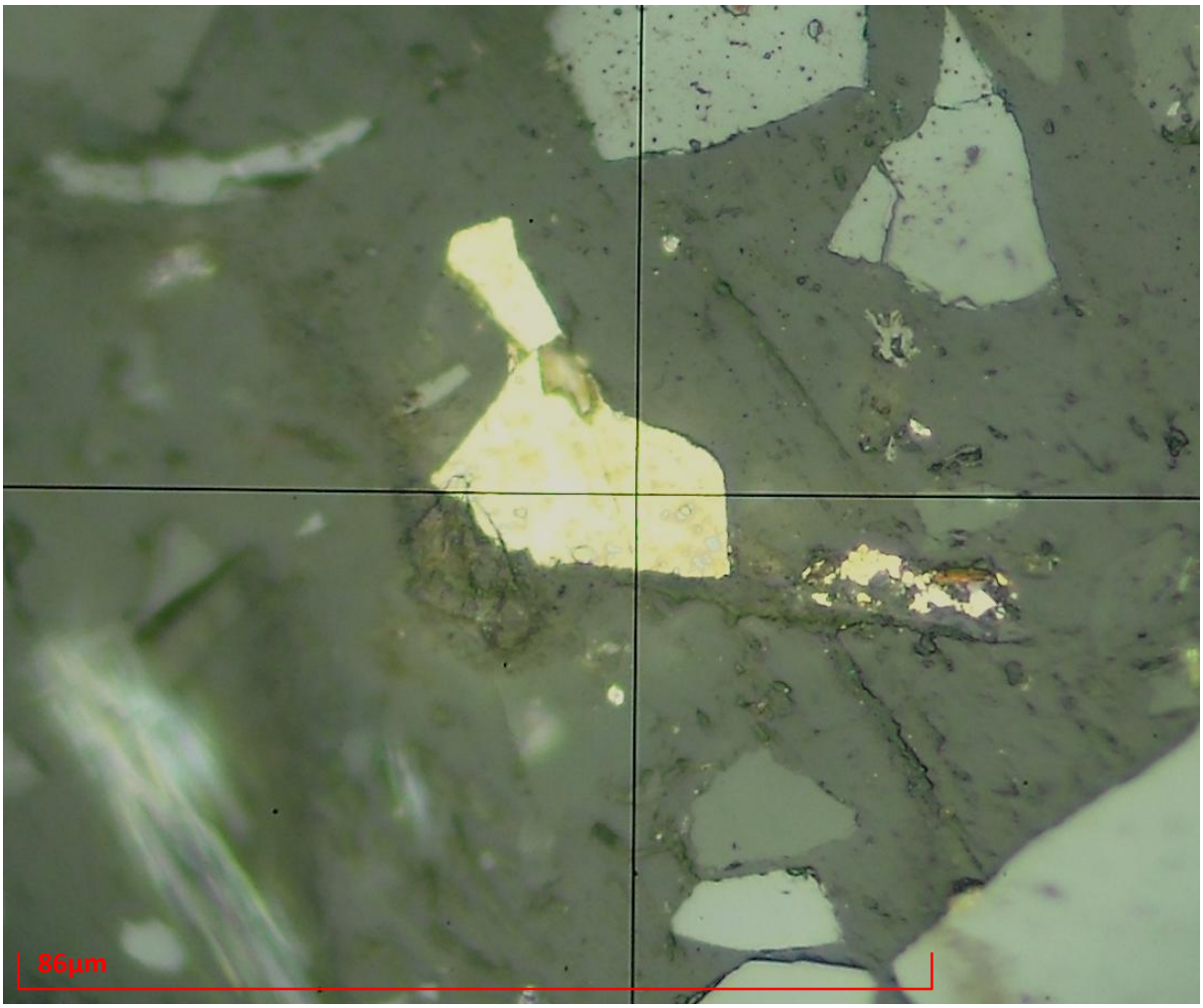

Figure 36: Reflected light microscopy image for sample TPH6.7.2T at 50x magnification.

Figure 37 illustrates single occurrences of pyrite (left) and chalcopyrite (right). These are the only occurrences of sulphide phases in the entire section, which was prepared from the sample extracted from 9.6m depth, in the tailings material. Both grains appear to be completely unaltered, indicating the highly anoxic conditions at the base of the TSF.

The abundances of sulphide phases in the tailings can therefore be concluded to be low, based on the microscopy images discussed in this section.

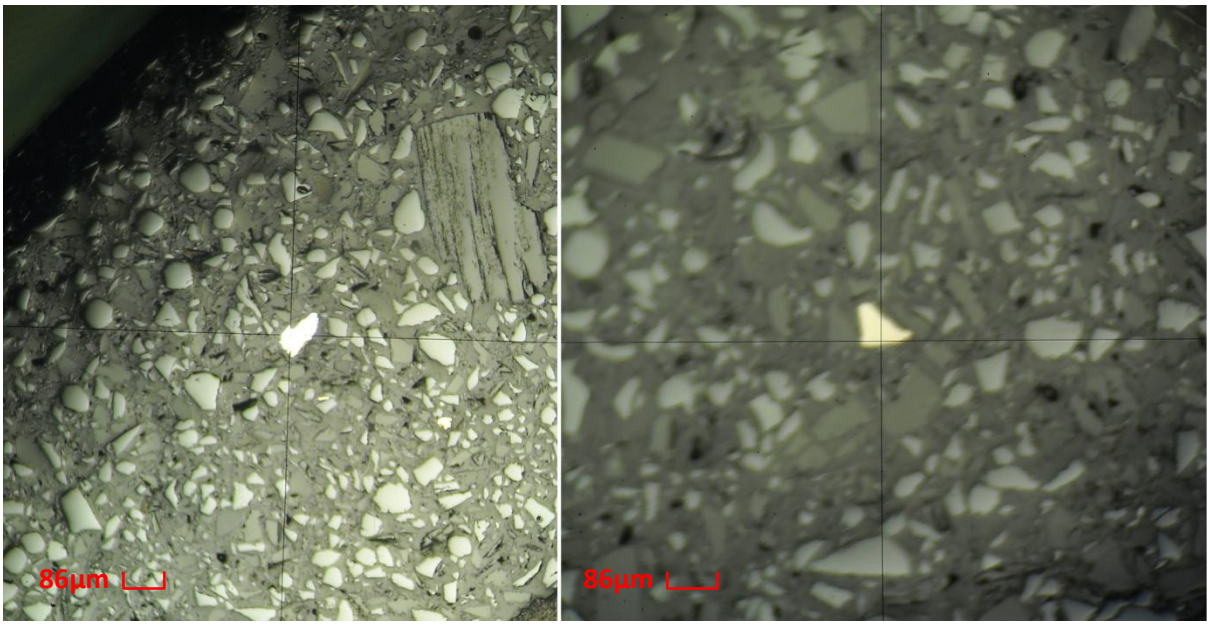

Figure 37: Reflected light microscopy images for sample TPH8.4.9B at 10x magnification.

5.1.5 Acid-Base Accounting and Net Acid Generation Potential

Acid-base accounting was performed at Waterlab® laboratories in Pretoria. The findings of the analysis are summarised below in *Table 11*. A duplicate sample, 4114D, was also tested to ensure reproducible results.

Table 11: Acid-Base Accounting Laboratory Results

Acid – Base Accounting Modified Sobek (EPA-600)	Sample Identification	
	Vadose Zone Hydrology TRPTS 1	Vadose Zone Hydrology TRPTS 1
Sample Number	4114	4114D
Paste pH	6.1	6.1
Total Sulphur (%) (LECO)	0.02	0.02
Acid Potential (AP) (kg/t)	0.62	0.62
Neutralisation Potential (NP)	8.50	9.50
Nett Neutralization Potential (NNP)	7.88	8.88
Neutralising Potential Ratio (NPR) (NP : AP)	13.73	15.34

The paste pH detected for the sample during acid-base accounting was 6.1. This indicates the pH of a sample mixed with distilled water to form a paste that has a liquid to solid ratio of 1:1. This indicates a slightly lowered pH that may be existent in the tailings at present. However, due to the nature of the test being performed over one hour, the paste pH value may be slightly skewed due to the time dependant reaction rates of sulphides and sulphates in the material, possibly generating acid in this time frame.

The total percentage sulphur in the sample was analysed with a LECO analyser and found to be 0.02%. The acid generation potential was calculated to be 0.062 kg of acid per ton of rock. This was calculated by multiplying the total percentage of sulphur by a factor of 31.25. The neutralisation potential was calculated, after treatment of the sample with a known volume of HCl and back-

titrating it with a known volume of NaOH. This determines the amount of unconsumed acid and the neutralisation potential of the rock can then be expressed as kg $CaCO_3$/ton of rock. This represents the theoretically available amount of calcite available in the rock, to neutralise acids.

The nett neutralisation potential was calculated by subtracting the acid generation potential from the neutralisation potential. This was found to be 7.88 kg $CaCO_3$/ton of rock in excess. The neutralisation potential ratio was found to be positive in the sample as well as in the duplicate sample at an average of 14. This indicates an unlikely ability of the rock material to generate acid. According to Price (1997) the tailings material is not potentially acid generating unless significant preferential exposure of sulphides exist, or extremely reactive sulphides in combination with insufficient reactive acid neutralisation potential are present.

5.1.6 Acid Leach Tests

Acid leach tests were performed on the tailings material collected from the auger holes. These analyses were performed on 18 August 2011 by Waterlab® laboratories in Pretoria. The leachable elements that were analysed for are listed below in *Table 12*.

Table 12: Elements analysed for during acid leach tests conducted in August 2011

Elements Analysed for in Leachate from Acid Leach Test					
Ag	Ce	Ho	Nb	Si	W
Al	Co	In	Nd	Sn	Y
As	Cr	Ir	Ni	Sr	Zn
Au	Cs	K	P	Ta	Zr
B	Cu	La	Pb	Te	F
Ba	Fe	Li	Pt	Th	Cl
Be	Ga	Mg	Rb	Ti	NO_2
Bi	Ge	Mn	Sb	Tl	NO_3
Ca	Hf	Mo	Sc	U	PO_4
Cd	Hg	Na	Se	V	SO_4

Leach tests were performed on each of the samples collected from the auger holes drilled in 2011 and the abundance of detected elements from the analyses are graphically illustrated below. *Figure 38* illustrates the abundances of the cations leached from samples collected from TAH01 during the acid leach tests. Ca, Mg, Na and Si were found to be the main leachable cations from the samples collected from this auger hole. It can also be observed that the abundances of these leached elements gradually increase with depth. This is a strong indication of the oxygen availability in the profile which may facilitate weathering and dissolution. Oxygen is illustrated to be depleted with depth in this profile as less weathering has taken place. This idea is supported by the abundances of leachable cations markedly increasing with depth, indicating that these elements may still be intact in less weathered mineral phases and also illustrates the accumulation of elements in pore fluid with depth. However, this could also be a function of additional mineral precipitates from permeating fluids in the tailings.

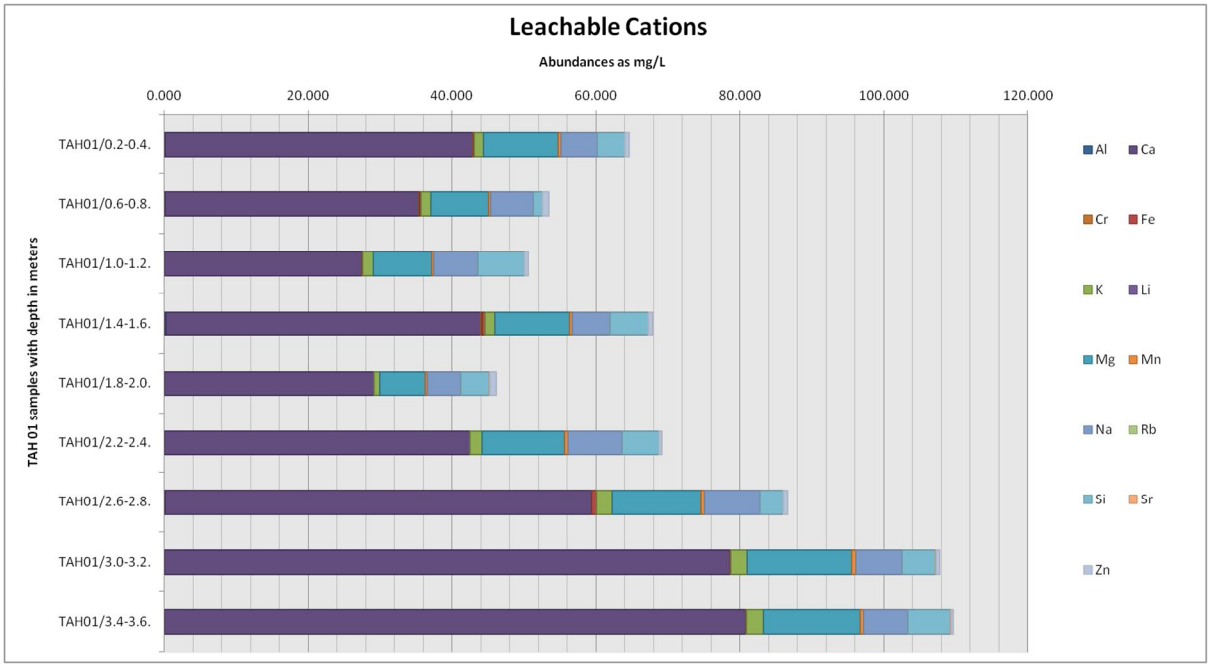

Figure 38: Leachable cations in samples collected from TAH01.

A corresponding graph for the leachable anions in the profile can be observed in *Figure 39*. This figure illustrates the leachable anion abundances from the same samples. However, the general trend of leachable elements does not indicate increasing abundances with depth. Nitrate concentrations decrease with depth and may be due to evaporative and desiccation effects with more nitrate available shallower in the profile. Other anion abundances remain fairly constant with variable amounts of sulphate being released. The concentrations of sulphate released may be an indication of changes in reef mineralogy during the material deposition cycle on the TSF. Leachable sulphate concentrations, however, do not indicate a clear trend in changing redox conditions in this profile.

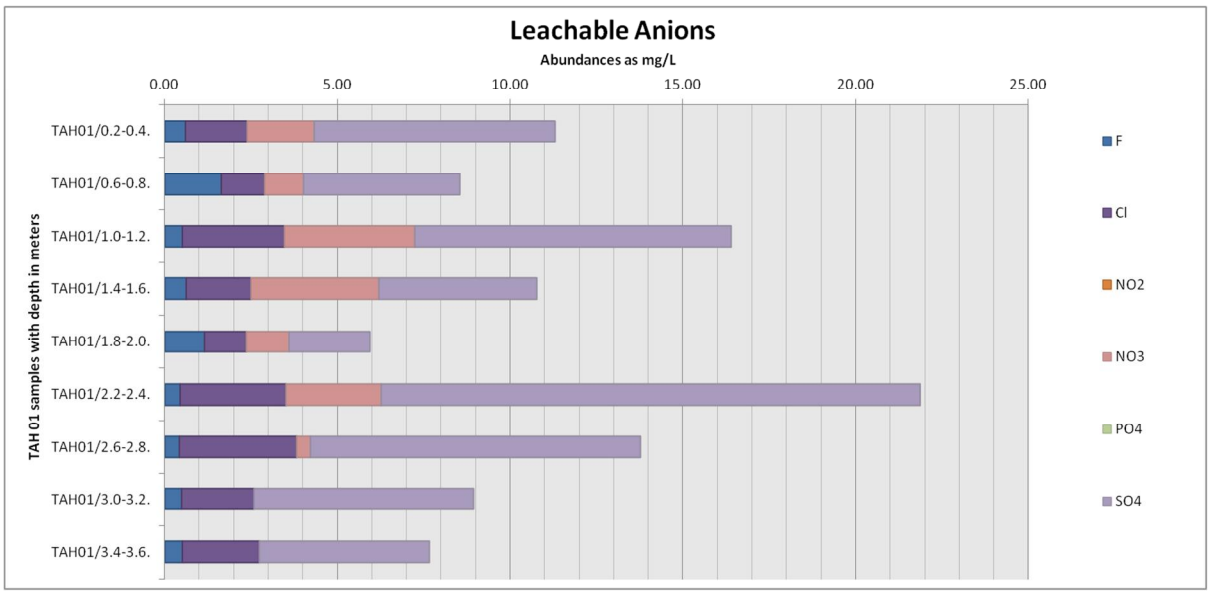

Figure 39: Leachable anions in samples collected from TAH01.

Figure 40 illustrates the abundances of the cations leached from samples collected from TAH02 during the acid leach tests. In this profile, Ca, Na, Mg and Si are also the main leachable elements. However, this profile does not supply clear information on the prevailing redox conditions as concentrations of these cations vary in an apparently random manner and do not indicate a trend of oxygen availability in the profile.

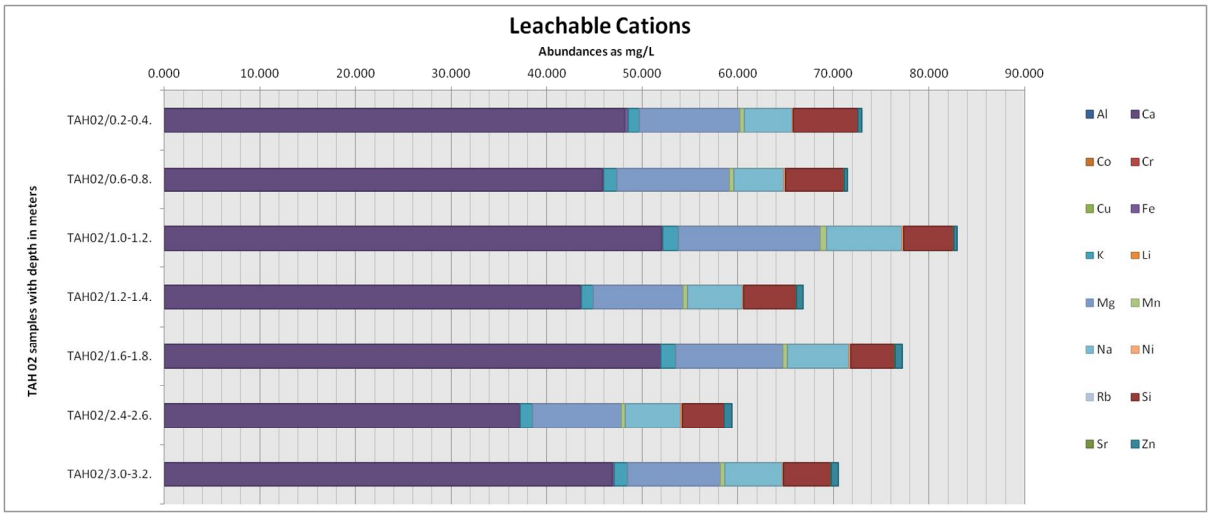

Figure 40: Leachable cations in samples collected from TAH02.

Figure 41 illustrates a corresponding graph indicating the leachable anions from the samples collected from TAH02. This graph illustrates no nitrate present which may indicate that the tailings material in this area has remained saturated for an extended period of time inhibiting nitrate precipitation from evaporative processes. Sulphate release is also variable throughout the profile and does not indicate a specific trend in redox conditions or oxygen content in the tailings material. Cl-abundances however, may reflect a fairly constant composition of the tailings material throughout this profile as the release concentrations of this conservative ion, remains fairly constant. This may indicate a saturated profile.

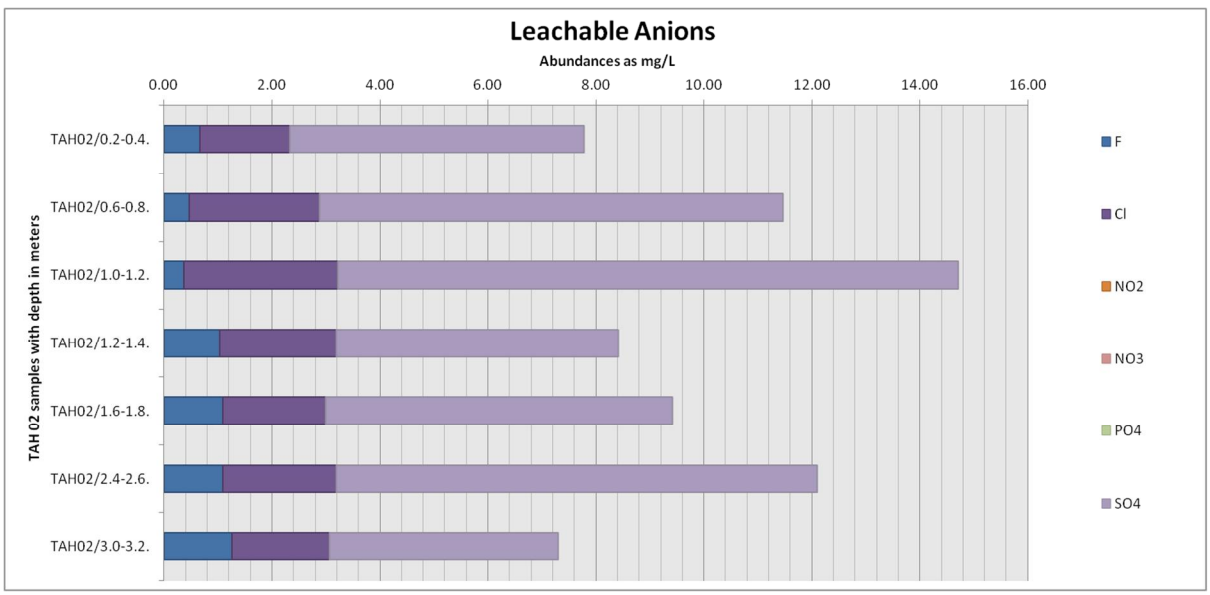

Figure 41: Leachable anions in samples collected from TAH02.

Figure 42 illustrates the abundances of the leachable cations from the samples collected from TAH03. The main leachable cations in this profile were found to be Ca, Mg, Na and Si. However, this profile illustrates the increased abundance of leachable elements with depth, indicating redox conditions changing from oxidising to reducing. This idea may indicate more weathered material shallower in the profile with fresher and less weathered material deeper in the profile, subsequently accompanied by more and less leachable ions respectively as well as increased cation concentrations in deeper pore fluids that may have accumulated over time.

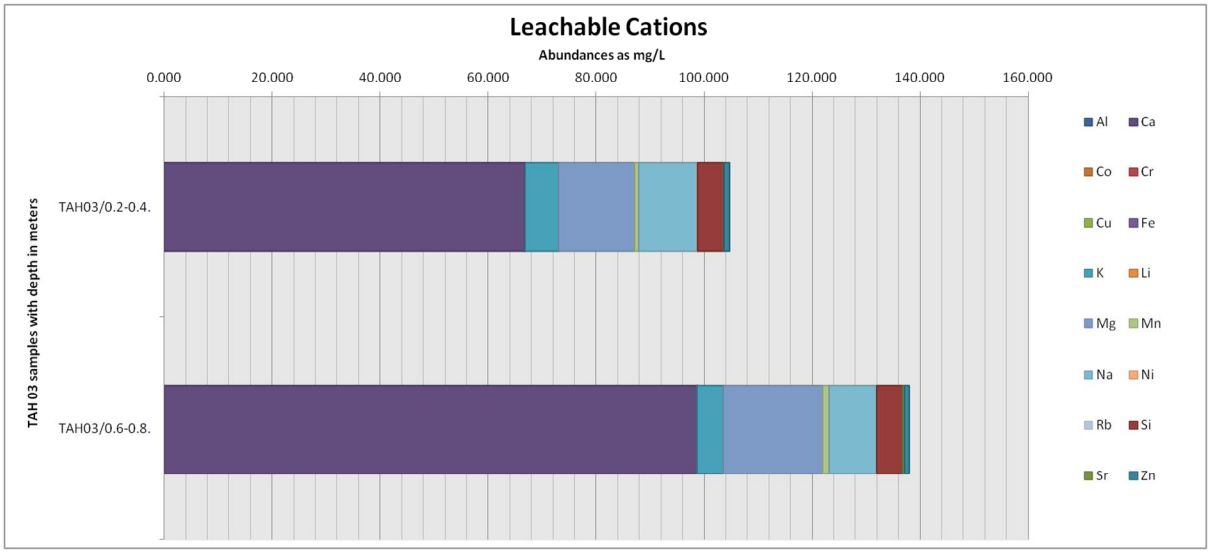

Figure 42: Leachable cations in samples collected from TAH03

Figure 43 illustrates a corresponding graph indicating the leachable anion abundances in the samples collected from TAH03. In this figure, more Cl and F are observed in the shallower part of the material which may indicate precipitation from evaporative processes as observed in *Figure 39* with nitrate abundances. This may indicate rapid evaporation and desiccation, subsequently increasing anion precipitation. However, the abundance of sulphates remains constant throughout the profile which may indicate relatively constant oxygen activity in the profile.

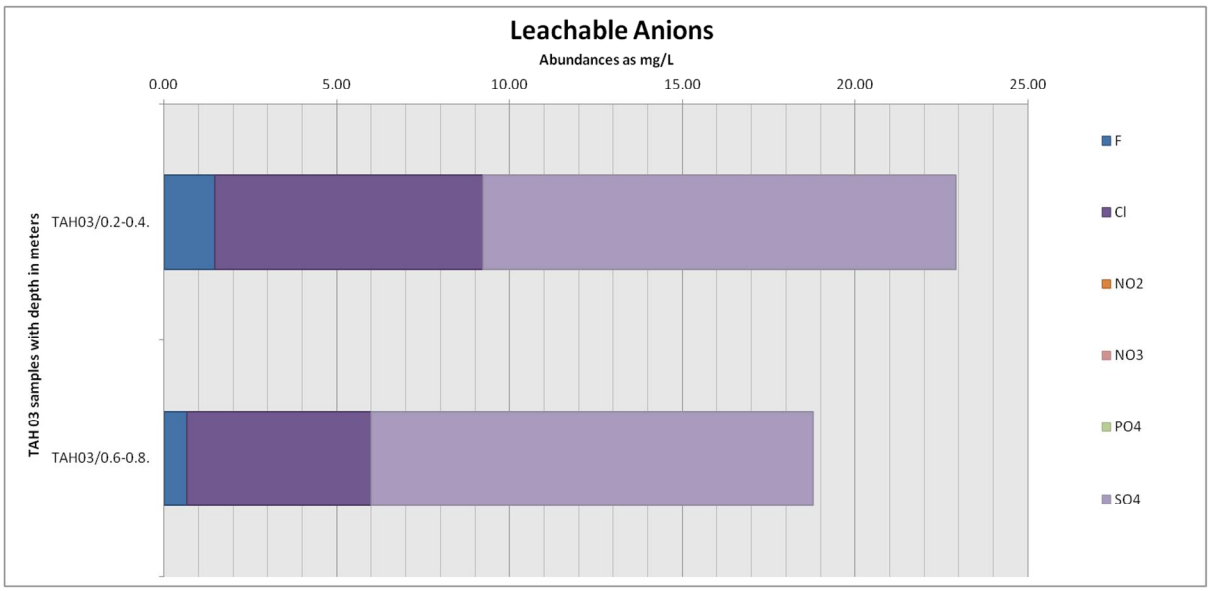

Figure 43: Leachable anions in samples collected from TAH03.

5.1.7 Inductively Coupled Plasma Scans

Water samples were collected from the toedrain of the tailings facility, two adjacent monitoring wells as well as the Steelpoort river during March and April of 2012. These samples were submitted to Waterlab® laboratories in Pretoria for inductively coupled plasma- optical emissions spectroscopy analyses. The results of the analyses are attached under Appendix C and are graphically illustrated in *Figure 44*.

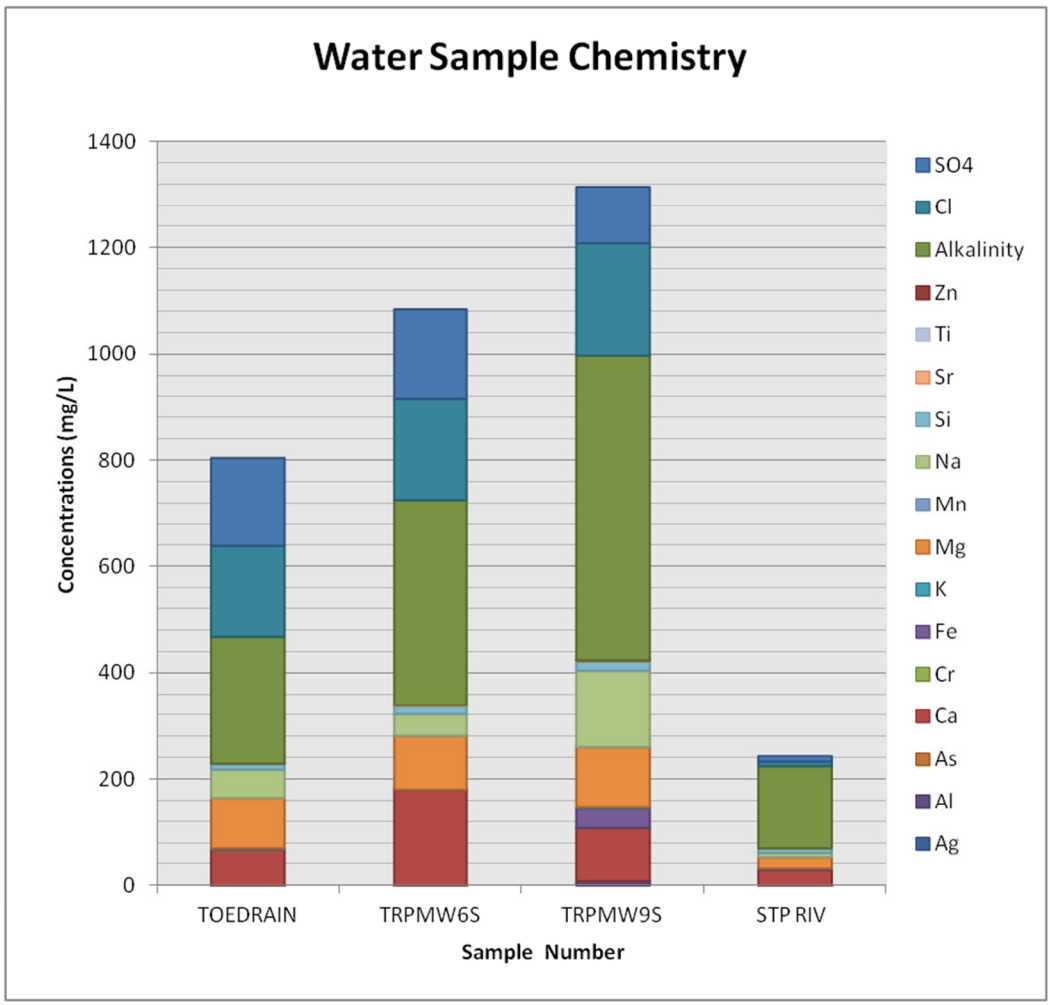

Figure 44: ICP-OES analysis results for collected water samples.

The sample TOEDRAIN was collected from a toedrain of the TSF to give a direct indication of the composition of fluids permeating the tailings. This sample was especially useful in the validation of geochemical models. The samples TRPMW6S and TRPMW9S were collected from shallow monitoring wells between the TSF and the Steelpoort river. Chemical data from these boreholes were expected to give an indication of the chemical evolution of hydro-chemistry in this area, following the drainage direction of the groundwater. The sample STP RIV was collected from the Steelpoort river west of the TSF. The chemical data obtained from this sample would give an indication if any contamination reached the river by groundwater flow and if the river is impacted by this contamination, making it a receptor. The water sampling locations are illustrated in *Figure 45*.

Figure 45: Water sampling positions around the tailings storage facility

Figure 46 illustrates stiff diagrams constructed using the major cation and anion concentrations in the water samples. From these diagrams, it can be observed that Ca and Mg are the most abundant cations in solution but show an abrupt decrease in the STP RIV sample. Abundant anions in each sample are CO_3 and HCO_3. These anions increase with distance from the tailings and are also indicated as alkalinity in *Figure 44*. However, Cl decreases steadily with distance from the tailings and abruptly decreases in the STP RIV sample. The same trend can be observed for SO_4.

Stiff diagrams act as a fingerprint to identify a specific water type. Similar diagrams or logical chemical evolution between diagrams may indicate a link between different samples, indicating a similar chemical fingerprint for each water sample. This may indicate a link between- or similar source area for each water sample. These diagrams appear to show a link between groundwater and surface water in this area with a large dilution factor present in the river, as a logical chemical evolution of the major ions takes place with distance.

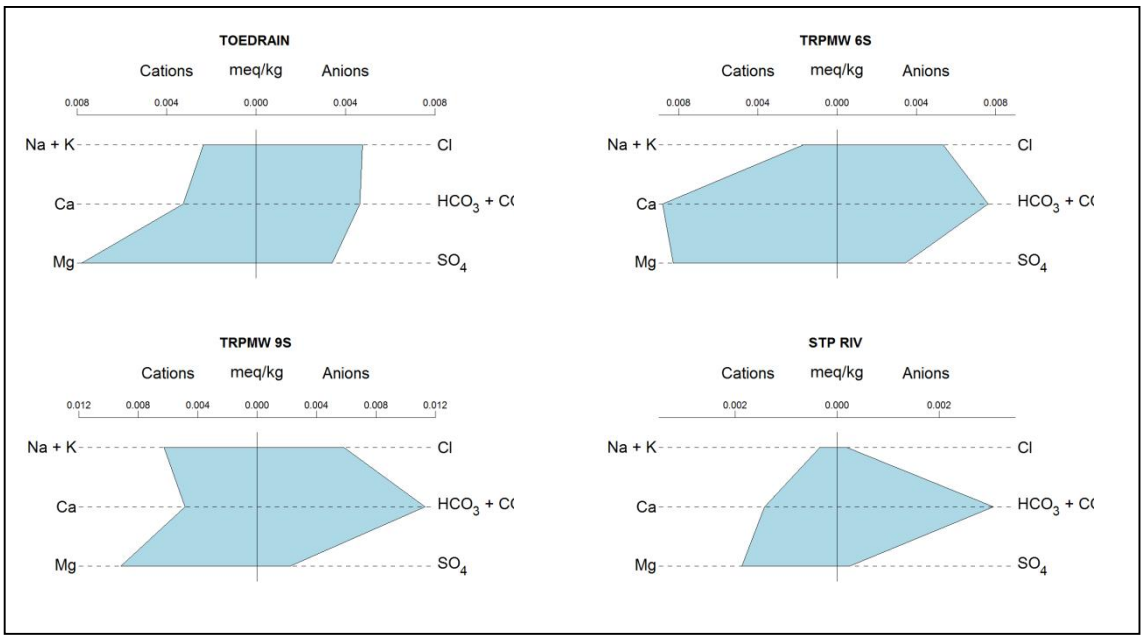

Figure 46: Stiff diagrams of major cations and anions in groundwater and surface water samples

Figure 47 also illustrates this possible link with a Piper diagram. The TOEDRAIN and TRPGWM6S samples plot in the quadrant representing Ca-SO_4 waters. This quadrant represents gypsum groundwaters and mine drainage. The TRPGWM9S and STP RIV samples plot in the quadrant representing Ca-HCO_3 waters. This quadrant represents shallow, fresh groundwaters. It should be noted that the TOEDRAIN and TRPGWM6S samples plot very close to the border line of the Ca-HCO_3 quadrant. This indicates that these samples have been only slightly influenced by mine drainage and if the SO_4 and Cl added from the tailings material were absent, these samples may also plot in the Ca-HCO_3 quadrant. This indicates that these samples may be linked by the same chemical fingerprint and contamination released from the tailings may reach the river. However, higher concentrations of major cations and anions were found in the groundwater as opposed to the river. This may be due to the dilution factor in the river. Therefore, the groundwater is believed to be the pathway in the system and groundwater users may be at higher risk of becoming potential receptors as opposed to river water users.

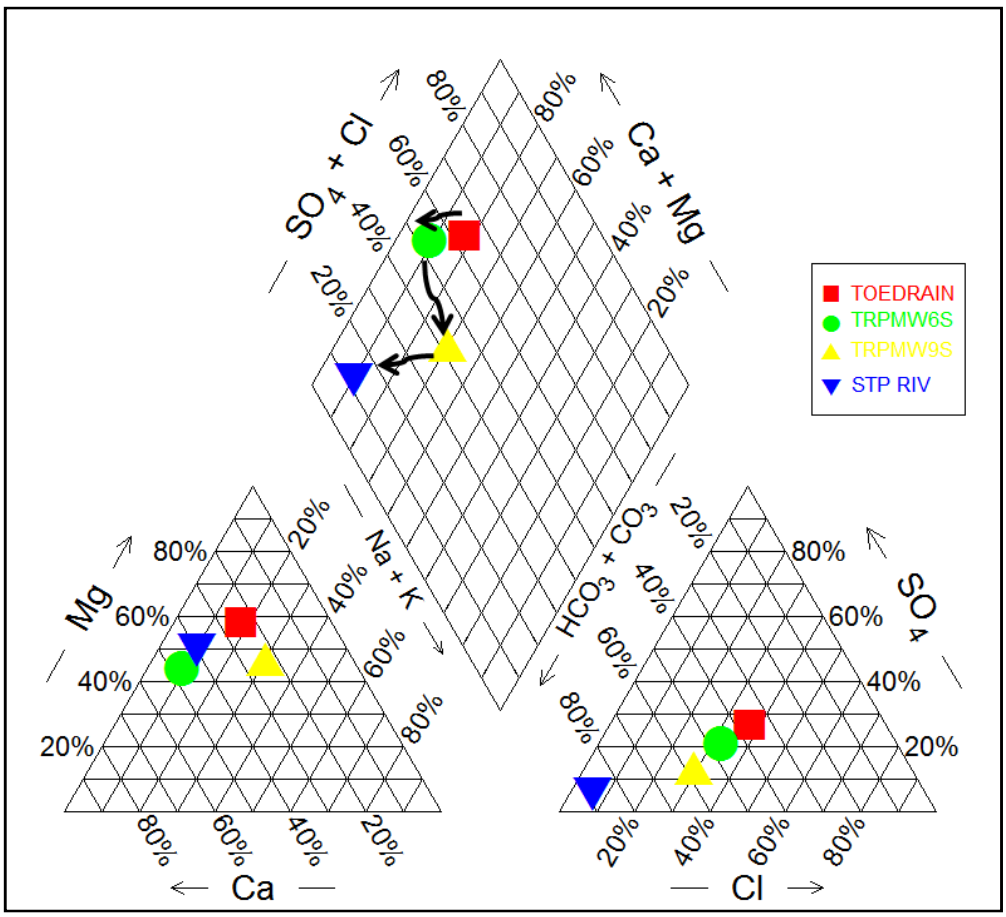

Figure 47: Piper diagram of groundwater sample chemical evolution

5.2 Hydraulic Testing

Hydraulic testing was performed on the tailings material as well as the underlying aquifer in the form of permeameter tests and pumping tests respectively. The values obtained from these tests were used to characterise fluid flow and groundwater flow velocities. The results of each test are described and discussed in the sections below.

5.2.1 Permeameter Tests

The values obtained from the falling head permeameter test are summarised below in Table 13. These values were interpreted to determine the saturated hydraulic conductivity of the tailings material. It is assumed that natural consolidation in the column will mimic field conditions in the TSF. Hydraulic conductivity for the tailings was calculated using the falling head permeameter equation in Craig (2004) and is denoted by the equation below:

$$K = 2.3\frac{al}{At_1}\log\frac{h_0}{h_1} \qquad \textit{Equation 6}$$

A hydraulic conductivity was calculated after each 30 minute interval of flow and an average value of 3.984 x 10^{-09} m.s^{-1} was obtained. This is in accordance with data published by Jorgensen *et al*. (1998) as well as Malmstrom *et al*. (2006).

Table 13: Summarised falling head permeameter test results

Time	Minutes	Seconds	Head (mm)	Drop (mm)	K (mm/s)
09:25	0.00	0.00	1530	0	
10:30	65.00	3900.00	1514	16	5.14568E-06
11:00	30.00	1800.00	1507	23	4.91478E-06
11:30	30.00	1800.00	1502	28	3.52455E-06
12:00	30.00	1800.00	1495	35	4.95413E-06
12:30	30.00	1800.00	1488	42	4.97738E-06
13:00	30.00	1800.00	1482	48	4.285E-06
13:30	30.00	1800.00	1477	53	3.58411E-06
14:00	30.00	1800.00	1471	59	4.31698E-06
14:30	30.00	1800.00	1466	64	3.61095E-06
15:00	30.00	1800.00	1461	69	3.62329E-06
15:30	30.00	1800.00	1456	74	3.63571E-06
16:00	30.00	1800.00	1451	79	3.64822E-06
16:30	30.00	1800.00	1448	82	2.19497E-06
17:00	30.00	1800.00	1444	86	2.93371E-06
17:30	30.00	1800.00	1438	92	4.41584E-06

This is indicative of a slow flow rate of water through the tailings material of an approximate order of magnitude of 10^{-4} m.d^{-1}. The amount of fluid that may discharge from the saturated tailings material (Q) was measured at approximately 0.34 L.d^{-1} through a cross sectional area of 1m^2, under a hydraulic gradient of approximately 1. However, the tailings material may not reach saturation throughout the profile under natural conditions. Therefore, the fluid discharged from the tailings may be less than 0.34 L.d^{-1} through the above mentioned cross sectional area and hydraulic gradient, as completely saturated flow does not necessarily occur throughout the tailings.

5.2.2 Pumping Tests – AQTESOLV

Two pumping tests were conducted on two monitoring wells adjacent to the TSF between 14 and 16 March 2012. The pumping test data was analysed to obtain hydraulic conductivity values for the underlying fractured aquifer using AQTESOLV software. The data obtained for TRPGWM06S is graphically illustrated below in *Figure 48*. The data obtained from this pumping test, conducted on the monitoring well closest to the tailings facility, was fitted with the Gringarten-Witherspoon curve assuming a single vertical fracture at depth. This method was chosen based on its provision of a hydraulic conductivity value for a fractured aquifer and provided a better fit than the Moench method. The underlying aquifer is also known to be fractured as it is composed of igneous rock, further supporting the use of this method. The curve provided by this method was fitted to the late time data to ensure that the hydraulic conductivity of the aquifer was calculated instead of the well bore storage. This yielded a K-value in the order of 0.46m/day for the underlying fracture network, assuming an anisotropy ratio of 0.5 between the horisontal and vertical axes.

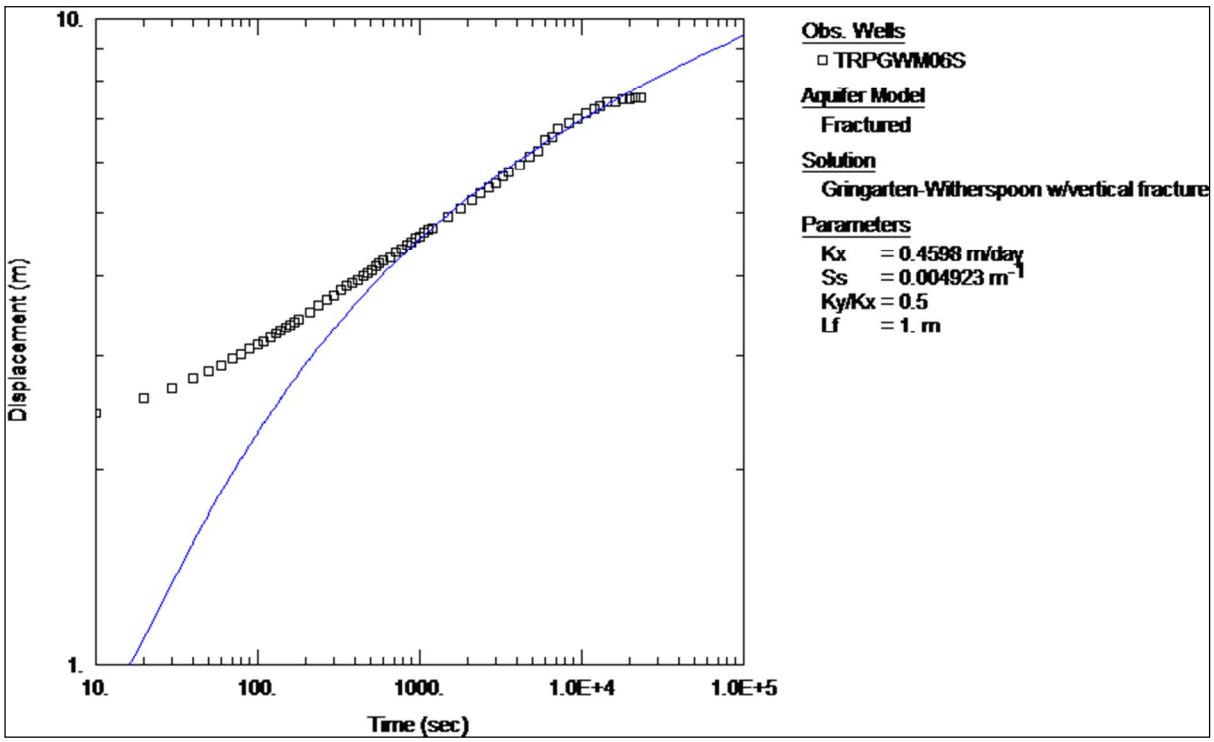

Figure 48: Pumping test data for TRPGWM06S fitted with Gringarten-Witherspoon on logarithmic axes

The linear flow velocity (equation below) in this portion of the aquifer was calculated as 0.015m/d of flow (Craig, 2004).

$$v = \frac{Ki}{\eta}$$ *Equation 7*

Where:

K: hydraulic conductivity
i: hydraulic gradient which is 0.0066 (calculated based on topography)
η: assumed porosity of 20% (comparatively low-conservative scenario)

This indicates a slow flow rate for groundwater in this portion of the aquifer and any accompanying contaminants may be transported at a rate equal to or slower than this rate. However, the properties of the aquifer will influence these flow and transport rate. This can be deduced from *Figure 49*. The flattening of the derivative curve around 10000 seconds and the abrupt dip in values that follows is indicative of a dual porosity aquifer. Therefore, components of a fractured and weathered aquifer system are both present in this portion of the aquifer and may influence the linear flow velocity of groundwater in different portions of the aquifer depending if the water moves through a more weathered, or more fractured portion.

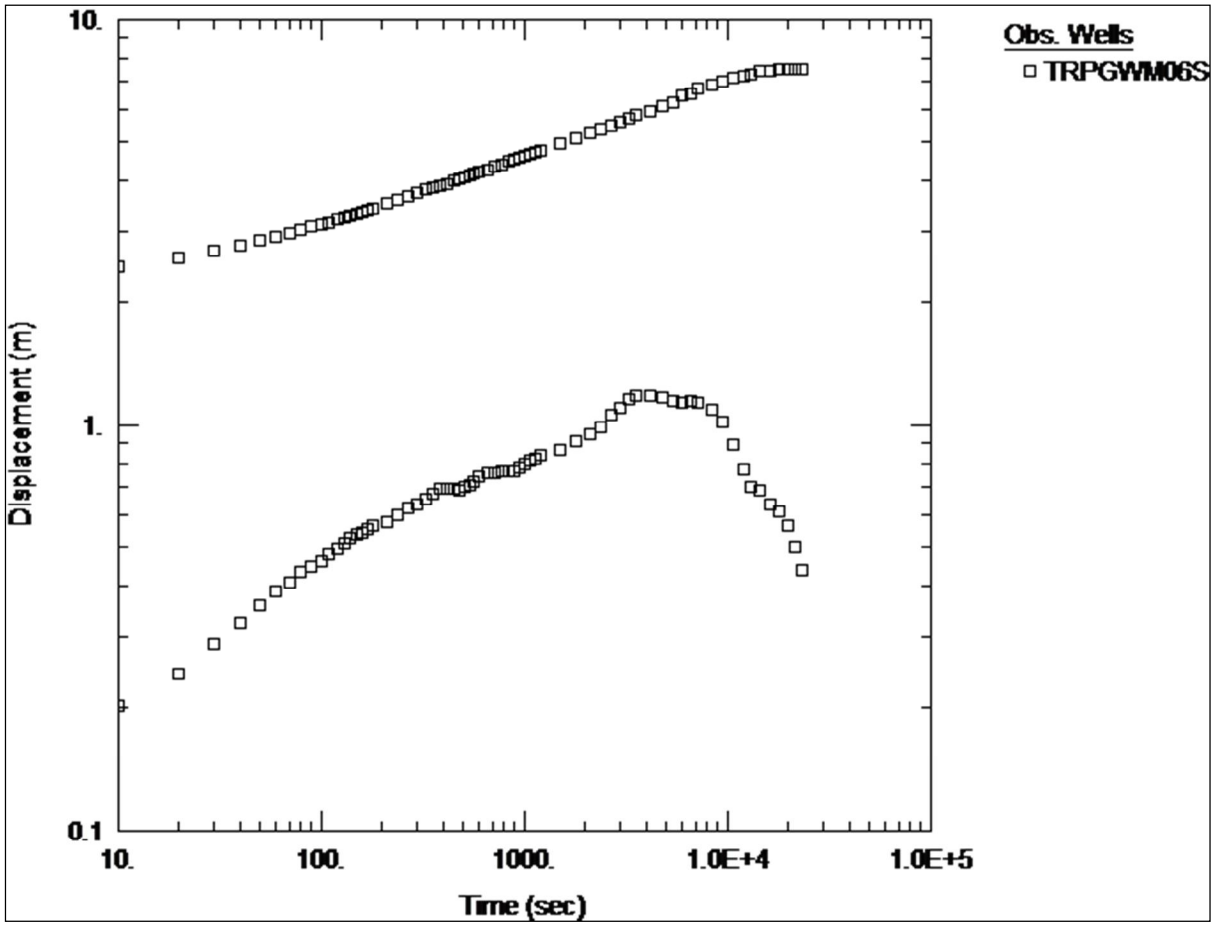

Figure 49: Derivative plot of TRPGWM06S

When comparing this information with that of TRPGWM09S, a slightly different situation is observed. This is indicated by *Figure 50*, which illustrates the pumping test data for the monitoring well TRPGWM09S. This well is situated closer to the Steelpoort river and further from the tailings facility. The data was also fitted with the Gringarten- Witherspoon curve for a single fracture, but provided a lower hydraulic conductivity in the order of 0.026m/day. The curve was also fitted to the late time data to ensure the representative calculation of the aquifer hydraulic conductivity, but used an anisotropy ratio of 0.1 between the vertical and horisontal axes. This improved the fit of the curve considerably but should be noted as an assumption. The linear flow velocity for this portion of the aquifer was calculated as 8.6×10^{-4} m/day, using the same assumptions for that of TRPGWM06S. This indicates a much slower rate of movement of groundwater than in the TRPGWM06S portion of the aquifer. It also indicates a much slower rate of contaminant advection due to groundwater stagnation and a higher salt load as indicated by *Figure 44* and *Figure 47*.

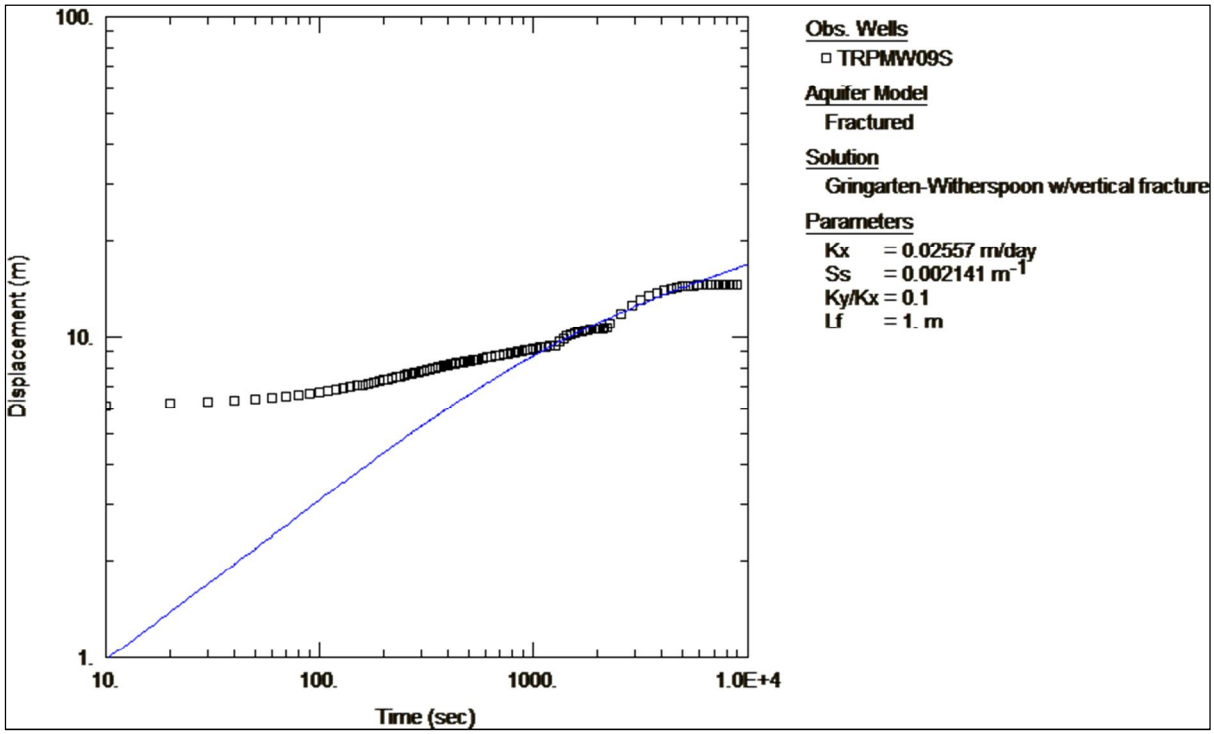

Figure 50: Pumping test data for TRPGWM09S fitted with Gringarten-Witherspoon

Another point to note in this figure is the doubling of the slope of the data at approximately 1000 and 2000 seconds. This change in the data's slope is possibly indicative of a low to no flow boundary encounter. The first doubling of the slope is believed to possibly indicate the Dwarsriver fault which is situated east of this monitoring well at a distance of approximately 550m. The second doubling of the slope may be a possible encounter of a second fault or could possibly indicate the encountering of the Steelpoort river. This may be supported by the levelling out of the data to provide a constant head reading around 10000 seconds with the waterlevel reaching 10.26m below groundlevel, close to the elevation of the river which is located at approximately 4m below the initial waterlevel in the borehole, measured at 5.95m. This may possibly indicate a hydraulic connection between the river and the aquifer, but more extensive pumping tests from more boreholes along the river are required to prove this conclusively.

Figure 51, the derivative plot of the data from TRPGWM09S, does however indicate that a fracture or fault structure was encountered between 1000 and 3000 seconds. The abrupt splitting of data and sharp slope change indicates a fracture or fault structure was encountered after which the water level became constant at around 4000 to 5000 seconds. The dip in derivative data between 300 and 1000 seconds indicates, similarly to that of TRPGWM06S, a dual porosity system. Therefore, components of a fractured and weathered aquifer system are also present in this portion of the aquifer at shallower depths and may influence the linear flow velocity of groundwater in different portions of the aquifer depending if the water moves through a more weathered, or more fractured portion.

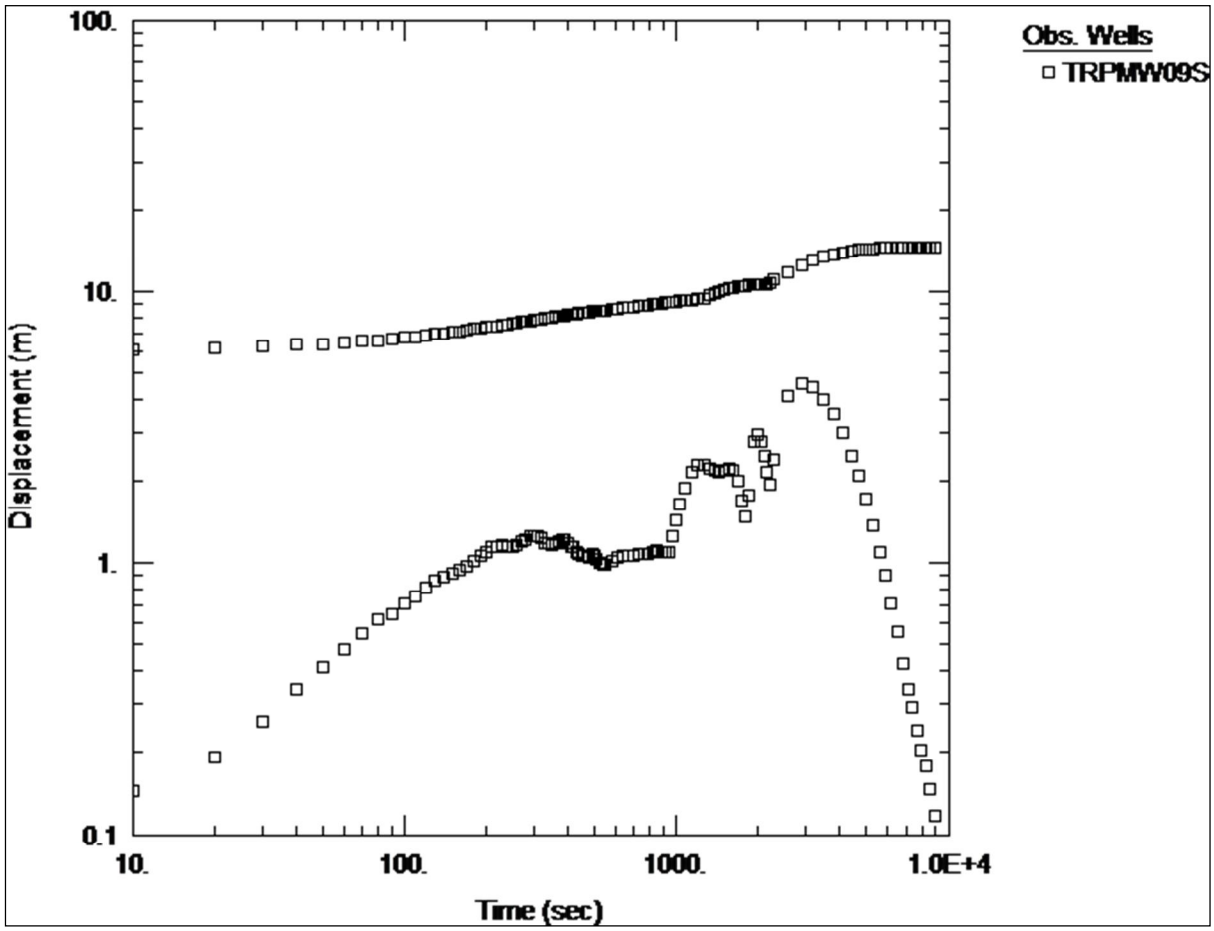

Figure 51: Derivative plot of TRPGWM09S

5.3 Geochemical and Unsaturated Flow Modelling

5.3.1 Geochemical Modelling – The Geochemist's Workbench

The modelling software used to determine the chemical changes taking place during fluid movement through the tailings-surface interface is The Geochemist's Workbench ©. The modelling software was used to calculate the breakdown of specific minerals, thought to be contributors to dissolved chemical components in groundwater and surface water, over a specified time period. This would give an indication of the geochemical processes taking place in the tailings causing contaminant release.

5.3.1.1 Model Construction and Assumptions

The model was constructed under the assumption that:

- Talc and chlorite are the phases most prone to breakdown as they are secondary in nature and may break down more rapidly than primary igneous minerals
- Chalcopyrite is considered to be prone to oxidise and dissolve readily in relation to primary igneous silicate minerals

- Oxygen fugacity from within the tailings to surface increases
- Oxygen fugacity from within the tailings to the aquifer decreases
- pH of the fluid in the tailings is slightly alkaline
- The leaching test values are a dilute representation of pore fluid within the tailings material
- Primary silicate phases as well as the chromite phase are practically insoluble in the scale of investigation based on literature values

The model was constructed using data from the acid leach tests, XRD analyses, ICP scans and literature, as follows:

- The acid leach test results were concentrated 20 times. The fluid to rock ratio in the leach test was noted as 20:1. Therefore, it was thought to be a reasonable assumption that the concentration of these values up to 20 times would give an indication of tailings pore fluid compositions as the leach test mobilises and dilutes pore fluids from a sample.
- The amount of fluid available for reaction was assumed to be an average of the measured gravimetric water content from the direct push probe samples for simplicity as the model would be a bulk composition simulation. This equated to 0.075kg of fluid per kg of rock material.
- The amounts of talc and chlorite present were taken as the average weight percentage throughout the tailings for simplicity as the model would be a bulk composition simulation. Rate constants were assigned to the phases as presented by Saldi *et al*. (2007) and Lowson *et al*. (2004) respectively.
- The amount of chalcopyrite present was taken as 0.01kg per kg of rock. This was assumed based on petrographic data as well as the acid-base accounting results. A rate constant was assigned to chalcopyrite as presented by Rimstidt *et al*. (1994)
- Oxygen fugacity was set to 2 orders of magnitude lower than the average atmospheric value of 0.21 to simulate a conservative case. The model was fitted with a sliding oxygen fugacity from 0.002 to atmospheric value to simulate discharge of the fluid from the tailings to the toedrain. A separate model was fitted with a sliding oxygen fugacity from 0.002 to 10^{-50} as a conservative case to simulate increasingly reducing conditions as tailings fluids discharge into the underlying fractured aquifer.
- After several model runs, a best fit of 60g of water addition upon discharge from the tailings was found to provide the best result, in terms of the short term calibration of the model to best provide long term calculations, and was therefore noted as an assumption.
- The concentrated leach test data was compared with the ICP analysis of the TOEDRAIN sample as well as the TRPGWM6S sample to determine the changes in fluid composition as illustrated in Figure 52. This data was used to calibrate the model to determine the neo-mineralised phases forming in and on the tailings, as well as the rate of mineral breakdown and contaminant input.
- The model was constructed to calculate geochemical changes within a 100 year period, to predict future concentrations of contaminants released from the material, with short term model runs only used for model calibration.

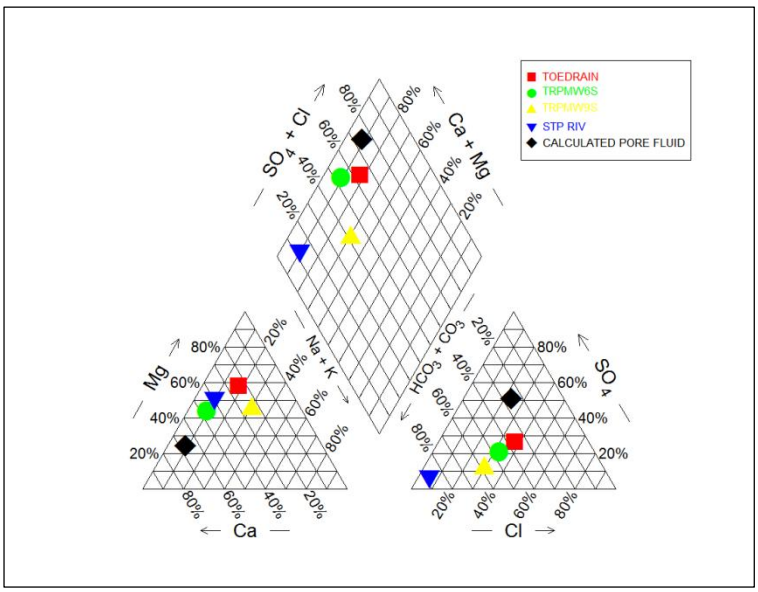

Figure 52: Piper diagram comparing groundwater, toedrain, river and tailings pore fluid compositions

5.3.1.2 Mineral Stability

The model constructed under the above mentioned assumptions calculated an immediate change in mineral abundances indicating breakdown as illustrated by *Figure 53*.

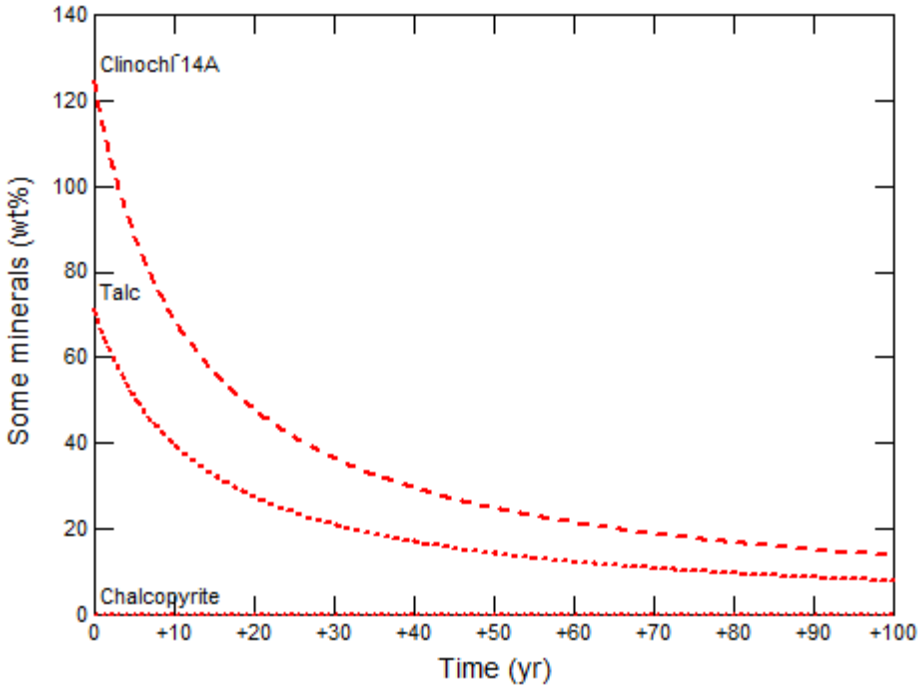

Figure 53: Modelled mineral phase breakdown

Figure 54: Precipitated salts and minerals on the tailings bank

This indicates that increased oxygen fugacity and fluid may accelerate mineral breakdown supporting the well known shrinking core model commonly used in tailings studies. Minerals exposed to atmospheric conditions and constant saturation may therefore produce more contaminants and salts as indicated by *Figure 54* which illustrates precipitated salts and discolouration on the saturated lower bank wall of the TSF.

According to the modelled data and factoring assumptions into account, talc, chalcopyrite and chlorite may be the major contributors to contamination in the short term. However, primary silicates and chromite may increase the contaminant load released from the material in the long term due to increased mineral breakdown and oxygen ingress.

The phases calculated by the model to form are illustrated below in *Figure 55* and *Figure 56*. The major phases calculated to form within the modelling period are gibbsite and a crystalline $CuFeO_2$ species. Gibbsite may possibly be derived from chlorite weathering and is precipitated from the solution as it has an alkaline pH value and no buffering Al is required to boost solution pH. This may also explain the low Al concentration in the analysed toedrain fluids. The $CuFeO_2$ phase, however, is considered less likely to form as intermediate salts are more likely to precipitate.

.

Goethite precipitation may also contribute to the lowering of the Fe-concentration in the toedrain sample and is also interpreted to be a possible precipitate of Fe in solution. Nontronite and beidellite are smectitic clay species which may form from the continuous alteration of chlorite and have a similar structure to this phase. However, talc may play a larger role in the formation of magnesian beidellite as this is a direct source of Mg. Calcic clinoptilolite is a low temperature zeolite and is interpreted to form at the base of the tailings where temperatures and pressures are elevated and may be a product of chlorite alteration.

The most likely phase to form from the permeating tailings pore fluid, which is also indicated by these figures, is predicted to be calcite. This phase may form due to the abundant Ca in the pore fluid solution and the possible change in CO_2 fugacity upon discharge from the tailings. This may also be substantiated by *Figure 54* which indicates precipitated salts on the tailings bank. Gypsum may also be a possible composition for these salts but is thought to be unlikely as the salts are only encountered on surface where a change in gas fugacity takes place which is not a driving force in the precipitation of gypsum.

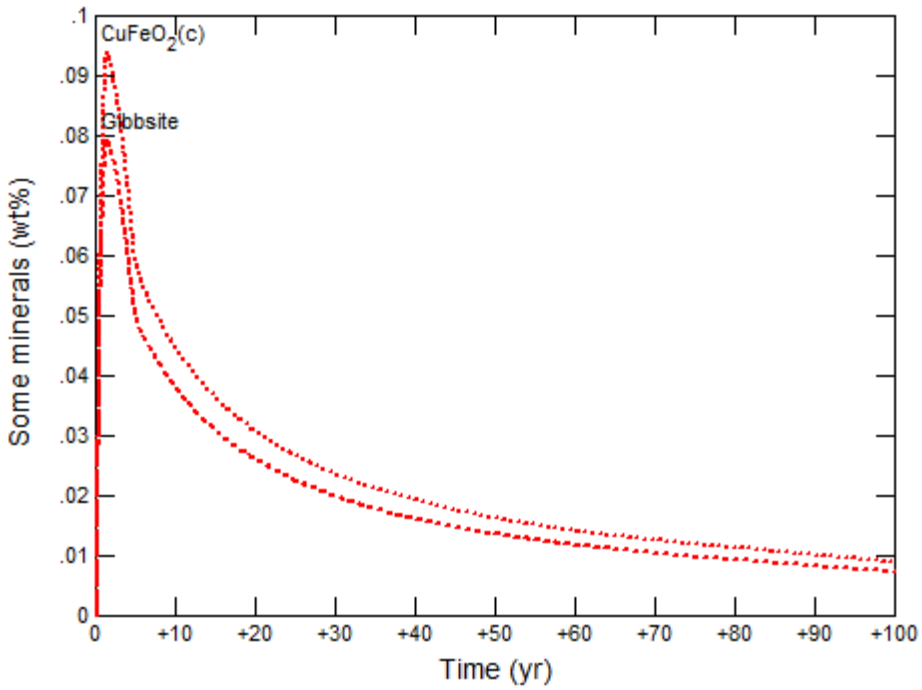

Figure 55: Model-calculated precipating major mineral phases

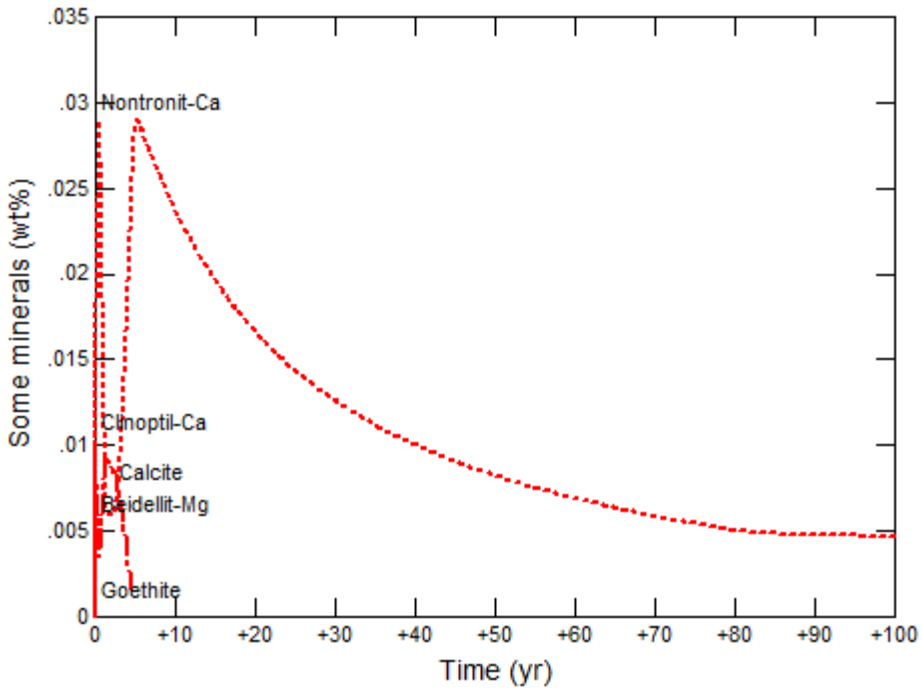

Figure 56: Model-calculated precipitated minor mineral phases

5.3.1.3 Liberated Contaminants

The modelled contaminants to be released from the tailings were a calibration of the model itself with respect to the pore fluid composition and the compositions of the TOEDRAIN and TRPGWM6S samples. However, it should be noted that these samples give a good indication of the composition of pore fluid discharge and contamination from the tailings and are therefore taken to represent the contaminant release from the material.

The modelled contaminant release is illustrated below in *Figure 57*.

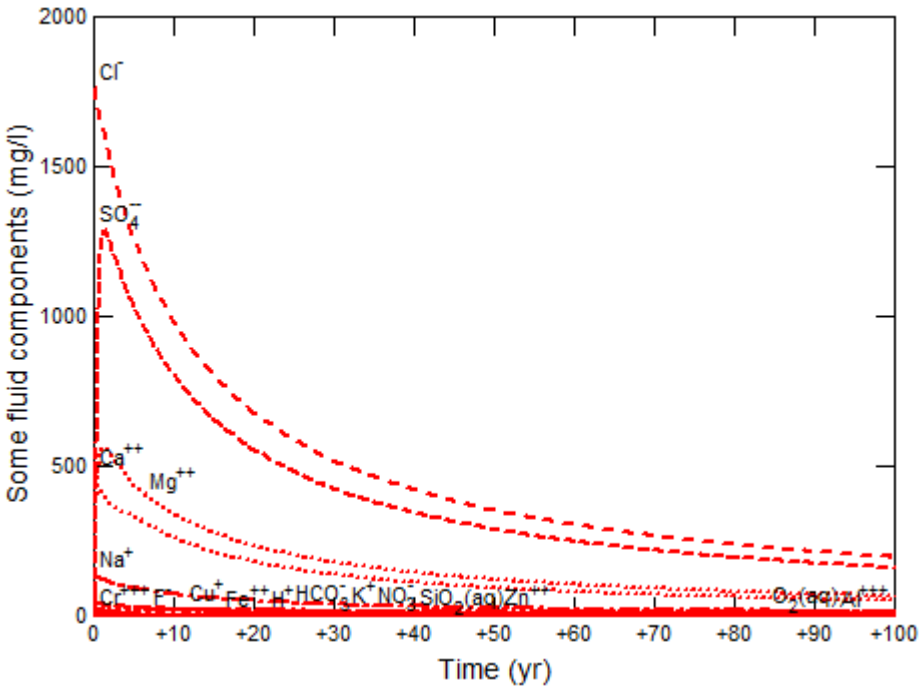

Figure 57: Modelled contaminant release from the tailings material as mg/L of constituents in contaminated water

This figure is of particular importance as it validates the model. The concentrations obtained from this model run were correlated with concentrations from the TOEDRAIN sample as well as the TRPGWM6S sample as illustrated in *Table 14* and *Figure 58*, as well as *Table **15*** and *Figure 59* respectively. Each data point was fitted with a standard error to determine if the sample concentrations and model concentrations correlate well within statistical error boundaries. The modelled concentrations were found to correspond well with the analytical values and the results obtained for mineral phase precipitation, formation and breakdown are therefore thought to be valid.

Table 14: Modelled and analysed concentrations of chemical constituents in TOEDRAIN sample

Constituent	Model (mg/L)	Analysed (mg/L)
Ca	52.49	66
Mg	76.28	96
SO_4	161	165
Cl	195.7	171
Al	0.05	0.156
Cr	0.04	0.025>
K	4.3	1.7
Si	2.7	9.5
NO_3	3.7	1.6

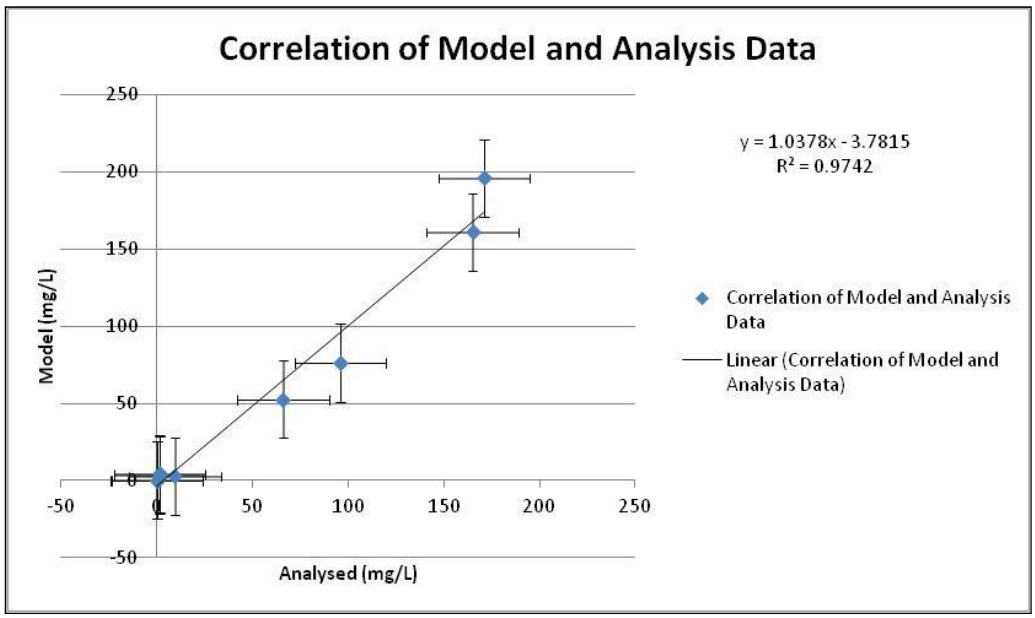

Figure 58: Correlation of modelled and analysed concentrations of chemical constituents in TOEDRAIN sample

Table 15: Modelled and analysed concentrations of chemical constituents in TRPGWM6S sample

Constituent	Model (mg/L)	Analysed (mg/L)
Ca	69.15	179
Mg	53.02	102
SO4	161.6	168
Cl	195.2	192
Al	0.02	0.177
Cr	0.04	0.025>
K	4.3	1.0>
Si	1.168	14.6
NO3	4.73	11

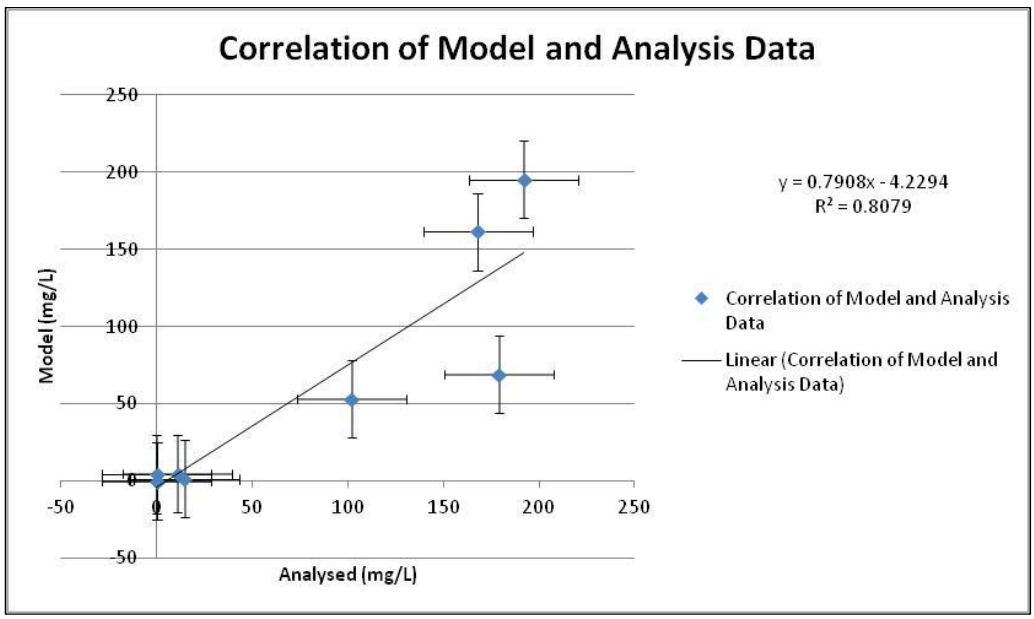

Figure 59: Correlation of modelled and analysed concentrations of chemical constituents in TOEDRAIN sample

5.3.2 Unsaturated Flow Modelling – HYDRUS

The modelling software used to determine the unsaturated hydraulic properties of the tailings material is HYDRUS1D 4. The model was used to calculate cumulative rainfall infiltration over a ten year period; change in water content over a period of ten years considering past meteorological data; water content at specified observation nodes in the profile over a ten year period; hydraulic conductivity of the material and underlying vadose zone at different degrees of saturation; and fluid flux from the bottom of the tailings. The modelled values are graphically illustrated and discussed in the following section.

5.3.2.1 Model Construction

The model was constructed using data measured from the direct push probe samples obtained from the TPH sampling point. Gravimetric water contents were measured from each sample tube and are summarised in *Table 16*.

Table 16: Measured gravimetric water contents from the TPH sampling locality

Sample Depth	Material Type	Initial Mass	Dry Mass	ΔMass	Gravimetric Water Content
0-1.2	Tailings	21	20.5	0.5	2.380952381
1.2-2.4	Tailings	17	16	1	5.882352941
2.4-3.6	Tailings	22	20	2	9.090909091
3.6-4.8	Tailings	31	30	1	3.225806452
4.8-6	Tailings	32	30	2	6.25
6-7.2	Tailings	38	34	4	10.52631579
7.2-8.4	Tailings	26	24	2	7.692307692
8.4-9.6	Tailings	29	24	5	17.24137931
9.6-10	Gravelly Sand	17	16	1	5.882352941

The tailings material is known to be of a -86µm grading and was therefore classified as a silty clay in soil terms. The underlying soil in the natural vadose zone was found to be a coarse gravelly sand.

Once these parameters were ascertained, the unsaturated flow model was constructed as follows:

- The sole simulation to be performed by the model was specified as water flow. Heat-, vapour- and CO_2 transport was not a modelling objective and was therefore omitted.
- Two sediment materials were specified, each representing the tailings and underlying soil. The combined depth of the materials in the profile was specified as 10m with measurement units specified as meters.
- Time units were specified as years with a starting time of 0 and an ending time of 10. Default values were used for maximum-, minimum- and initial time step. Ten years was chosen as the model simulation time based on the saturated hydraulic conductivity calculated from the falling head permeameter testing. Theoretically, under saturated conditions, this would be the time frame for contaminated fluid to move from the top, to the base of the tailings.
- The number of time variable boundary conditions was specified as ten. These conditions represent rainfall data.
- Default values were used for the printing information section as well as in the iteration criteria section. However, in iteration criteria section, water content tolerance was specified as 0.0001 to allow the model to run to a value near desiccation if required.

- The mobile-immobile dual porosity hydraulic model with water content and mass transfer was used to simulate flow as two sediment materials exist in the profile.
- The sediment hydraulic parameters were chosen based on the sediment characteristics such grading, bulk density and saturated hydraulic conductivity. This was performed using the neural network prediction function of HYDRUS.
- The upper boundary condition of the profile was specified as Atmospheric BC with surface runoff with a free draining lower boundary condition as the underlying soil material is coarser than the tailings material. The initial condition of the system in terms of fluids was specified in water contents.
- The graphical discretisation tool of HYDRUS was used to discretise the water content- and material distribution of the profile as well as to specify model observation nodes at 1m intervals in the profile.

5.3.2.2 Model Execution and Results

After model construction was completed, the model was executed and the following parameters were calculated and interpreted with respect to the tailings storage facility. The model was constructed to illustrate a conservative scenario which assumes complete infiltration of rainfall.

Cumulative Rainfall Infiltration

Assuming a completely unsaturated top of the tailings material, the infiltration of rainfall would take place rapidly and infiltrate into deeper levels in the TSF profile. This is directly linked to the amount of rainfall in a particular year of the simulation. The time dependent boundary condition linked to rainfall in the simulation, was based on the mean annual precipitation of the area since 2001. Therefore, a curve can be observed indicating similar trends to rainfall per year. Evaporative losses were omitted from the calculation to create a conservative scenario indicating the maximum amount of fluid recharged into the tailings. Based on these assumptions, the model calculated a maximum cumulative rainfall infiltration of approximately 3500mm per decade. This is illustrated in *Figure 60*.

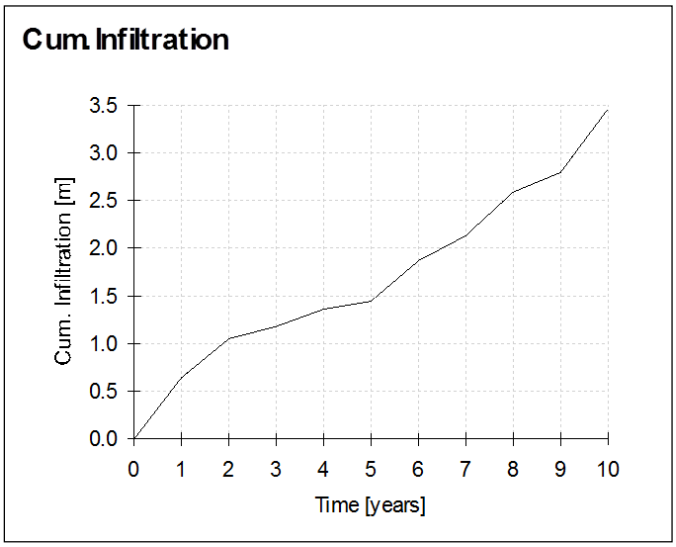

Figure 60: Cumulative rainfall infiltration per decade for the tailings material

Change in Water Content Considering Past Meteorological Data

Initial soil moisture content was specified at different depths in the soil profile as mentioned in the model construction section. However, when simulating rainfall events in the model, these moisture contents vary due to the infiltration of rainwater and percolation through the profile. This variation is illustrated by *Figure 61*, where water content is illustrated with depth for each year of the simulation. Each year is indicated by a different colour and T-value in the legend. As illustrated, the void space, which was assumed to be between 20 and 30% for the tailings material grading by the model, becomes completely filled with fluid after the ten year duration of the model simulation. The coarser underlying soil material also becomes saturated after 7 years in the simulation. This could be explained by the smaller porosity of the coarser material allowing for less fluid to saturate the material.

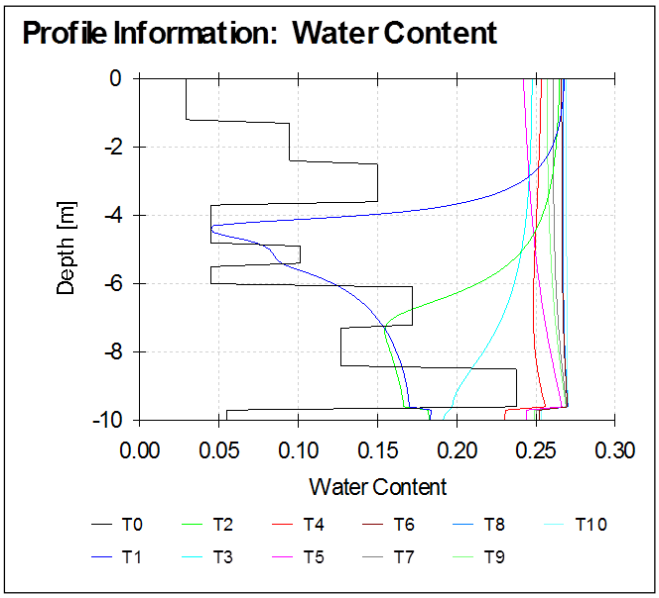

Figure 61: Tailings water content at different depths and times

The possible reason for the saturation of the material will be explained in the following sections. Another important simulation pertaining to the material water content, as generated by the model, is graphically illustrated in *Figure 62*. This figure illustrates the water contents present at each specified observation node in the profile with time. Each node number is denoted by the prefix N. It can be observed that the curve for each node moves sequentially forward relative to the time axis in a chronological order while the curve also indicates an increase and decrease in water content with time with a similar trend to that of annual rainfall. The sequential shifting of each curve may possibly indicate a piston flow regime with water movement taking place due to a change in pressure head by infiltration. The data can also be observed to contain an inverse logarithmic trend indicating faster infiltration at the top of the profile and slower infiltration lower in the profile due to higher degrees of saturation. Node ten can also be observed to have an anomalous curve which indicates the saturation of the underlying soil material at a lower water content and is illustrated well relative to node 9 which is located at the bottom of the tailings material. Node nine also shows an anomalously high final water content. This is due to ponding of fluids at the boundary between the coarser and finer sediments due to higher suction values in the tailings material.

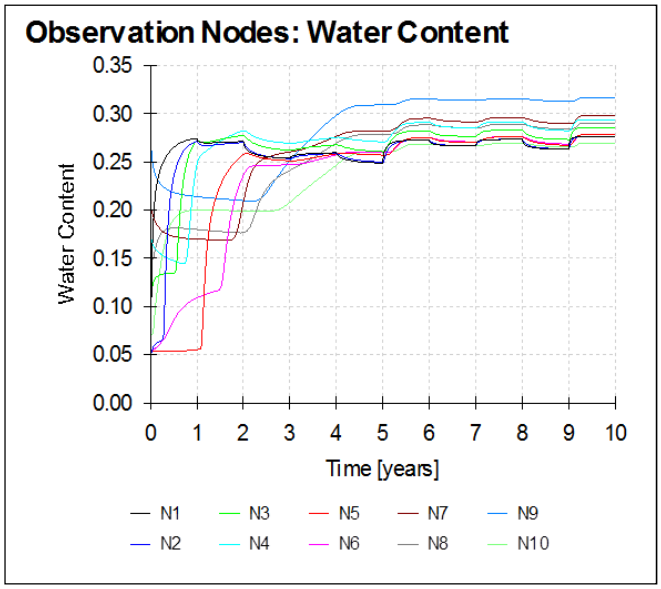

Figure 62: Water content at profile observation nodes at different simulation times

Cumulative Bottom Flux

The cumulative fluid flux from the bottom of the tailings is a function of the cumulative infiltration and the change in fluid content stored pore as pore water in the tailings. This parameter is important to quantify the possible amount of leachate released from the tailings into the vadose zone and possibly the groundwater. Assuming complete infiltration of rainfall as well as the possibility of changes in pore fluid content, the model calculated an average cumulative discharge of 1.9m per decade, from the base of the tailings, as indicated by *Figure 63*. This indicates approximately 0.19m of discharge per year through a cross-sectional area of $1m^2$. Therefore, approximately $190L/m^2/y$ of leachate is released through the foot of the tailings as a conservative scenario, completely discounting lateral fluid discharge. However, as it is known that tailings water is released through the tailings wall into toedrains, the volume of leachate released into the groundwater environment is expected to be significantly less.

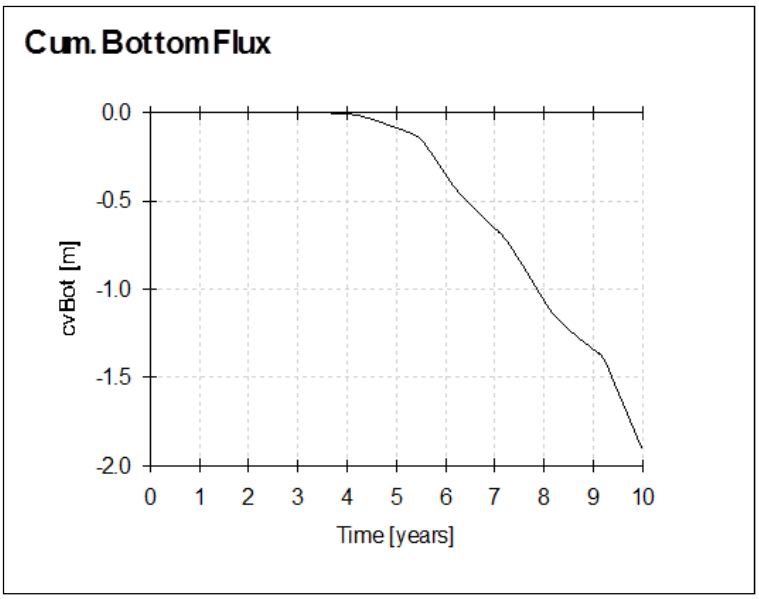

Figure 63: Cumulative fluid flux from the foot of the tailings as a conservative case

Unsaturated Hydraulic Conductivity

The saturated hydraulic conductivity was measured to be approximately 1.2m/decade ($3.29x10^{-4}$m/d). Based on the textural class and moisture contents of the tailings profile and assuming a porosity of 25%, the model predicted a hydraulic conductivity value in the same order of magnitude, for the saturated tailings profile. The model was therefore assumed to be acceptably representative based on its agreement with experimental data. The model also calculated unsaturated hydraulic conductivities for the tailings material and based on the varying degrees of saturation from the top to the bottom of the tailings, water could be conducted through the material at rates of between 10^{-8} m/decade and 1m/decade. These values were calculated between water contents of approximately 5 and 27% respectively. This is illustrated by *Figure 64* in which M1 represents the tailings material.

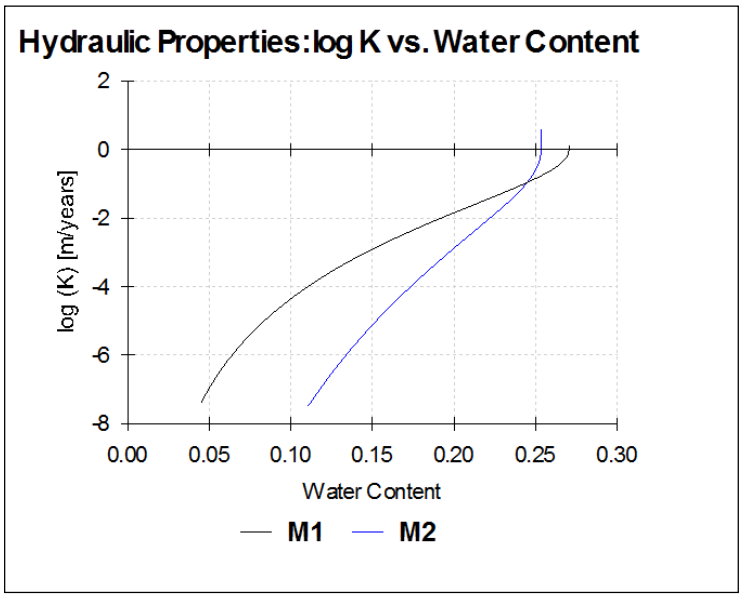

Figure 64: Unsaturated hydraulic conductivities at different water contents in the tailings material (M1) and the underlying, natural gravelly sand vadose zone (M2)

M2 in *Figure 64* illustrates the underlying gravelly sand of the natural vadose zone. Water is predicted to move at faster rates at higher degrees of saturation and slower rates at lower degrees of saturation in this material. The natural vadose zone is therefore less conductive than the tailings at most pore water content values below approximately 24% which may explain the fluid ponding in the lower areas of the tailings profile. The unsaturated hydraulic conductivity of the underlying vadose zone was calculated to range between 10^{-8} m/decade and $10^{0.5}$m/decade. These values were calculated for water contents ranging approximately between 11 and 26% respectively.

6. CONCLUSIONS

Based on the data collected; analyses and tests performed; assumptions and interpretations made; and models calculated, the following conclusions could be made:

1. The chemical composition of the tailings material is dominated by the major elements Mg, Ca, Fe, Si, Al and Cr based on XRF results. The dominant trace elements contributing to the tailings material composition are Sc, Ni, Zn and Co.
2. The mineralogical composition of the tailings material consists of the following:
    - Annite $KFe_3(Al, Si)_3O_{10}(OH, F)_2$
    - Anthophyllite $(Mg_{0.76}, Fe_{1.24})(Mg_{4.95}, Fe_{0.05})Si_8O_{22}(OH)_2$
    - Diopside $(Ca, Mg)Si_2O_6$
    - Enstatite $(Mg_{1.568}, Fe_{0.432})Si_2O_6$
    - Magnesiohornblende $Na_{0.46}Ca_{1.7}Mg_{3.44}Fe_{1.72}Al_{1.08}Si_{6.92}O_{23}(OH)$
    - Lizardite $Mg_3Si_2O_5(OH)_4$
    - Chromite $NiCr_2O_4$
    - Anorthite $CaAl_2Si_2O_8$
    - Talc $Mg_3Si_4O_{10}(OH)_2$
    - Chlorite (Clinochlore) $Mg_{5.1}Al_{1.2}Si_3Cr_{0.7}O_{10}(OH)_8$
    - Phlogopite $KMg_3(Al, Si)_3O_{10}(OH,F)_2$
    - Muscovite $KAl_3Si_3O_{10}(OH)_2$
    - Tremolite $Ca_2Mg_5Si_8O_{22}(OH)_2$
    - Chalcopyrite $CuFeS_2$
3. The dissolution potential of the mineral phases is considered to be low even under oxidising, saturated conditions as the alkaline fluid draining through the tailings material favours slightly lower reaction rate constants. This causes primary minerals to break down in a geological time scale, superseding the scale of investigation as well as the life of mine. However, alteration phases such as talc and chlorite as well as the sulphide phase, chalcopyrite, are likely to break down in the scale of investigation. This may form precipitated salts, clay minerals and possible low temperature zeolites at the interface between the tailings and earth surface conditions.
4. The major contaminants released by the tailings material are Ca, Mg, SO_4 and Cl which may increase groundwater salinity, but due to groundwater alkalinity, the probability of acid rock drainage formation is low. Trace heavy metal contamination is considered unlikely as these elements were either undetected or detected in low concentrations in toedrain fluids. These trace metals are mainly associated with the chromite phase which is considered practically insoluble in the tailings redox conditions. Chromite is considered to break down in reducing, acidic conditions, both of which were not found to be present in the tailings storage facility.
5. The fluid discharge from the tailings was identified as 2m per decade with ingress of 3m per decade from rain water. The hydraulic conductivity of the tailings material was found to range between 10^{-8} and 1m/decade. These values were calculated between water contents of approximately 5 and 27% respectively. The unsaturated hydraulic conductivity of the underlying vadose zone was calculated to range between 10^{-8} and $10^{0.5}$m/decade. These values were calculated for water contents ranging approximately between 11 and 26% respectively. Fluid and contaminant movement through the tailings material is considered as porous medium flow.

6. The hydraulic conductivity of the aquifer was found to be 0.46m/d in the area of the aquifer underlying the tailings. The hydraulic conductivity of the aquifer was found to be 0.026m/d in the area of the aquifer closer to the Steelpoort river. Two no flow boundaries were encountered during the pumping tests which were interpreted as part of the Dwarsriver fault system. The second derivative of the pumping test curves indicated that the aquifer is a dual-porosity system. However, water and contaminant movement is considered predominantly as fracture flow.

The interconnection between the fractured rock aquifer underlying the tailings storage facility and the tailings material is evident in the water chemistry analysed. A contaminant load is imposed on the aquifer by permeating fluids. This contaminant load is generated by geochemical processes causing mineral breakdown in the tailings material. However, no acid rock drainage is likely to form and no significant heavy metal contamination is likely to take place. Based on the study, only groundwater salinity will be elevated by discharge of the chemical constituents released by geochemical processes from the tailings material. The Steelpoort river also shows a different chemical signature than the groundwater and tailings fluids which; along with the increase in chemical concentrations in the groundwater closer to the river, indicating stagnation and evaporation; as well as no flow boundaries indicated by pumping tests; indicates that the river may not be significantly impacted by chemical discharge from the tailings.

7. REFERENCES

1. Appelo, C.A.J., 2010, Geochemistry, Groundwater and Pollution, A.A. Balkema Publishers, Leiden, Netherlands

2. Bear, J., Bachmat, Y., 1967, *A Generalised Theory on Hydrodynamic Dispersion in Porous Media*, IAHS Publ. no. 72, 524 pages, pp. 7-16

3. Bethke, C. M., 2011, *Geochemical and Biogeochemical Reaction Modelling*, Cambridge University Press, pp. 397-400

4. Bowen, N. L., 1928, *The Evolution of Igneous Rocks*, Princeton University Press, Princeton, New Jersey

5. Cawthorn, R.G., Eales, H.V., Walraven, F., Uken, R., Watkeys, M.K., 2006, The Bushveld Complex, In: Johnson, M.R., Anhaeusser, C.R., Thomas, R.J. (Eds.), The Geology of South Africa, Geological Society of South Africa, Johannesburg/ Council for Geoscience, Pretoria, 261-281

6. Craig, R.F. (2004). Craig's Soil Mechanics, 7th Ed. Spon Press. Abingdon, Oxon.

7. Dippenaar, M.A. 2008, Characterisation of Some Fractured-Rock Aquifers in Limpopo Province, South Africa: Review and Case Study, M.Sc. thesis, University of Pretoria

8. Essington, M.E., 2004. Soil and Water Chemistry: An integrative Approach, CRC Press, Boca Raton Florida

9. Garrels, R.M., Christ, C.L. 1965, Solutions, Minerals and Equilibria, Jointly published by Harper & Row, New York, Evanston & London and John Weatherhill, inc., Tokyo, pp. 450

10. Geelhoed, J.S., Meeussen, J.C.L., Hillier, S., Lumsdon, D.G., Thomas, R.P., Farmer, J.G., Paterson, E. 2004, Identification and geochemical modelling of processes controlling leaching of Cr(VI) and other major elements from chromite ore processing residue, Geochimica et Cosmochimica Acta, Vol. 66, No. 22, pp. 3927–3942

11. Hartzer, F.J., 1995, Transvaal Supergroup inliers: geology, tectonic development and relationship with the Bushveld complex, South Africa, Journal of African Earth Sciences, vol. 21, no. 4, pp. 521-547

12. Hem, J.D. 1985, Study and Interpretation of the Chemical Characteristics of Natural Water 3rded., U.S Geological Survey, 604 South Pickett street, Alexandria, VA 22304, pp. 264

13. Johnson's Soil Augers, (Compiler). (2008, cited August 31st, 2011), Johnson Bucket Auger (Thompson Type), (Internet). (South Africa). (Publisher Unknown). (approx. 1p.) http://www.johnsonsoilauger.co.za/Types.aspx

14. Jorgensen, P.R., McKay, L.D., Spliid, N.H., 1998, Evaluation of chloride and pesticide transport in a fractured clayey till using large undisturbed columns and numerical modelling, Water Resources Research, vol. 34, no. 4, pp.539–553

15. Kalmaz, E.V., Barbierri, J.L. 1980, MATHEMATICAL MODELING AND COMPUTER SIMULATION OF RADIOACTIVE AND TOXIC CHEMICAL SPECIES DISPERSION IN POROUS MEDIA IN THE VICINITY OF URANIUM RECOVERY OPERATIONS, Ecological Modelling, vol. 13, pp. 159-181

16. Klein, C., Dutrow, B., 2008, The Manual of Mineral Science, John Wiley & Sons Inc., pp. 90-99

17. Koski, R.A., Munk, L., Foster, A.L., Shanks III, W.C., Stillings, L.L. 2008, Sulfide oxidation and distribution of metals near abandoned copper mines in coastal environments, Prince William Sound, Alaska, USA, Applied Geochemistry, vol. 23, pp. 227–254

18. Kotas, J., Stasicka, Z. 1999, Chromium occurrence in the environment and methods of its speciation, Environmental Pollution, vol. 107, pp. 263-283

19. Lefebvre, R., Hockley, D., Smolensky, J., Gelinas, P. 2001, Multiphase transfer processes in waste rock piles producing acid mine drainage 1: Conceptual model and system characterization and Multiphase transfer processes in waste rock piles producing acid mine drainage 2. Applications of numerical simulation, Journal of Contaminant Hydrology, vol. 52, pp. 165-186

20. Linklater, C.M., Sinclair, D.J., Brown, P.L. 2005, Coupled chemistry and transport modelling of sulphidic waste rock dumps at the Aitik mine site, Sweden, Applied Geochemistry, vol. 20, pp. 275-293

21. Lowson, R.T., Comarmond, M.C.J., Rajaratnam, G., Brown, P.L. 2004, The kinetics of the dissolution of chlorite as a function of pH and at 25°C, Geochimica et Cosmochimica Acta, Vol. 69, No. 7, pp. 1687–1699

22. Malmstrom, M.E., Gleisner, M., Herbert, R.B., 2006, Element discharge from pyritic mine tailings at limited oxygen availability in column experiments, Applied Geochemistry, vol. 21, pp. 184–202

23. McCandless, T.E., Ruiz, J., Adair, B.I., Freydier, C., 1999, Re-Os isotope and Pd/Ru variations in chromitites from the Critical Zone, Bushveld Complex, South Africa, Geochimica et Cosmochimica Acta, vol. 63, pp. 911-923

24. Molson, J.W., Fala, O., Aubertin, M., Bussiere, B. 2005, Numerical simulations of pyrite oxidation and acid mine drainage in unsaturated waste rock piles, Journal of Contaminant Hydrology, vol. 78, pp. 343-371

25. Moncur, M.C., Jambor, J.L., Ptacek, C.J., Blowes, C.W. 2009, Mine drainage from the weathering of sulfide minerals and magnetite, Applied Geochemistry, vol. 24, pp. 2362-2373

26. Moncur, M.C., Ptacek, C.J., Blowes, C.W. Jambor, J.L. 2004, Release, transport and attenuation of metals from an old tailings impoundment, Applied Geochemistry, vol.20, pp. 639-659

27. Mondofacto Ltd. (Compiler). (October 9th, 1997, cited April 24th, 2011). Fick's Law of Diffusion. (Internet). (Place unknown). (Publisher Unknown). (approx. 1p.) http://www.mondofacto.com/facts/dictionary?fick's+law+of+diffusion

28. Parkhurst, D.L., Appelo, C.A.J., 1999, The PHREEQC modelling databases, U.S. Geological Survey

29. Piatak,N.M., Seal II, R.R., Hammarstrom, J.M. 2004, Mineralogical and geochemical controls on the release of trace elements from slag produced by base- and precious-metal smelting at abandoned mine sites, Applied Geochemistry, vol. 19, pp. 1039–1064

30. Price, W.A. (1997). DRAFT Guidelines and Recommended Methods for the prediction of Metal leaching and Acid Rock Drainage at Minesites in British Columbia. British Columbia Ministry of Employment and Investment, Energy and Minerals Division, Smithers, BC, p.143.

31. Radojevic, M., Bahskin, V.N. 2006, Practical Environmental Analysis, Royal Society of Chemistry, pp. 457

32. Rimstidt, J.D., Chermak, J.A., Gagen, P.M. 1993, Rates of Reaction of Galena, Sphalerite, Chalcopyrite, and Arsenopyrite with Fe(III) in Acidic Solutions, In Environmental Geochemistry of Sulfide Oxidation; Alpers, C., et al.; ACS Symposium Series; American Chemical Society: Washington, DC

33. Rockware (Compiler). (2004-2011, cited September 6th, 2011). The Geochemist's Workbench. (Internet). (Place unknown). (Publisher Unknown). (approx. 1p.) http://www.rockware.com/product/overview.php?id=132

34. Saldi, G.D., Kohler, S.J., Marty, N., Oelkers, E.H. 2007, Dissolution rates of talc as a function of solution composition, pH and temperature, Geochimica et Cosmochimica Acta, vol. 71, pp. 3446–3457

35. SANS [South African National Standards]. 2003. Development, Maintenance and Management of Groundwater Resources Part 4: Test-pumping of Water Boreholes. SANS 10299-4:2003. ISBN 0626-14912-6.South Africa.

36. Šimůnek,J., van Genuchten, R., 2009, *Listing of Programs, Reports, and Publications on the HYDRUS CD*, PC-Progress, pp.3-4

37. Stimmie, C., Richters, E., Thompson, H., Perret, S., Matete, M., Abdallah, K., Kau, J., Mulibana, E., 2001, Hydro- institutional mapping in the Steelpoort river basin, South Africa. Working Paper 17 (South Africa Working Paper No. 6) Colombo, Sri Lanka: International Water Management Institute.

38. Strassberg,G., Maidment, D.R., Lynn, E.K. (cited April 25th, 2011), Dilution Attenuation Factors in Susceptibility Assessments: A GIS based method, (Internet). (Center For Research in Water Resources: The University of Texas at Austin). (Publisher Unknown). (approx. 3p.). http://proceedings.esri.com/library/userconf/proc02/pap0927/p0927.htm

39. University of Arizona, (Compiler). (2007, cited April 24th, 2011), Mass Transfer Equations: Fick's Law, (Internet). (Place unknown). (Publisher Unknown). (approx. 1p.) http://blowers.chee.arizona.edu/cooking/mass/fickslaw.html

40. van der Sloot, H.A. (September 18th, 2007 cited April 24th, 2011), Test Methods, pH Dependence Leaching Tests, (Internet). (Energy Research Centre of the Netherlands). (Publisher Unknown). (approx. 1p.). http://www.leaching.net/leaching/test-methods/

41. Van Tonder, G., Bardenhagen, I., Riemann, K., Van Bosch, J., Dzanga, P., Xu, Y. 2002, *Manual on pumping test analysis in fractured rock aquifers*, WRC Report No. 1116/1/02. Water Research Commision. Pretoria

42. Vermaak, C. F., Hendriks, L. P. 1976, A review of the mineralogy of the Merensky Reef, with specific reference to new data on the precious metal mineralogy, Economic Geology, vol. 71, pp. 1244-1269

43. Verral, D.P., Read, W.W., Narayan, K.A. 2008, Predicting salt advection in groundwater from saline aquaculture ponds, Journal of Hydrology, vol. 364, pp. 201-206

44. Walvaren, F., Hartzer, F.J., 1986, Geological Map Series 2430, Pilgrim's Rest, Mapped by Engelbrecht. L.N.J., Schwellnus, J.S.I., Coertze, F.J., Malherbe, S.J., Russell, H.D., Van Rooyen, D.P., Cooke, R. & Claasen, P.J. 1948-56; Jantsky, G.J., 1979, Brandl, G. 1980-81, Michaluk, E. & Hartzer, F.J. 1982., Schutte, I.C. 1975-76. Geological Survey and Department of Mineral and Energy Affairs, Government Printer, Pretoria

45. Weight, W.D., 2008, Hydrogeology Field Manual, 2nd Ed. McGraw-Hill, pp. 395-499

46. Wilson, M. J., 2004, Weathering of the primary rock-forming minerals: processes, products and rates, Clay Minerals, vol. 39, pp. 233-266

47. Winter, J., 2001, An Introduction to Igneous & Metamorphic Petrology, Prentice hall, pp293-308

48. Yadav, S.K., Chakrapani, G.J. 2006, Dissolution kinetics of rock–water interactions and its implications, CURRENT SCIENCE, vol. 90, pp. 932-937

49. Yellishetty, M., Ranjith, P.G., Kumar, D.L. 2009, Metal concentrations and metal mobility in unsaturated mine wastes in mining areas of Goa, India, Resources, Conservation and Recycling, vol. 53,pp. 379–385

8. APPENDICES

UNIVERSITEIT VAN PRETORIA
UNIVERSITY OF PRETORIA
YUNIBESITHI YA PRETORIA

Faculty of Natural & Agricultural Sciences
XRD & XRF Facility
Geology Department
Pretoria 0002, South Africa

Direct Telephone: (012) 420-2722
Direct Telefax: (012) 362 5219
E-Mail: wiebke.grote@up.ac.za
http://www.up.ac.za/academic/science

CLIENT: Matthys Dippenaar (for honours student)

DATE: 22 August 2011

SAMPLES: 11 Samples (Tailings – eastern Bushveld)

ANALYSIS: Qualitative and Quantitative XRD

The samples were prepared for XRD analysis using a back loading preparation method.
They were analysed using a PANalytical X'Pert Pro powder diffractometer with X'Celerator detector and variable divergence- and receiving slits with Fe filtered Co-Kα radiation. The phases were identified using X'Pert Highscore plus software. Graphical representations of the qualitative result follow below.
The relative phase amounts (weight %) was estimated using the Rietveld method (Autoquan Program). Errors are on the 3 sigma level in the column to the right of the amount. Amorphous phases, if present were not taken into consideration in the quantification. The quantitative results are listed below.

Comment: Chromite, a phase with a spinel structure, which may contain other elements in solid solution and not necessarily Ni – but the structure of Nichromite (in the qualitative program) just fitted best.
The samples do contain a phase with the structure of a phyllosilicate. Since the XRF showed very low potassium values, the phase Annite was identified. Annite is the iron-rich end member of the biotite mica group.

If you have any further queries, kindly contact the laboratory.

Analyst:

Wiebke Grote

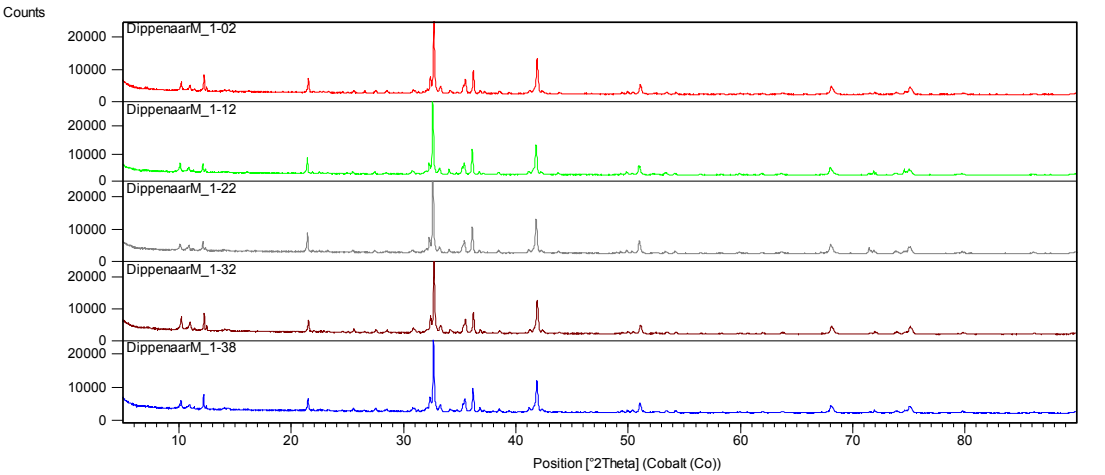
Counts
DippenaarM_1-02
DippenaarM_1-12
DippenaarM_1-22
DippenaarM_1-32
DippenaarM_1-38
20000
10000
0
10
20
30
40
50
60
70
80
Position [°2Theta] (Cobalt (Co))

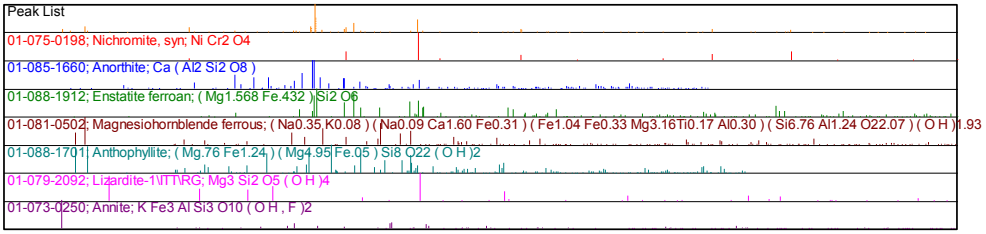
Peak List
01-075-0198; Nichromite, syn; Ni Cr2 O4
01-085-1660; Anorthite; Ca (Al2 Si2 O8)
01-088-1912; Enstatite ferroan; (Mg1.568 Fe.432) Si2 O6
01-081-0502; Magnesiohornblende ferrous; (Na0.35 K0.08) (Na0.09 Ca1.60 Fe0.31) (Fe1.04 Fe0.33 Mg3.16 Ti0.17 Al0.30) (Si6.76 Al1.24 O22.07) (O H)1.93
01-088-1701; Anthophyllite; (Mg.76 Fe1.24) (Mg4.95 Fe.05) Si8 O22 (O H)2
01-079-2092; Lizardite-1\ITT\RG; Mg3 Si2 O5 (O H)4
01-073-0250; Annite; K Fe3 Al Si3 O10 (O H , F)2

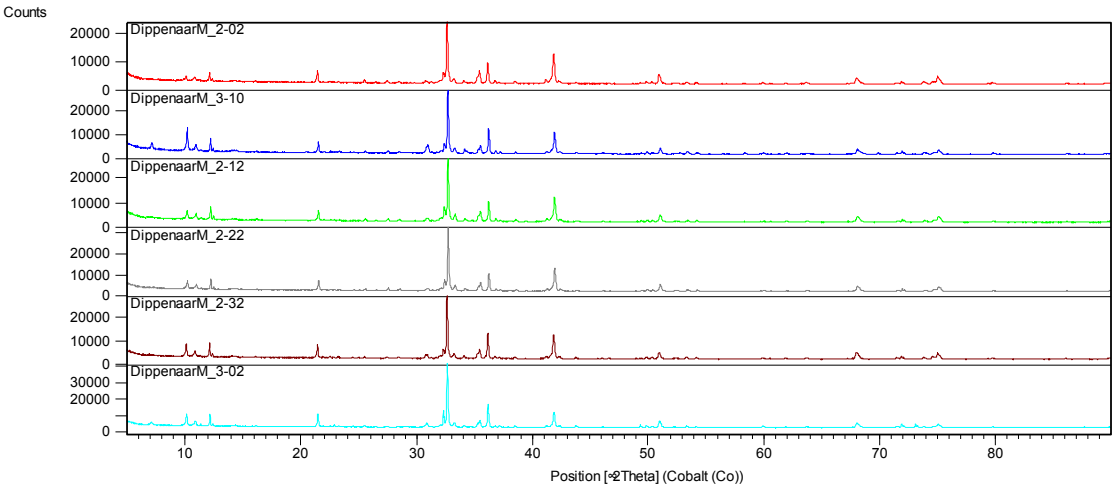
Counts
DippenaarM_2-02
DippenaarM_3-10
DippenaarM_2-12
DippenaarM_2-22
DippenaarM_2-32
DippenaarM_3-02
20000
10000
0
30000
10
20
30
40
50
60
70
80
Position [°2Theta] (Cobalt (Co))

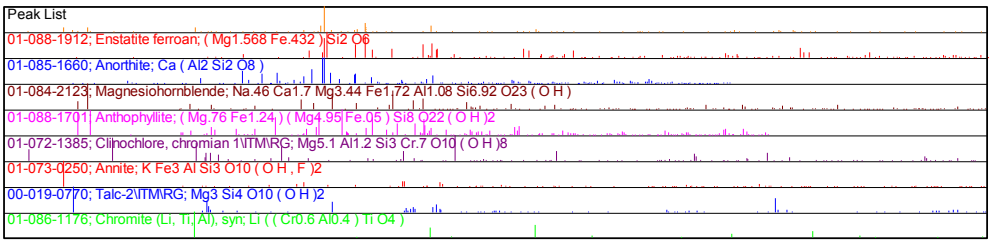
Peak List
01-088-1912; Enstatite ferroan; (Mg1.568 Fe.432) Si2 O6
01-085-1660; Anorthite; Ca (Al2 Si2 O8)
01-084-2123; Magnesiohornblende; Na.46 Ca1.7 Mg3.44 Fe1.72 Al1.08 Si6.92 O23 (O H)
01-088-1701; Anthophyllite; (Mg.76 Fe1.24) (Mg4.95 Fe.05) Si8 O22 (O H)2
01-072-1385; Clinochlore, chromian 1\ITM\RG; Mg5.1 Al1.2 Si3 Cr.7 O10 (O H)8
01-073-0250; Annite; K Fe3 Al Si3 O10 (O H , F)2
00-019-0770; Talc-2\ITM\RG; Mg3 Si4 O10 (O H)2
01-086-1176; Chromite (Li, Ti, Al), syn; Li ((Cr0.6 Al0.4) Ti O4)

Matt 1-02

	weight%	3 σ error
Annite_	2.73	0.63
Anthophyllite_	5.81	0.99
Enstatite(Fe)_	31.63	1.5
Hornblende	7.19	1.32
Lizardite	0	0
Chromite_Fe_	21.25	0.9
Plagioclase		
Anorthite_	26.93	1.95
Talc C-1_	4.47	1.08

Matt 1-12

	weight%	3 σ error
Annite_	3.63	0.87
Anthophyllite_	3.2	0.87
Diopside_	3.08	1.08
Enstatite(Fe)_	39.16	1.74
Hornblende	7.51	1.35
Lizardite	0	0
Chromite_Fe_	21.84	0.9
Plagioclase		
Anorthite_	21.58	1.83

Matt 1-22

	weight%	3 σ error
Annite_	3.38	0.72
Anthophyllite_	3.59	0.87
Diopside_	2.7	0.99
Enstatite(Fe)_	40.72	1.5
Hornblende	8.75	1.02
Chromite_Fe_	22.49	0.87
Plagioclase		
Anorthite_	12.8	1.23
Talc C-1_	5.57	1.35

Matt 1-32

	weight%	3 σ error
Annite_	3.35	0.75
Anthophyllite_	9.54	2.1
Enstatite(Fe)_	28.65	1.59
Hornblende	5.25	1.23
Lizardite	0.33	0.36
Chromite_Fe_	19.66	0.96
Plagioclase		
Anorthite_	28.11	2.01
Talc C-1_	5.11	1.08

Matt 1-38

	weight%	3 σ error
Annite_	3.43	0.78
Anthophyllite_	4.47	1.08
Enstatite(Fe)_	32.75	1.35
Hornblende	8.18	1.2
Lizardite	1.06	0.54
Chromite_Fe_	20.39	0.84
Plagioclase		
Anorthite_	29.72	1.86

Matt 2-02

	weight%	3 σ error
Annite_	2.32	0.78
Anthophyllite_	6.45	1.29
Enstatite(Fe)_	37.71	1.56
Hornblende	7.04	1.14
Lizardite	1.3	0.6
Chromite_Fe_	22.72	0.87
Plagioclase		
Anorthite_	22.47	1.83

Matt 2-12

	weight%	3 σ error
Annite_	2.82	0.63
Anthophyllite_	8.33	0.99
Enstatite(Fe)_	30.47	1.65
Hornblende,		
Magnesium Iron_	5.56	1.23
Chromite_Fe_	19.56	0.9
Plagioclase		
Anorthite_	26.65	1.95
Talc C-1_	6.61	1.08

Matt 2-22

	weight%	3 σ error
Anthophyllite_	3.39	0.93
Chlorite IIb-2_	0.44	0.57
Enstatite(Fe)_	35.21	1.83
Hornblende	7.7	1.38
Chromite_Fe_	21.26	1.05
Plagioclase		
Anorthite_	26.46	2.16
Talc C-1_	5.54	1.32

Matt 2-32

	weight%	3 σ error
Diopside_	3.43	0.93
Enstatite(Fe)_	36.32	1.8
Hornblende	7.95	1.47
Illite1Mt_	3.84	0.66
Chromite_Fe_	21.92	0.99
Phlogopite		
ferrian 1M_	1.64	0.93
Plagioclase		
Anorthite_	20.24	1.83
Talc C-1_	4.66	1.26

Matt 3-02

	weight%	3 σ error
Annite_	7.59	1.35
Anthophyllite_	12.79	1.89
Diopside_	6.95	1.26
Enstatite(Fe)_	29.78	1.89
Hornblende,		
Magnesium Iron_	4.73	1.5
Chromite_Fe_	18.37	1.02
Plagioclase		
Anorthite_	13.71	1.86
Talc C-1_	6.08	1.83

Matt 3-10

	weight%	3 σ error
Annite_	6.73	1.23
Chlorite IIb-2_	6.34	1.92
Enstatite(Fe)_	32.72	1.46
Hornblende,		
Magnesium Iron_	7.62	1.98
Chromite_Fe_	14.76	1.02
Plagioclase		
Anorthite_	27.21	1.79
Talc C-1_	4.62	1.47

UNIVERSITEIT VAN PRETORIA
UNIVERSITY OF PRETORIA
YUNIBESITHI YA PRETORIA

Faculty of Natural &
Agricultural Sciences
XRD & XRF Facility
Geology Department
Pretoria 0002, South Africa

Direct Telephone: (012) 420-2722
Direct Telefax: (012) 362 5219
E-Mail: wiebke.grote@up.ac.za
http://www.up.ac.za/academic/science

CLIENT: Altus Huisamen

DATE: 26 March 2012

SAMPLES: 13 Samples

ANALYSIS: Qualitative and Quantitative XRD

The samples were prepared for XRD analysis using a back loading preparation method.
They were analysed using a PANalytical X'Pert Pro powder diffractometer with X'Celerator detector and variable divergence- and receiving slits with Fe filtered Co-Kα radiation. The phases were identified using X'Pert Highscore plus software.

The relative phase amounts (weight %) were estimated using the Rietveld method (Autoquan Program). Errors are on the 3 sigma level in the column to the right of the amount. Amorphous phases, if present were not taken into consideration in the quantification. The quantitative results are listed below.

Comments:

- Errors reported for phases occurring in minor amounts are sometimes larger than that of the quantity reported, indicating the possible absence of those phases.
- Chromite, a spinel may contain other elements, apart from their ideal composition, in solid solution.
- Mineral names may not reflect the actual compositions of minerals identified, but rather the mineral group (i.e "Muscovite" and "Biotite" would represent the mineral group "Mica" and "Tremolite" and "Hornblende" the mineral group "Amphibole").
- Due to preferred orientation effects results may not be as accurate as shown in the table.
- Since X-ray diffraction patterns are directly related to crystal structures, X-ray identification is, in principal, better suited to the recognition of structural groups and structural varieties than chemical species.

If you have any further queries, kindly contact the laboratory.

Analyst:

Wiebke Grote

TPH 0-1.2T				TPH 0-1.2B				TPH 1.2-2.4B		
	weight%	3 σ error			weight%	3 σ error			weight%	3 σ error
Anthophyllite_	7.54	1.56		Anthophyllite	4	1.02		Anthophyllite_	4.67	1.5
Chlorite	1	0.81		Chlorite	11	1.6		Chromite	21.88	1.17
Chromite	26.43	1.32		Chromite	19.31	1.26		Enstatite	45.09	2.4
Enstatite	32.38	1.92		Enstatite	30	1.89		Muscovite	1.9	0.9
Muscovite	2.79	0.69		Lizardite	1.45	0.39		Plagioclase Anorthite_	15.83	2.34
Plagioclase Anorthite	18.47	2.31		Muscovite	1.7	0.54		Talc	3.98	1.71
Talc	6.22	1.23		Plagioclase Anorthite_	20.48	2.13		Tremolite_	6.65	1.5
Tremolite_	5.17	1.62		Talc	5.21	1.08				
				Tremolite	6.88	1.11				
TPH 2.4-3.6B				**TPH 3.6-4.8B**				**TPH 4.8-6B**		
	weight%	3 σ error			weight%	3 σ error			weight%	3 σ error
Anthophyllite_	4.21	1.44		Anthophyllite_	2.72	1.02		Anthophyllite_	2.64	0.6
Biotite	5.36	1.05		Biotite	2.46	0.81		Chromite	23.98	1.2
Chromite	22.49	0.87		Chromite	27.44	0.96		Enstatite	35.14	1.95
Diopside	2.64	1.32		Diopside	2.9	1.23		Lizardite	0.28	0.45
Enstatite	45.86	1.77		Enstatite	38.92	1.56		Muscovite_2M1_	3.47	0.72
Hornblende	4.92	1.26		Hornblende	4.62	1.11		Plagioclase Anorthite_	24.42	2.43
Plagioclase Anorthite_	9.2	1.26		Plagioclase Anorthite_	15.11	1.77		Talc	2.1	1.08
Talc	5.32	1.14		Talc	5.84	0.87		Tremolite_	7.96	1.38
TPH 6-7.2T				**TPH 6-7.2B**				**TPH 7.2-8.4T**		
	weight%	3 σ error			weight%	3 σ error			weight%	3 σ error
Anthophyllite_	9.46	1.89		Anthophyllite_	12.71	2.64		Anthophyllite_	9.21	1.89
Biotite	3.56	0.6		Biotite	3.26	0.9		Biotite	3.89	0.87
Chromite_	27.48	0.93		Chromite_	19.86	1.14		Chromite_	25.98	1.14
Diopside	2.18	0.93		Diopside	2.84	1.38		Diopside	1.4	0.87
Enstatite	34.82	1.47		Enstatite	27.77	1.86		Enstatite	34.73	1.86
Hornblende	3.82	0.93		Hornblende	3.29	1.38		Hornblende	3.83	1.02
Plagioclase Anorthite_	13.07	1.59		Plagioclase Anorthite_	24.38	2.34		Plagioclase Anorthite_	15.3	1.71
Talc	5.61	0.78		Talc	5.87	1.35		Talc	5.66	1.08

TPH 8.4-9.6T				**TPH 7.2-8.4B**				**TPH 8.4-9.6B**		
	weight%	3 σ error			weight%	3 σ error			weight%	3 σ error
Biotite	6.5	1.3		Anthophyllite_	7.8	1.2		Anthophyllite_	5.23	1.23
Chromite	10.3	0.6		Biotite	4.64	1.05		Biotite	2.35	0.9
Diopside	2.03	0.87		Chromite	26.33	1.02		Chromite_	30.81	1.2
Enstatite	14.1	1.17		Diopside	0.84	0.87		Diopside	1.36	0.72
Kaolinite	14.23	1.17		Enstatite	35.18	1.65		Enstatite	34.96	1.74
Plagioclase Anorthite	39.43	2.01		Hornblende	4.16	0.93		Plagioclase Anorthite	14.78	1.53
Quartz	5.51	0.45		Plagioclase Anorthite_	16.13	1.95		Talc	5.61	1.41
Talc	7.9	1.17		Talc	4.92	0.9		Tremolite	4.91	1.32
TPH 9.6-10										
	weight%	3 σ error								
Chlorite	15.97	2.34								
Chromite_	3.62	0.48								
Enstatite	8.52	1.5								
Kaolinite	34.19	2.01								
Plagioclase Anorthite_	30.66	1.86								
Quartz	7.05	0.9								

UNIVERSITEIT VAN PRETORIA
UNIVERSITY OF PRETORIA
YUNIBESITHI YA PRETORIA

XRF REPORT:

Direct Telephone: (012) 420-2137
Direct Telefax: (012) 420-2661
E-Mail: jeanette.dykstra@up.ac.za

Pretoria 0002 South Africa
http://www.up.ac.za/academic/science/

Faculty of Natural & Agricultural Sciences
XRD & XRF Facility
Geology Department

CLIENT: Matthys Dippenaar

DATE: 19-Mar-12

ANALYSIS: The samples were prepared as pressed powder briquettes.
The ARL9400 XP+ Sequential XRF and Uniquant software was used for semi-quantitative analyses.
The software analyse for all elements in the periodic table between Na and U, but only elements found above the detection limits were reported.
The values were normalised, as no LOI was done to determine crystal water and oxidation state changes.
All elements were expressed as oxides

	NimNcert	NIMN	0-1.2T	0-1.2B	1.2-2.4B	2.4-3.6B	3.6-4.8B	4.8-6B	6-7.2T
SiO_2	**52.64**	48.78	26.87	28.30	30.13	30.22	26.60	28.31	27.13
TiO_2	**0.2**	0.16	0.62	0.59	0.55	0.59	0.64	0.61	0.61
Al_2O_3	**16.5**	23.10	13.38	13.47	13.58	13.47	13.42	13.41	13.07
Fe_2O_3	**8.91**	8.04	19.01	18.29	18.08	17.44	19.19	18.34	19.21
MnO	**0.18**	0.16	0.22	0.22	0.23	0.22	0.23	0.22	0.23
MgO	**7.5**	5.16	15.51	15.95	15.51	16.17	15.43	15.90	15.38
CaO	**11.5**	11.28	2.64	2.89	3.19	3.16	2.67	2.89	2.67
Na_2O	**2.46**	2.86	0.54	0.59	0.90	0.72	0.57	0.63	0.65
K_2O	**0.25**	0.27	0.12	0.13	0.17	0.14	0.11	0.12	0.11
P_2O_5	**0.03**	0.02	0.02	0.03	0.04	0.03	0.02	0.01	0.01
Cr_2O_3	**0.0044**	*<0.01*	20.49	19.00	16.84	17.15	20.53	18.97	20.27
NiO	**0.0153**	0.01	0.13	0.12	0.12	0.12	0.12	0.12	0.12
V_2O_5	**0.0393**	0.03	0.22	0.21	0.19	0.19	0.23	0.21	0.21
ZRO2	**0.0031**	*<0.01*	*<0.01*	*<0.01*	*<0.01*	*<0.01*	*<0.01*	*<0.01*	*<0.01*
SO_3		*<0.01*	0.01	0.03	0.19	0.22	0.04	0.08	0.10
WO_3		*<0.01*	0.01	0.01	0.02	0.01	0.01	0.01	0.01
BaO		*<0.01*	*<0.01*	*<0.01*	*<0.01*	*<0.01*	*<0.01*	*<0.01*	*<0.01*
Cl		0.02	0.03	0.03	0.13	0.03	0.03	0.03	0.07
CuO	**0.0018**	*<0.01*	0.01	*<0.01*	0.01	0.01	*<0.01*	*<0.01*	*<0.01*
ZnO		0.01	0.04	0.04	0.04	0.03	0.04	0.04	0.05
Co_3O_4		0.01	0.04	0.04	0.04	0.04	0.04	0.04	0.04
CeO_2		*<0.01*	0.02	*<0.01*	0.02	0.02	*<0.01*	*<0.01*	*<0.01*
SrO		0.03	0.01	0.01	0.01	0.01	0.01	0.01	0.01
MoO3		0.01	0.01	0.01	0.01	0.01	0.01	0.01	0.01
Total	**100.23**	99.97	99.93	99.95	99.97	99.98	99.94	99.95	99.96

ppm	0-1.2T	0-1.2B	1.2-2.4B	2.4-3.6B	3.6-4.8B	4.8-6B	6-7.2T	6-7.2B	7.2-8.4T
As	3.00	3.00	3.00	3.00	5.18	3.00	3.00	3.00	3.00
Cu	32.57	44.16	39.90	36.42	30.67	31.94	39.04	29.20	25.94
Ga	39.67	35.79	29.04	32.99	37.42	35.13	35.59	34.40	35.21
Mo	11.03	9.92	14.29	10.11	10.45	10.83	13.04	10.10	10.79
Nb	11.46	13.78	11.41	12.86	12.97	13.78	12.91	12.64	12.73
Ni	1118.13	1046.39	984.73	1019.30	1098.22	1046.52	1072.59	1027.93	1032.10
Pb	14.89	7.73	15.74	6.28	3.00	17.71	5.96	6.99	13.09
Rb	15.73	14.06	16.41	14.76	15.18	15.34	15.49	13.82	13.59
Sr	60.29	73.34	72.19	71.69	65.20	70.52	63.94	66.74	65.31
Th	24.34	24.67	18.44	20.56	24.51	23.58	24.32	23.73	23.08
U	24.99	26.47	20.99	22.56	26.40	24.91	23.55	23.62	24.86

W	129.46	80.23	209.29	39.30	79.42	93.45	126.43	56.44	71.31
Y	14.72	14.63	12.56	14.87	14.56	14.13	14.68	14.00	14.55
Zn	408.20	369.18	378.60	341.42	395.37	376.24	429.99	368.93	368.58
Zr	29.22	37.03	30.84	32.47	32.50	28.69	30.97	32.34	36.07
Cl*	73.10	97.93	767.20	130.50	93.68	107.78	344.60	115.13	145.39
Co	174.81	165.20	166.33	148.06	175.88	162.41	177.13	162.50	165.47
Cr	143023.36	132033.65	118859.82	120517.54	142611.58	132145.47	141568.18	132514.08	132448.43
F	100.00	100.00	100.00	100.00	100.00	100.00	100.00	100.00	100.00
S	20.96	25.57	164.44	184.11	40.52	74.78	105.25	99.66	89.42
Sc	14.87	15.70	18.00	18.39	15.81	16.81	14.89	17.48	16.53
V	1202.01	1119.57	1027.81	1042.27	1207.20	1128.20	1195.51	1132.14	1128.09
Cs	9.43	9.43	9.43	9.43	9.43	9.43	9.43	9.43	9.43
Ba	18.32	24.49	32.51	26.97	17.96	26.05	20.85	24.34	20.90
La	6.07	4.26	5.40	5.42	7.58	10.98	8.23	4.26	8.23
Ce	4.88	4.88	4.88	4.88	4.88	4.88	4.88	4.88	4.88

If you have any further queries, kindly contact the laboratory.

Analyst: J.E. Dykstra
Senior Technical Assistant (XRF)

6-7.2B	7.2-8.4T	7.2-8.4B	8.4-9.6T	8.4-9.6B	9.6-10
28.31	28.32	26.26	42.53	25.59	47.90
0.61	0.60	0.66	0.41	0.66	0.31
13.38	13.31	13.54	32.96	13.24	40.77
18.35	18.43	19.25	6.66	19.72	3.56
0.22	0.22	0.22	0.09	0.23	0.05
15.90	15.84	15.29	3.44	15.29	0.32
2.84	2.84	2.67	6.08	2.47	4.40
0.65	0.63	0.55	0.71	0.56	0.39
0.12	0.12	0.10	0.25	0.09	0.21
0.02	0.02	0.02	0.07	0.02	0.07
19.02	19.07	20.90	6.24	21.50	1.55
0.12	0.12	0.12	0.04	0.13	0.01
0.21	0.20	0.23	0.08	0.24	0.03
<0.01	*<0.01*	*<0.01*	*<0.01*	*<0.01*	*<0.01*
0.10	0.09	0.03	0.21	0.06	0.27
<0.01	0.01	0.01	0.01	0.01	*<0.01*
<0.01	*<0.01*	*<0.01*	0.01	*<0.01*	0.01
0.03	0.04	0.02	0.10	0.03	0.10
<0.01	0.01	*<0.01*	*<0.01*	*<0.01*	*<0.01*
0.04	0.04	0.05	0.01	0.05	0.01
0.03	0.04	0.04	0.01	0.04	0.01
<0.01	*<0.01*	*<0.01*	0.01	0.02	*<0.01*
0.01	0.01	0.01	0.03	0.01	0.03
0.01	0.01	*<0.01*	0.01	0.01	*<0.01*
99.97	99.96	99.97	99.96	99.94	100.00

7.2-8.4B	8.4-9.6T	8.4-9.6B	9.6-10
3.00	3.00	3.00	3.00
16.36	18.62	15.53	16.05
37.30	26.68	38.78	22.76
11.63	1.60	12.15	1.00
12.79	5.67	14.08	3.10
1072.33	267.24	1075.25	67.99
9.87	3.35	13.33	3.00
12.65	10.39	13.87	4.55
64.92	240.75	56.13	205.38
26.56	3.77	27.68	3.00
25.90	3.00	24.70	3.00

81.48	58.33	89.53	8.85
15.13	7.61	16.75	5.02
416.44	112.59	429.74	42.54
33.89	41.52	34.76	37.63
66.98	620.98	117.51	588.91
173.51	63.57	180.56	20.46
145400.41	46252.13	149564.07	10830.79
100.00	100.00	100.00	100.00
26.19	391.57	50.67	177.21
17.47	9.86	16.40	8.08
1241.08	430.70	1274.58	138.57
9.43	30.72	9.43	36.21
15.27	151.30	12.91	173.81
8.87	4.26	7.22	5.38
4.88	4.88	4.88	18.93

UNIVERSITEIT VAN PRETORIA
UNIVERSITY OF PRETORIA
YUNIBESITHI YA PRETORIA

XRF REPORT:

Direct Telephone: (012) 420-2137
Direct Telefax: (012) 420-2661
E-Mail: jeanette.dykstra@up.ac.za

Pretoria 0002 South Africa
http://www.up.ac.za/academic/science/

Faculty of Natural & Agricultural Sciences
XRD & XRF Facility
Geology Department

CLIENT: Matthys Dippenaar (batch 2)

DATE: 16-Aug-11

ANALYSIS: The samples were prepared as pressed powder briquettes.
The ARL9400 XP+ Sequential XRF and Uniquant software was used for analyses.
The software analyse for all elements in the periodic table between Na and U, but only elements found above the detection limits were reported.
The values were normalised, as no LOI was done to determine crystal water and oxidation state changes.
All elements were expressed as oxides

	GSNcert	GSN	MATT1-02	MATT1-12	MATT1-22	MATT1-32	MATT1-38	MATT2-02	MATT2-12
SiO_2	**65.8**	62.95	34.48	31.81	30.09	35.62	35.81	33.69	34.63
TiO_2	**0.68**	0.59	0.53	0.57	0.58	0.50	0.55	0.55	0.52
Al_2O_3	**14.67**	18.49	15.62	14.17	13.71	15.43	15.42	14.91	15.51
Fe_2O_3	**3.75**	3.37	14.31	16.42	17.04	13.95	14.06	15.24	14.26
MnO	**0.06**	0.05	0.18	0.21	0.22	0.18	0.19	0.20	0.19
MgO	**2.3**	2.03	16.14	16.19	15.96	16.49	16.15	16.22	16.14
CaO	**2.5**	2.56	4.66	3.78	3.62	4.78	5.00	4.24	4.77
Na_2O	**3.77**	3.88	0.85	0.74	0.78	0.81	0.88	0.79	0.85
K_2O	**4.63**	5.08	0.18	0.14	0.13	0.21	0.20	0.16	0.19
P_2O_5	**0.28**	0.30	0.02	0.02	0.02	0.02	0.02	0.02	0.03
Cr_2O_3	**0.008**	0.01	12.52	15.40	16.63	11.59	11.27	13.51	12.17
NiO	**0.0043**	*<0.01*	0.10	0.11	0.11	0.10	0.09	0.10	0.10
V_2O_5	**0.01**	0.01	0.15	0.18	0.19	0.13	0.13	0.15	0.14
SO_3	**0.03**	0.09	0.09	0.13	0.76	0.03	0.05	0.06	0.38
WO_3		0.06	0.01	0.01	0.01	0.01	*<0.01*	*<0.01*	*<0.01*
Cl		0.15	0.03	0.03	0.04	0.03	0.03	0.03	0.03
CuO		0.02	*<0.01*	*<0.01*	*<0.01*	*<0.01*	*<0.01*	*<0.01*	*<0.01*
ZnO		0.01	0.03	0.04	0.03	0.02	0.02	0.03	0.03
Co_3O_4		0.01	0.03	0.03	0.03	0.03	0.02	0.03	0.02
CeO_2		*<0.01*	0.01	*<0.01*	*<0.01*	*<0.01*	*<0.01*	*<0.01*	*<0.01*
SrO		0.07	0.01	0.01	0.01	0.01	0.01	0.01	0.01
MoO3		0.01	0.01	0.01	0.01	0.01	0.01	0.01	0.01
BaO		0.14	*<0.01*	*<0.01*	*<0.01*	*<0.01*	*<0.01*	*<0.01*	*<0.01*
Total	**99.82**	**99.86**	**99.96**	**99.97**	**99.97**	**99.95**	**99.94**	**99.94**	**99.97**

ppm	GSNcert	GSN	1-02	1-12	1-22	1-32	1-38	2-02	2-12
As	**1.6**	3.00	3.00	3.00	3.00	3.00	3.00	3.00	3.00
Cu	**20**	93.26	11.69	12.14	14.91	9.81	11.43	12.54	11.68
Ga	**22**	20.44	26.16	28.75	29.21	24.33	24.80	27.26	26.23
Mo	**1.2**	1.00	8.39	12.76	10.88	8.22	7.21	10.02	9.15
Nb	**21**	21.06	7.47	11.27	9.75	7.64	8.16	9.45	7.83
Ni	**34**	31.94	869.94	969.19	980.53	845.69	815.98	896.41	863.56
Pb	**53**	48.47	4.69	3.00	3.00	8.32	4.77	5.28	3.05
Rb	**185**	183.83	13.58	13.12	12.74	12.77	14.61	14.27	13.16
Sr	**570**	571.57	115.29	84.75	76.93	115.32	122.49	100.43	115.43
Th	**42**	42.24	13.35	20.78	20.50	11.99	13.21	16.50	14.07
U	**8**	7.04	12.70	16.99	19.82	9.48	11.90	14.20	12.35

W*	**450**	495.69	100.49	19.77	28.31	40.97	27.21	23.81	6.00
Y	**19**	10.79	12.75	14.08	13.25	13.09	12.42	14.09	11.99
Zn	**48**	72.83	240.04	288.11	300.12	231.69	225.42	254.67	231.68
Zr	**235**	210.06	29.13	25.68	30.93	27.14	29.20	29.51	27.93
Cl*	**450**	895.51	87.32	59.09	142.47	36.95	82.33	47.00	41.70
Co	**65**	63.17	133.76	144.62	155.17	125.46	122.28	133.53	122.90
Cr	**55**	71.69	92710.74	112311.84	120685.18	86233.00	83240.63	99440.21	90124.33
F*	**1050**	502.28	100.00	100.00	100.00	100.00	100.00	100.00	100.00
S*	**140**	114.35	157.81	266.42	1521.86	71.38	110.30	151.21	771.24
Sc	**7**	4.52	19.57	17.63	17.71	18.88	19.63	18.54	18.51
V	**65**	61.11	758.56	927.37	986.14	713.85	704.76	820.71	744.52
Cs	**5**	9.43	9.43	9.43	9.43	9.43	9.43	9.43	9.43
Ba	**1400**	1305.90	36.18	25.61	21.71	44.30	45.82	34.21	41.49
La	**75**	58.88	13.68	15.20	16.07	15.00	13.30	16.55	16.87
Ce	**135**	151.10	4.88	4.88	4.88	4.88	4.88	4.88	4.88

If you have any further queries, kindly contact the laboratory.

Analyst: J.E. Dykstra
Senior Technical Assistant (XRF)

QI30308.MATTHYS2.16-08-2011.xls

MATT2-22	MATT2-32	MATT3-02	MATT3-10
33.47	31.04	31.44	35.99
0.53	0.59	0.58	0.51
15.05	14.01	14.43	19.40
14.80	16.98	16.55	13.27
0.20	0.22	0.22	0.18
15.97	16.29	15.92	12.47
4.57	3.56	3.73	5.23
0.86	0.70	0.77	0.64
0.17	0.13	0.15	0.21
0.04	0.02	0.03	0.02
13.07	15.96	15.41	11.55
0.11	0.11	0.12	0.09
0.15	0.18	0.17	0.13
0.89	0.04	0.34	0.11
<0.01	*<0.01*	*<0.01*	*<0.01*
0.03	0.02	0.06	0.03
0.01	*<0.01*	*<0.01*	*<0.01*
0.03	0.04	0.03	0.03
0.03	0.03	0.03	0.02
0.02	0.01	*<0.01*	0.02
0.01	0.01	0.01	0.01
<0.01	*<0.01*	0.01	0.01
<0.01	*<0.01*	*<0.01*	*<0.01*
99.98	**99.95**	**99.99**	**99.94**

2-22	2-32	3-02	3-10
3.00	3.00	3.00	3.00
14.29	8.88	13.50	13.40
26.54	30.28	27.47	21.92
9.92	10.37	10.17	7.89
7.46	10.77	9.97	7.94
878.00	983.36	950.01	731.44
3.00	3.00	3.00	3.00
12.81	14.14	12.77	13.06
108.16	79.50	89.19	124.44
15.89	19.86	17.11	13.78
12.30	19.63	15.72	9.42

11.27	6.00	8.89	6.00
12.84	14.48	14.67	12.50
244.75	291.46	268.17	208.61
29.18	30.76	29.15	32.41
67.62	7.58	242.86	73.94
133.43	147.70	144.94	109.70
96798.74	116390.72	110656.74	85012.47
100.00	100.00	100.00	100.00
1859.01	89.09	614.40	197.00
17.59	18.46	16.83	15.64
791.34	947.04	902.02	711.61
9.43	9.43	9.43	9.43
35.85	21.31	26.04	60.84
18.70	14.32	12.31	20.08
4.88	4.88	4.88	4.88

WATERLAB (Pty) Ltd

Reg. No.: 1983/009165/07 V.A.T. No.: 4130107891

Building D
The Woods
41 De Havilland Cresent
Persequor Techno Park
Meiring Naudé Drive
Pretoria

P.O. Box 283
Persequor Park, 0020
Tel: +2712 – 349 – 1066
Fax: +2712 – 349 – 2064
e-mail: admin@waterlab.co.za

SANAS Accredited Testing Laboratory
No. T0391

CERTIFICATE OF ANALYSES
GENERAL WATER QUALITY PARAMETERS

Date received: 2012 - 03 - 19 **Date completed:** 2012 - 03 - 28

Project number: 215 **Report number: 34574** **Order number: 0418**

Client name: University of Pretoria – Geology Department **Contact person: Mr. M.A Dippenaar**

Address: Private Bag X20, Hatfield, 0028 **e-mail:** altus.huisamen@mtd.blackberry.com

Telephone: 012 804 8120 **Facsimile: -** **Mobile: -**

Analyses in mg/ℓ (Unless specified otherwise)	**Method Identification**	**Sample Identification**		
		TRPMW6S	**TOEDRAIN**	**TRPMW9S**
Sample Number		819	820	821
pH – Value at 25°C *	WLAB001	7.4	8.3	7.6
Electrical Conductivity in mS/m at 25°C	WLAB002	157	121	171
Total Dissolved Solids at 180°C *	WLAB003	1 180	814	1 076
Total Alkalinity as $CaCO_3$	WLAB007	388	240	576
Chloride as Cl *	WLAB046	192	171	210
Sulphate as SO_4	WLAB046	168	165	108
Fluoride as F	WLAB014	<0.2	<0.2	<0.2
Nitrate as N*	WLAB046	11	1.6	2.3
Ortho Phosphate as P *	WLAB046	<0.2	<0.2	<0.2
ICP-OES Scan *	WLAB015	See Attached Report: 34574-A		
% Balancing	---	95.5	98.5	98.1

*** = Not SANAS Accredited**
Tests marked "Not SANAS Accredited" in this report are not included in the SANAS Schedule of Accreditation for this Laboratory.

[s] = Analyses performed by a Sub-Contracted Laboratory

A. van de Wetering

Technical Signatory

WATERLAB (Pty) Ltd

Reg. No.: 1983/009165/07 V.A.T. No.: 4130107891

Building D
The Woods
41 De Havilland Cresent
Persequor Techno Park
Meiring Naudé Drive
Pretoria

P.O. Box 283
Persequor Park, 0020
Tel: +2712 – 349 – 1066
Fax: +2712 – 349 – 2064
e-mail: admin@waterlab.co.za

SANAS Accredited Testing Laboratory
No. T0391

CERTIFICATE OF ANALYSES
GENERAL WATER QUALITY PARAMETERS

Date received: 2012 - 05 - 04 **Date completed:** 2012 - 05 – 08

Project number: 215 **Report number: 35085** **Order number: 0419**

Client name: University of Pretoria **Contact person: Mr. M.A. Dippenaar**

Address: Private Bag X20, Geology Department, Hatfield, 0028 **e-mail: altus@gptglobal.co.za madip@up.ac.za**

Telephone: - **Facsimile: -** **Mobile: 083 352 0223**

Analyses in mg/ℓ (Unless specified otherwise)	**Method Identification**	**Sample Identification**
		STP RIV
Sample Number		3084
Total Alkalinity as $CaCO_3$	WLAB007	156
Chloride as Cl *	WLAB046	7
Sulphate as SO_4	WLAB046	12
Fluoride as F	WLAB014	<0.2
Nitrate as N*	WLAB046	4.5
ICP-OES Scan *	WLAB015	See Attached Report: 35085-A
% Balancing	---	97.7

*** = Not SANAS Accredited**
Tests marked "Not SANAS Accredited" in this report are not included in the SANAS Schedule of Accreditation for this Laboratory.

[s] = Analyses performed by a Sub-Contracted Laboratory

Ard van de Wetering

Technical Signatory:

WATERLAB (PTY) LTD

CERTIFICATE OF ANALYSIS

Project Number : **215**
Client : **University of Pretoria**
Report Number : **35085-A**

Sample Origin	Sample ID	Note: all results in parts per million (ppm) unless specified otherwise										
		Ag	**Al**	**As**	**B**	**Ba**	**Be**	**Bi**	**Ca**	**Cd**	**Co**	**Cr**
		mg/l	mg/l	mg/l	mg/l	mg/l	mg/l	mg/l	mg/l	mg/l	mg/l	mg/l
Lowest Reported Concentration		<0.025	<0.100	<0.010	<0.025	<0.025	<0.025	<0.025	<2	<0.005	<0.025	<0.025
STP RIV	3084	<0.025	0.228	<0.010	<0.025	<0.025	<0.025	<0.025	29	<0.005	<0.025	<0.025

Sample Origin	Sample ID											
		Fe	**K**	**Li**	**Mg**	**Mn**	**Mo**	**Na**	**Ni**	**P**	**Pb**	**Sb**
		mg/l	mg/l	mg/l	mg/l	mg/l	mg/l	mg/l	mg/l	mg/l	mg/l	mg/l
Lowest Reported Concentration		<0.025	<1.0	<0.025	<2	<0.025	<0.025	<2	<0.025	<0.025	<0.020	<0.010
STP RIV	3084	0.133	<1.0	<0.025	23	<0.025	<0.025	8	<0.025	<0.025	<0.020	<0.010

Sample Origin	Sample ID									
		Se	**Si**	**Sn**	**Sr**	**Ti**	**V**	**W**	**Zn**	**Zr**
		mg/l	mg/l	mg/l	mg/l	mg/l	mg/l	mg/l	mg/l	mg/l
Lowest Reported Concentration		<0.020	<0.2	<0.025	<0.025	<0.025	<0.025	<0.025	<0.025	<0.025
STP RIV	3084	<0.020	7.5	0.084	0.103	<0.025	<0.025	<0.025	<0.025	<0.025

Cu
mg/l
<0.025
<0.025

Constituent	Model (mg/L)	Analysed (mg/L)
Ca	52.49	66
Mg	76.28	96
SO_4	161	165
Cl	195.7	171
Al	0.05	0.156
Cr	0.04	0
K	4.3	1.7
Si	2.7	9.5
NO_3	3.7	1.6
pH	8.02	8.3

Regression line confidence interval

x	Cl	y+Cl	y-Cl
-40	35.40	-9.89	-80.70
-20	34.27	9.73	-58.81
0	33.37	29.59	-37.15
20	32.73	49.70	-15.75
40	32.35	70.08	5.38
60	32.26	90.74	26.23
80	32.44	111.69	46.80
100	32.90	132.91	67.10
120	33.63	154.39	87.13
140	34.61	176.13	106.91
160	35.82	198.09	126.46
180	37.23	220.26	145.80
200	38.82	242.61	164.97

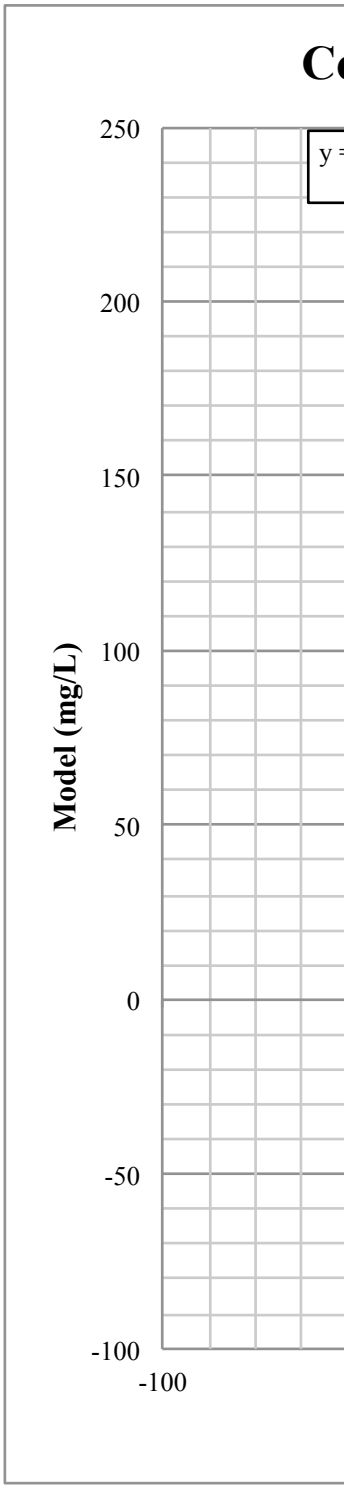

orrelation of Modelled and Analysed Water Chemical Dat

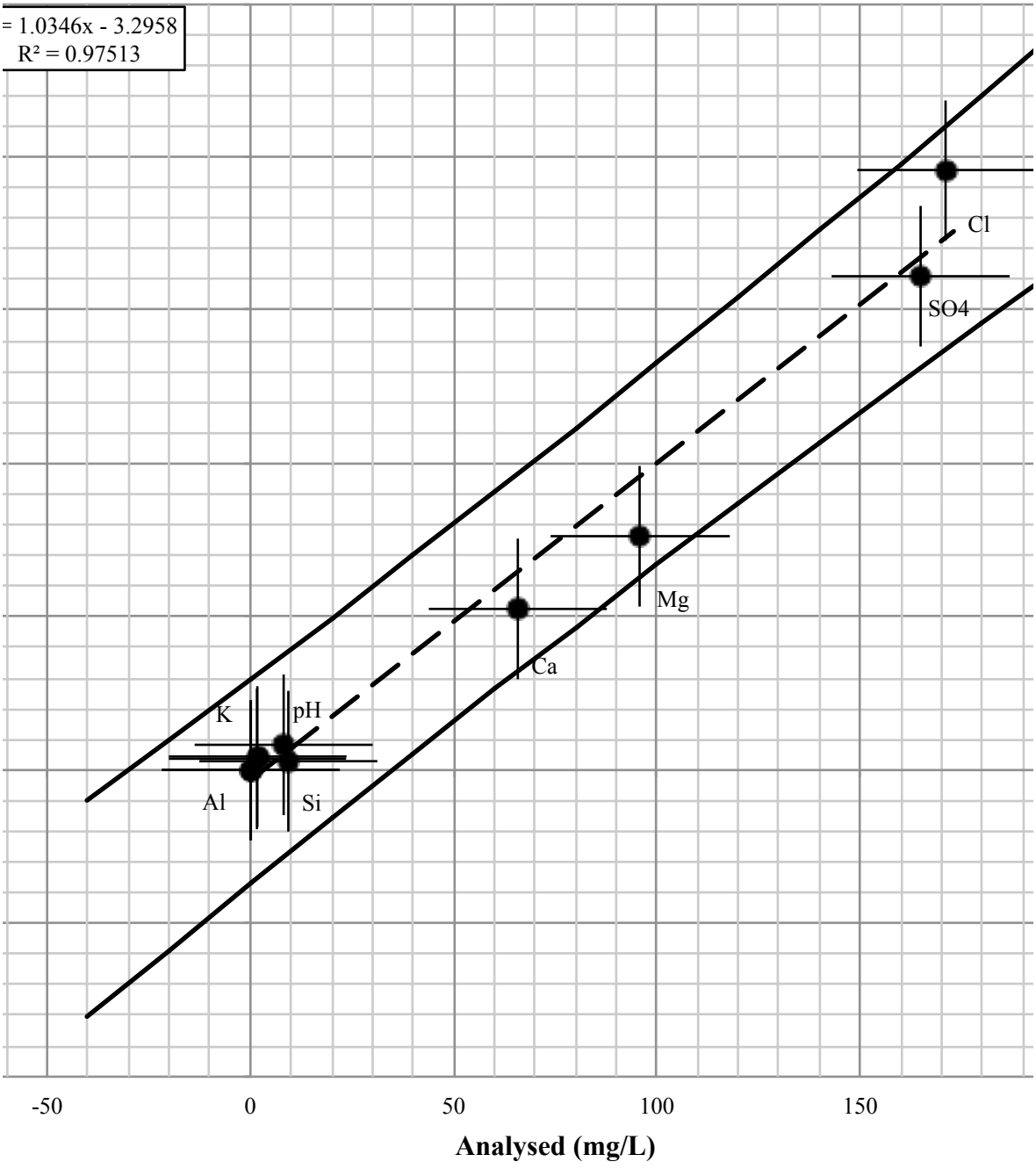

a